The Tropical Momentum Budget in Aquaplanet Simulations with an Ensemble of Global Climate Models

Master's Thesis in Meteorology
by

Freia Then

January 2020

INSTITUTE FOR METEOROLOGY AND CLIMATE RESEARCH
KARLSRUHE INSTITUTE OF TECHNOLOGY (KIT)

Advisor:	Dr. Aiko Voigt
Second Advisor:	Prof. Dr. Peter Knippertz

Abstract

A large share of the global population lives in the tropics. Their societies and economies are vulnerable to changes in precipitation patterns. The highest amount of precipitation occurs around the intertropical convergence zone (ITCZ). Yet simulations imply uncertainty about how the ITCZ might respond to climate change. Further investigation of the underlying mechanisms will facilitate a deeper understanding of these uncertainties. The energetic framework is part of this effort. It links the ITCZ to cross-equatorial energy transport and net energy input at the equator. While this theory is in agreement with some findings, other studies show deviations from its assumptions. One cause of these discrepancies might be activity of eddies within the Hadley cell. To investigate this hypothesis, measures and indices of eddy activity for the momentum budget are applied on TRACMIP AquaControl simulations. The data set consists of present-day aquaplanet simulations from 11 models with a slab ocean and parametrized ocean heat transport. In the tropics, the annual mean meridional momentum flux divergence shows three peaks in the upper troposphere. The maxima in the Southern and Northern Hemisphere weaken and migrate poleward within the corresponding Hadley cell during the summer months. The equatorial minimum is weak in spring and autumn, when both Hadley cells are equally strong, and becomes more prominent in the summer and winter months. This thesis finds that the eddy influence on the Hadley cell is weak in the winter, while it is stronger in summer. Eddies are the driving force in the Hadley cell at the poleward edge. Closer to the common border of the Hadley cells, their influence is less significant. Eddies also influence the Southern Hemisphere cross-equatorial Hadley cell in the deep tropics. This influence is mostly caused by changes in deviating meridional wind rather than fluctuation of the zonal wind. Eddy influence can differ between models by factor 2 and 4, depending on the indices. This uncertainty is predominantly due to the mean meridional circulation, rather than the eddy terms. The migration of the ITCZ is accompanied by changes in eddy influence, whereas changes in cross-equatorial energy transport do not coincide with eddy influence on the upper branch of the Hadley cell. Thus, the results of this thesis suggest that eddies can explain one part of the deviations from the energetic framework. An investigation of eddies in the energy budget and shallow circulations in the deep tropics could yield further insights in this regard.

Zusammenfassung

Ein großer Anteil der Weltbevölkerung lebt in den Tropen. Ihre Volkswirtschaften sind gegenüber Änderungen in Niederschlagsmustern verwundbar. Der stärkste Niederschlag tritt um die Innertropische Konvergenzzone (ITCZ) auf. Doch gekoppelte Ozean-Atmosphären-Simulationen stimmen nicht darin überein, wie sich die ITCZ mit dem Klimawandel verändert. Weitere Untersuchungen der zugrundeliegenden Mechanismen können das Verständnis der Unsicherheiten in den Simulationen verbessern. Das Energetische Modell ist Teil dieser Bestrebungen. Es verknüpft die ITCZ mit dem Energietransport über den Äquator. Während diese Theorie mit manchen Forschungsergebnissen übereinstimmt, zeigen andere Studien Abweichungen von deren Grundannahmen. Diese Abweichungen könnten mit Eddy-Aktivität innerhalb der Hadley-Zelle zusammenhängen. Um diese Hypothese zu untersuchen, werden Methoden und Indizes für Eddy-Aktivität auf TRACMIP AquaControl Simulationen angewandt. Dieser Datensatz besteht aus Aquaplanet-Simulationen unter heutigen Klimabedingungen von 11 Modellen mit einem Grenzschichtozean und einem parametrisierten Wärmefluss im Ozean. In den Tropen zeigt die meridionale Divergenz des Impulsflusses in der oberen Troposphäre drei Extrema. Die beiden Maxima in der Süd- und Nordhemisphäre innerhalb des jeweiligen Hadley-Zelle sind im Sommers schwächer. Das äquatoriale Minimum ist im Frühling und Herbst schwach, während beide Hadley-Zellen ungefähr gleich stark sind, und wird in den Sommer- und Wintermonaten stärker. Diese Arbeit zeigt, dass der Einfluss von Eddys im Winter gering ist, während er im Sommer hoch ist. Eddys treiben die Hadley-Zelle an deren polwärtiger Kante an. Näher an der gemeinsamen Kante der Hadley-Zellen ist der Einfluss schwächer. Eddys beeinflussen die winterliche Hadley-Zelle der Südhemisphären in der Nähe des Äquators. Dieser Einfluss liegt aber vor allem in Schwankungen des meridionalen Windes und nicht des zonalen Windes begründet. Der Eddy-Einfluss auf den Impulshaushalt kann zwischen den Modellen um einen Faktor 2 bis 4 unterscheiden, abhängig vom Index. Diese Unsicherheit geht vor allem von der Divergenz durch den mittleren zonalen Fluss aus und nicht in der Eddy-Komponente. Die Verlagerung der ITCZ wird von Änderungen im Eddy-Einfluss begleitet, wohingegen Änderungen im Energietransport über den Äquator nicht mit einer Änderung des Eddy-Einflusses zusammenfallen. Somit legen die Ergebnisse dieser Arbeit nahe, dass Eddys einen Teil der Abweichung vom Energetischen Modell erklären können. Das Untersuchen von Eddys in der Energiebilanz und flacher Zirkulationen in der Nähe des Äquators könnten weitere Erkenntnisse in diesem Rahmen ergeben.

Contents

1 Introduction

Today, 40% of the global population live in the tropics. This share may even rise to 50% in 2030 (Edelman et al., 2014). The tropical rain belt is the main source of precipitation in the tropics (Fig. 1.1a) and is visible as a distinct peak of precipitation in the zonal-mean (Fig. 1.1b). The tropical rain belt, via its strength and spatial pattern, strongly shapes the availability of fresh water and thus has a strong socioeconmic impact, e.g., on farming practices. Hence, it is important to advance the understanding of the mechanisms that govern the tropical rain belt. Additionally, the climate of the Earth is changing rapidly. The emission reductions pledged under the Paris Agreement[1] might lead to a 3°C increase of the global mean surface temperature (Olhoff and Christensen, 2018) until the end of the 21st century. Therefore, and together with the expected increase of people living in the tropics, it becomes even more important to understand the impact of climate change on the tropical rain belt. But the response of the ITCZ to climate changes remains uncertain in coupled ocean-atmosphere global climate models (Byrne et al., 2018). Its positions, for example, could shift to the South or North depending on the model. Conceptual and theoretical work can help to better understand the impact of a changing climate on the tropical rain belt (Bony et al., 2015).

The tropical rain belt is fueled by surface convergence of moist air and subsequent convection of

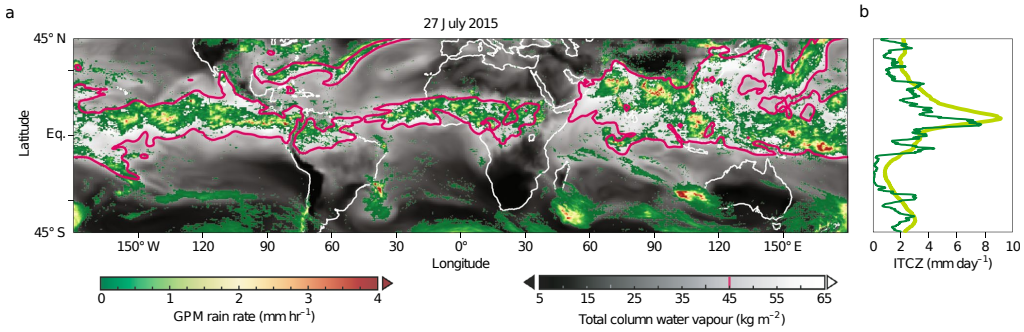

Figure 1.1: (a) Rainfall (colored shading) on July 27th, 2015, and the high atmospheric moisture enveloping it (indicated by the red 45 mm contour of column-integrated water vapour, the full field of atmospheric moisture content is in grey shades) from GPM, global precipitation measurement. (b) The dark green line shows the precipitation rate of the July 27th, 2015 and the light green line the climatological mean of July 27th. Adapted from Biasutti et al. (2018)

this air. Therefore, maximum precipitation can be found in a zone of maximum mass convergence, the Intertropical Convergence Zone (ITCZ). In today's atmosphere the ITCZ is situated at 6° N in the annual and zonal mean (Adler et al., 2003). As reviewed by Schneider et al. (2014), the ITCZ is linked to the zonal-mean transport of mass in the tropics, i.e., the Hadley circulation, which itself is linked to the energy budget of the atmosphere. As a result, the latitudinal position of the

[1] The nationally determined contributions under the Paris Agreement of the United Nations Framework Convention on Climate Change (NDCs) can be found online `https://www4.unfccc.int/sites/NDCStaging/Pages/All.aspx`

ITCZ δ is correlated to the cross-equatorial energy transport and inversely correlated to the net energy input at the equator.

$$\delta \propto -\frac{\text{cross-equatorial energy transport at the equator}}{\text{net energy input at the equator}} \tag{1.1}$$

The net energy input consists of the incoming solar radiation, the outgoing longwave radiation and the ocean heat flux (Frierson et al., 2013). According to Eq. 1.1, the location of the ITCZ is shifted towards the equator, if the net energy input is increased. This can be caused, for example, by changes in cloud patterns or because of increased CO_2 concentration in the atmosphere. The ITCZ is shifted off the equator, when the atmosphere in one hemisphereis more strongly heated than in the other hemisphere. This requires cross-equatorial energy transport at the equator. More specifically, the ITCZ is shifted towards the hemisphere which is more strongly heated. Such a hemispheric imbalance can be caused, for example, by the eccentricity of the Earth orbit or the strength of meridional ocean heat transport, e.g., the Atlantic meridional overturning circulation.

This energy-based theory has become known as the "energetic framework" and is powerful to understand the climate-related influences on the latitudinal position of the ITCZ. For some data this theory works (Adam et al., 2016; Donohoe and Voigt, 2017). Other datasets deviate from this theory (Biasutti et al., 2018; Wei and Bordoni, 2018). Biasutti et al. (2018) hypothesize this to be caused, amongst other things, by the influence of eddies on the Hadley cell being neglected away from its poleward boundary.

Eddies are deviations from the zonal mean (i.e., midlatitude low pressure systems) that carry energy and momentum. The momentum transport by eddies is known to be capable of influencing the dynamics of the Hadley cell. The Hadley cell is the tropical cell of the general circulation. Generally, it transports moist air close to the Earth's surface from the subtropics to the tropics. In the upper troposphere, the Hadley cell transports energy from the tropics to the subtropics. The strength of the Hadley cell is characterized by its mass transport, which in turn is influenced by the meridional gradient of heating and the eddy momentum activity (Vallis, 2006). The thermodynamical relationship from the energetic framework could therefore be distorted by the influence of eddy momentum transport.

The influence of eddy momentum transport on the Hadley cell has been subject to scientific studies in the last decades. Two idealized cases of the Hadley cell can be found in the literature. Held and Hou (1980) and Lindzen and Hou (1988) describe a Hadley cell in the absence of eddies. In this case, the gradient of heating drives the Hadley cell fully and the transport in the upper troposphere conserves the angular momentum. This corresponds well with the energetic framework in which the mass transport is governed by thermodynamical quantities only. On the other hand, there could be a Hadley circulation mainly driven by eddies in which the heating gradient holds a smaller role (Vallis, 2006). Walker and Schneider (2005), Walker and Schneider (2006) and Bordoni and Schneider (2008) quantified the influence of eddies on the Hadley cell from a dynamical point of view. The metrics developed by these studies may shed light onto why, and in which cases, the energetic framework fails due to a strong impact of eddies.

In this thesis, the metrics are utilized to investigate whether the tropical climate deviates from the assumption of a negligible impact of eddies. In addition to the characterization of eddies, the thesis furthermore investigates whether circumstances, in which the energetic framework fails, can be related to a strong impact of eddies. The analysis particularly focuses on the seasonal cycle.

2 State of the Art

This chapter introduces the concepts referred to in this thesis. It starts with the introduction of the basic concept of the energetic framework in Section 2.1 and Section 2.2. Section 2.3 describes the angular momentum in the Earth's atmosphere and the associated constraint for the eastward wind u. This constraint is then used in Section 2.4 to characterize a Hadley cell directly driven by the meridional gradient of diabatic heating, the Held and Hou model. In this model, eddies do not influence the upper branch of the Hadley cell. Section 2.5 describes the method of eddy decomposition (Peixoto and Oort, 1992), in which an atmospheric component is split into two components, the mean and the deviation from it. Using this method, Section 2.6 discusses the implications of eddy influence of the Hadley cell following the argument of Vallis (2006).

2.1 Moist Static Energy

The thermodynamic budget is approximated by the dry static energy equation. This depiction of dry static energy is derived from the first law of thermodynamics (Eq. 2.1).

$$dU = Tds - pd\alpha \tag{2.1}$$

Equation 2.1 describes that a change in internal energy dU is either due to the heating rate Tds with temperature T and entropy change ds or due to work $pd\alpha$ with the pressure p and the specific volume α. The heating rate Q in the atmosphere is related to radiation, latent heat and conduction. The air is considered an ideal gas. Consequently, the internal energy is given by $dU = C_v dT$ with the heat capacity C_v at constant volume. Following up, a new expression for the first law of thermodynamics (Eq. 2.2) is found by taking into account the aforementioned considerations and taking the full derivative of Equation 2.1.

$$C_v \frac{DT}{Dt} = Q - p\frac{D\alpha}{Dt} \tag{2.2}$$

Combined with the Equation of state for ideal gases (Eq. 2.3) in which R is the specific gas constant for dry air and with the Mayer's equation (Eq. 2.4), it results in Equation 2.5.

$$p\frac{D\alpha}{Dt} + \alpha\frac{Dp}{Dt} = R\frac{DT}{Dt} \tag{2.3}$$

$$C_p = C_v + R \tag{2.4}$$

$$C_p \frac{DT}{Dt} - \alpha\frac{Dp}{Dt} = Q \tag{2.5}$$

In Equation 2.6, a scale analysis for the synoptic scale is applied to the subtrahend from Equation 2.5 (see Holton and Hakim, 2012, p. 85).

$$\omega = -g\rho\frac{Dz}{Dt} \tag{2.6}$$

Here, $\omega = \frac{Dp}{Dt}$ is the vertical velocity in the atmosphere, g the gravitational acceleration and z the height. The resulting Equation 2.7 is further simplified using the definition of dry static energy $s = C_pT + \Phi$ with the geopotential $\Phi = gz$.

$$C_p\frac{DT}{Dt} + g\frac{Dz}{Dt} = Q \tag{2.7}$$

This results in the dry static energy budget equation (Eq. 2.8). Dry static energy captures the energy of dry air in the atmosphere.

$$\frac{Ds}{Dt} = Q \tag{2.8}$$

In an atmosphere that holds moisture, the energy contribution from condensation is not negligible. Consequently, the dry static energy is an incomplete measure of thermodynamic energy in such an atmosphere. Neelin and Held (1987) find an additional expression for condensation to extend the static energy for moist atmospheres. To yield a similar equation as Equation 2.8 for a moist atmosphere, the heating term is split into its three components $Q = g\frac{\partial(F^R+F^S)}{\partial p} + Q_{LH}$, with vertical fluxes of energy due to radiation and diffusion of sensible heat F^R and F^S, respectively, and latent heat per mass unit Q_{LH}. The latter is also defined in the water budget equation of the atmosphere (Eq. 2.9) with latent heat of condensation L and specific humidity q. F_L denotes the vertical energy flux due to evaporation and condensation.

$$\frac{D(Lq)}{Dt} = -Q_{LH} + g\frac{\partial F^L}{\partial p} \tag{2.9}$$

Using this relationship and considering the definition of moist static energy, Equation 2.10 for the moist static energy budget is found.

$$\frac{Dh}{Dt} = \frac{D(s+Lq)}{Dt} = g\frac{\partial(F^R+F^S+F^L)}{\partial p} \tag{2.10}$$

Moist static energy connects thermodynamics and moisture budget of the atmosphere where kinetic energy can be neglected.

2.2 The Energetic Framework

The energetic framework aims to link the zonal mean ITCZ to the meridional energy transport. For this, the energetic framework uses the moist static energy budget (Eq. 2.10). But as it is concerned with the zonal mean and net mass transport, this framework uses the mass-weighted integral (denoted as $\frac{1}{g}\int_{p_T}^{p_B} dp$ or $<>$) of the zonal mean (denoted as $[]$) moist static energy budget (Eq. 2.11).

$$\frac{1}{g}\int_{p_T}^{p_B}\left[\frac{Dh}{Dt}\right]dp = \frac{1}{g}\int_{p_T}^{p_B}\left(\frac{\partial\left[\bar{h}\right]}{\partial t} + \nabla\cdot\left[\overline{\mathbf{v}h}\right]\right)dp = F_B - F_T \tag{2.11}$$

The energetic framework assumes steady state in which the time tendency of the moist static energy vanishes, $\frac{\partial h}{\partial t} = 0$. Furthermore, the zonal average of the zonal divergence vanishes, $\frac{\partial}{\partial x}\left[\overline{\mathbf{v}h}\right] = 0$, and the vertical divergence of energy flux vanishes over an integrated atmospheric column, $\frac{\partial}{\partial z}[\overline{vh}] = 0$. Hence, the divergence $\nabla \cdot \left[\overline{\mathbf{v}h}\right]$ simplifies to the meridional gradient of the energy transport $\frac{\partial}{\partial y}\left[\overline{\mathbf{v}h}\right]$ (Eq. 2.12).

$$\frac{1}{g}\int_{p_T}^{p_B}\left(\frac{\partial\left[\bar{h}\right]}{\partial t} + \nabla\cdot\left[\overline{\mathbf{v}h}\right]\right)dp = \frac{\partial}{\partial y} < [\overline{vh}] > \tag{2.12}$$

F_B is the vertical heat flux at the pressure level p_B at the bottom of the atmosphere and F_T the vertical heat flux at the top of the atmosphere at pressure level p_T. According to Neelin and Held (1987), the vertical heat flux at the top of the atmosphere F_T is comprised of radiative fluxes at the top of the atmosphere with $\mathscr{S}$, the incoming shortwave radiation, and the outgoing longwave radiation $\mathscr{L}$: $F_T = F_R = -\mathscr{S} + \mathscr{L}$. The vertical heat flux at the bottom of the atmosphere F_B is fully described by the ocean heat uptake, $F_B = -\mathscr{O}$. Hence, the difference between heat flux at the top of the atmosphere and its bottom can be described by the incoming shortwave radiation, the outgoing longwave radiation and the ocean heat uptake (Eq. 2.13).

$$F_B - F_T = \mathscr{S} - \mathscr{L} - \mathscr{O} \tag{2.13}$$

The net energy input is balanced by the divergence of meridional moist static energy flux in an atmospheric column. This is inferred by the mass-weighted integral of the relationship in Equation 2.11. Using the considerations from the paragraphs above, the notation of the relationship as in Bischoff and Schneider (2014) is found (Eq. 2.14).

$$\mathscr{S} - \mathscr{L} - \mathscr{O} = \frac{\partial}{\partial y} < [\overline{vh}] > \tag{2.14}$$

In the following, the underlying picture of the Hadley cell which leads to Equation 2.14 is described in more detail. The energetic framework implies that moist static energy is transported equatorwards by the mean meridional circulation (Figure 2.1). Moist air masses converge at the ITCZ and cause precipitation there. The convection lifts the air into the upper troposphere. The potential energy of the air increases, while the latent heat decreases in this process. The ultimately dry air masses diverge above the area of convergence and therefore transport dry static energy poleward in the upper troposphere. In the subtropics, the air subsides and diverges at the bottom of the atmosphere. Some air flows back to the ITCZ taking up moisture on its way, while the poleward energy transport is accomplished by eddies.

Following this description, the ITCZ is located where the vertically integrated moist static energy transport vanishes. The ITCZ would thus coincide with the equator in an atmosphere in which the net energy input was equal in both hemisphere. However, this is not the case in today's atmosphere. The net energy input of the Northern Hemisphere is larger, mainly due to the meridional overturning circulation in the Atlantic and Pacific (Frierson et al., 2013). They transport warm surface water from the Southern into the Northern Hemisphere (Figure 2.1). In the Northern Hemisphere polar region, the water cools, sinks and flows in the deep ocean back to the Southern

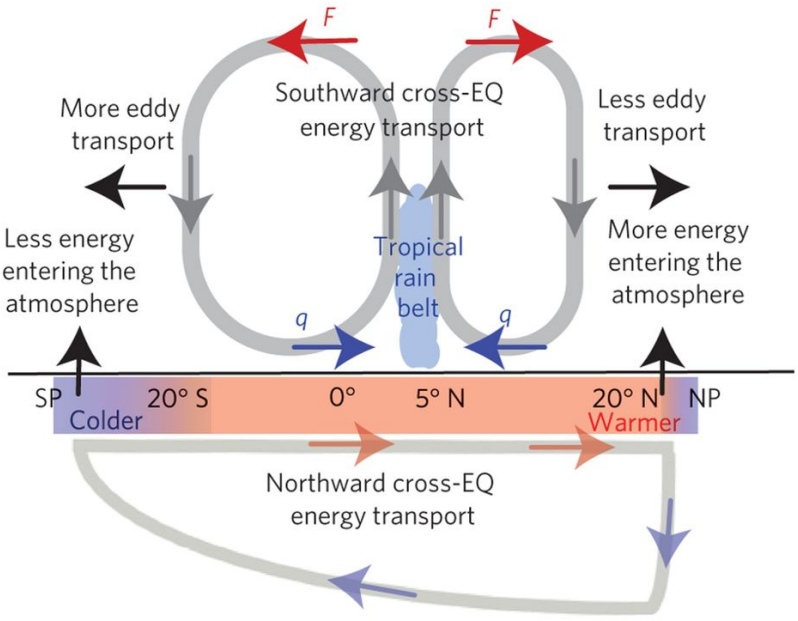

Figure 2.1: The Hadley cell in the energetic framework. The meridional moist static energy transport in form of meridional moisture transport q and energy transport F is directly connected to the position of the tropical rain belt. The tropical rain belt is shifted to 5° N because of the northward ocean heat transport. SP, South Pole; NP, North Pole; cross-EQ, cross-equatorial. Figure adapted from Frierson et al. (2013) Figure 3.

Hemisphere. It resurfaces in the upwelling regions around Antarctica where it cools the Southern Hemisphere. The Southern Hemisphere Hadley cell compensates the inter-hemispheric energy imbalance by transporting energy from the Northern Hemisphere across the equator. Hence, the Southern Hemisphere Hadley cell is stronger in the annual mean than its Northern Hemisphere counterpart. In consequence, the ITCZ is located in the Northern Hemisphere in present-day climate (for argument see Schneider et al. (2014) and Adam et al. (2016); for precipitation climatology see Adler et al. (2003)). Bischoff and Schneider (2014) argue that the position of the ITCZ can be approximated by properties of the energy balance at the equator. They achieve this by expanding the equation 2.14 to the first order. The resulting Equation 2.15 suggests that the position of the ITCZ δ is proportional to the meridional moist static energy flux $< vh >_0$ (cross-equatorial energy transport) and inversely proportional to the net energy input at the equator.

$$\delta \approx \frac{1}{a} \frac{< \overline{vh} >_0}{(\mathscr{S}_0 - \mathscr{L}_0 - \mathscr{O}_0)} \tag{2.15}$$

The relationship described by Equation 2.15 is particularly true in the annual mean (Schneider et al., 2014). Yet it does not represent all mechanisms of seasonal migration of the ITCZ in some seasons (Adam et al., 2016). The analysis of observational data does not show a linear correlation as depicted in Equation 2.15 but rather a relationship in which the annual cycle follows an ellipsis (Biasutti et al., 2018). Simulation with aquaplanet set-ups deviate from observational data. In these simulations, the months follow a triangular shape (see Fig. 2.2 or Biasutti and Voigt (2019) and Wei and Bordoni (2018)). These deviations from the linear relationship in the annual cycle of the ITCZ found in observations and simulations might be causes by shortcomings of the energetic framework (Biasutti et al., 2018).

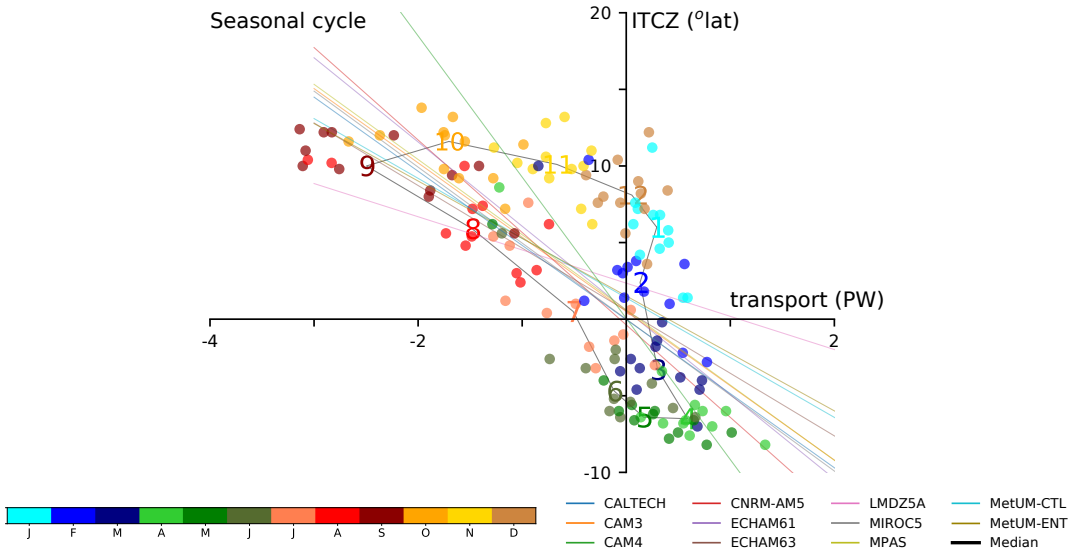

Figure 2.2: The annual cycle of the ITCZ and the cross-equatorial energy transport of the TRACMIP Aqua-Control model ensemble. The multiyear monthly mean values for each month and each simulation of TRACMIP AquaControl (small circles) are colored according to the month they represent. Colored numbers denote the model median of a month, starting with 1 for January. The thin lines display the linear regressions for each simulation colored according to the model used. Figure adapted from Biasutti and Voigt (2019, Fig. 2a).

This is mainly due to two factors. The energetic framework assumes that the meridional energy transport of the atmospheric column is in the direction of the upper troposphere energy transport (polewards). But as the Hadley cell retreats from a position far in the opposite hemisphere back to the equator, a near-surface shallow circulation develops. This circulation counteracts the energy transport in the upper troposphere, as it transports energy in the opposite direction. This changes the overall stratification of energy transport, the gross moist stability, in some cases to the point where the bottom moist static energy transport is stronger than the transport in the upper troposphere. In this case, the gross moist stability changes its sign from positive to negative. Negative gross moist stability is in conflict with the energetic framework (e.g. Wei and Bordoni (2018)). Moreover, precipitation in the tropics, when a shallow circulation occurs, is not always generated from deep convection. Instead, shallow circulations also contribute to the precipitation (Back and Bretherton, 2006). This potentially disconnects the precipitation signal used to calculate the ITCZ from the general circulation. The energetic framework assumes further that the Hadley cell responds directly to the changes in the energetic balance. This should be the case in an angular momentum conserving Hadley cell. But if the Hadley cell is dominated by eddies, the relationship is not as straight-forward. In this scenario, the Hadley cell would be dependent on eddy activity rather than a shift in the energy budget (Walker and Schneider, 2005).

2.3 Angular Momentum in the Earth's Atmosphere

The angular momentum in the atmosphere of the Earth (Eq.2.16 and Fig. 2.3) depends on the latitude ϕ, the radius of the Earth a, the angular velocity of the Earth Ω and the eastward wind u (Peixoto and Oort, 1992).

$$M = (a\Omega\cos\phi + u)a\cos\phi \tag{2.16}$$

Equation 2.16 can be split into two components. The planetary component M_Ω (Eq. 2.17) is constant in time and depends mostly on the angular velocity of the Earth:

$$M_\Omega = a^2\cos^2\phi\Omega \tag{2.17}$$

The second is the relative component M_R (Eq. 2.18) which fluctuates throughout the year, as it depends on the zonal wind u.

$$M_R = a\cos\phi u \tag{2.18}$$

Since the planetary component exceeds the relative one by far, the maximum of angular momentum is typically found in vicinity of the equator (Peixoto and Oort, 1992).

Following the argument of Hide (1969), if there were a closed contour of angular momentum in the meridional plane in a steady state, axisymmetric set-up (independent of longitude (Held and Hou, 1980)), advection of the angular momentum flux and the mass flux across the contour would exactly equal zero. In contrast, the net frictional flux cannot be zero, even if viscosity is very small. It implies that there is a downward gradient of angular momentum that cannot be balanced in the free atmosphere. The maximum of planetary angular momentum is located at the equator, since $\cos\phi \to 1$ for $\phi \to 0$. Additionally, the angular momentum conserving wind u_M, the upper boundary of the zonal wind speed, is $u_M = 0$ at the equator (Eq. 2.19). Therefore, the zonal wind is easterly and the maximum of angular momentum can be reached at the equator with $M_{max} = \Omega a^2$.

$$u_M = a\Omega\frac{\sin\phi}{\cos\phi} \tag{2.19}$$

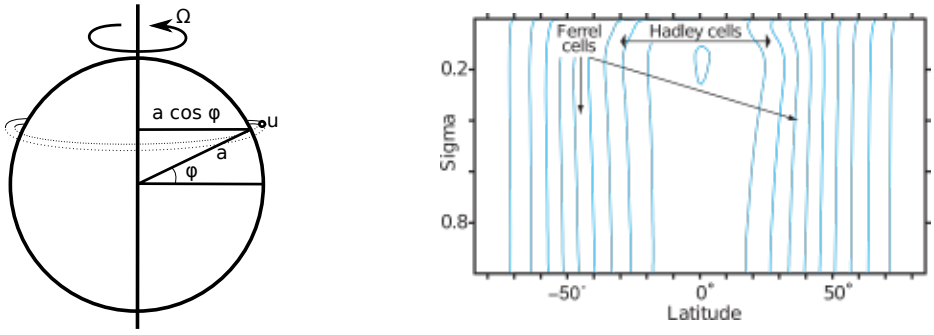

Figure 2.3: Schematic diagram (left) of the angular momentum component around the rotational axis of the Earth, adapted from Peixoto and Oort (1992). Variables denote the latitude ϕ, the zonal wind u, the Earth's angular velocity Ω and its radius a. Temporal and zonal mean of angular momentum in January are from reanalysis data for the years 1980-2001 (Kallberg et al., 2004). The contour intervals (right) are $0.1\Omega a^2$, decreasing monotonically from the equator to the poles. Figure adapted from (Schneider, 2006).

An indicator of eddy activity in the upper troposphere of the tropics is the deviation of u (in simulations or measurements) from u_M. Eddy activity is considered negligible, if u exceeds 90% of u_M. In this case, the flow can be called angular momentum conserving (Walker and Schneider, 2005, 2006).

2.4 The Held and Hou model

The Held and Hou model describes the Hadley circulation in an atmosphere, in which large scale eddies cannot form. The model pictures a Hadley cell which is directly governed by the meridional energy gradient. Held and Hou (1980) describe a model of the Hadley cell using the Boussinesq approximation in an isentropic, dry atmosphere at a steady state on a meridional ϕ - vertical z plane (cf. Fig. 2.4).

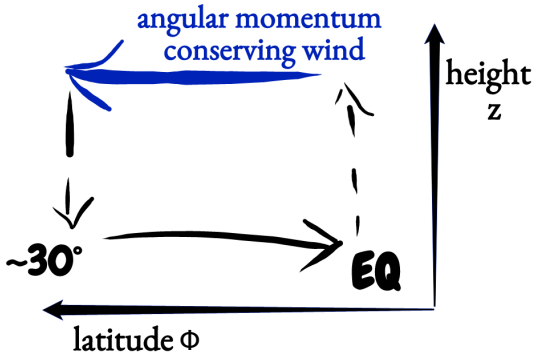

Figure 2.4: Schematic diagram of the Hadley circulation in Held and Hou (1980). Arrows describe the direction of mass transport. EQ: Equator.

The buoyancy b for a stratified fluid is defined as in Equation 2.20 which includes the gravitational acceleration g, the local potential temperature $\delta\theta$ and the global-mean potential temperature θ_0.

$$b = g\frac{\delta\theta}{\theta_0} \tag{2.20}$$

Hence, the buoyancy changes directly in response to changes in the potential temperature ratio. Accordingly, the buoyancy is strongest at the equator, where θ deviates most from θ_0. Therefore, the air rises at the equator due to differential heating. Yet the ascent of the air parcel is constrained by the maximum height of the model $z = H$. From there on, the wind is redirected horizontally as an angular momentum conserving wind $u(H) = u_M$, whereas ϕ denotes the latitude, a the radius and Ω the angular velocity of the Earth.

$$u_M = a\Omega\frac{\sin\phi}{\cos\phi} \tag{2.21}$$

The thermal forcing of the model is given by the Newtonian cooling $\frac{D\theta}{Dt} = \frac{\theta_E - \theta}{\tau}$. Therefore, it depends on the meridional profile of the radiative equilibrium potential temperature $\theta_E(\phi, z)$.

$$\frac{\theta_E(\phi,z)}{\theta_0} = 1 - \frac{2}{3}\Delta_H P_2(\sin\phi) + \Delta_V\left(\frac{z}{H} - \frac{1}{2}\right) \tag{2.22}$$

The radiative equilibrium temperature $\theta_E(\phi, z)$ (Eq. 2.22) is dependent on the fractional temperature change between equator and pole Δ_H and with the Legendre polynomial P_2 in the horizontal dimension, along with the fractional temperature change between the ground and the top of the atmosphere Δ_V and the fraction of the height z, as well as the maximum model height H.

When the air parcel has a potential temperature θ below the potential temperature, the air parcel will sink, as illustrated in Figure 2.4. This happens at $\approx 30°$. The return flow to the equator is slowed down by friction to a point where it is almost non-existent.

For a clearer understanding of the consequences of this model, we can look at the vertically averaged atmosphere, proposed by Held and Hou (1980). The border of a Hadley cell is found in this model, when an air parcel carried by the angular momentum conserving wind has a lower potential temperature than the vertically averaged radiative equilibrium temperature and the air on average is descending.

It is a rather easy task to find the vertically averaged radiative equilibrium temperature from Equation 2.22. Using $P_2(a\phi) = {}^{(3(a\phi)^2-1)}/_2$ and choosing $z = {}^H/_2$, the vertically averaged radiative equilibrium temperature can be written as in Equation 2.23.

$$\theta_E = \theta_0(1 + \frac{1+\Delta_H}{3}) - \theta_0\Delta_H(\frac{a\phi}{a})^2 \tag{2.23}$$

It is more complicated, however, to derive an equation for the potential temperature, assuming the zonal wind to be $u = 0$ at the bottom and u_M at $z = H$. For this purpose, the thermal wind balance (Eq. 2.24) is used which connects the vertical profile of zonal wind u with the meridional gradient of buoyancy b, given that the geostrophic wind approximation is permissible. In this Equation (Eq. 2.24), f is the Coriolis parameter and a the Earth's radius.

$$f\frac{\partial u}{\partial z} = -\frac{1}{a\cos\phi}\frac{\partial b\cos\phi}{\partial\phi} \tag{2.24}$$

To find a vertical average potential temperature θ_M from Equation 2.41, the definitions of b (Eq. 2.20) and u_M (Eq. 2.21) are inserted into Equation 2.41. In order to produce a vertical average, the resulting equation is integrated over the full height of the model ($\frac{1}{g}\int_0^H$) and divided by H. Additionally, the small angle approximation is applied to this equation, i.e. $\sin\phi \approx \phi$ and $\cos\phi \approx \phi$.

$$\frac{1}{a\theta_0}\frac{\partial\theta}{\partial\phi} = -\frac{2\Omega^2 a\phi^3}{gH} \tag{2.25}$$

Equation 2.25 relates the meridional gradient of the vertically averaged potential temperature θ to angular momentum conserving wind. Equation 2.25 can be transformed into Equation 2.26 by meridional integration and imposing conservation of potential temperature within the Hadley cell, along with a continuous solution at the border of the Hadley cell. R denotes the thermal Rossby number $R = {}^{gH\Delta_H}/_{\Omega^2 a^2}$.

$$\theta_M = \theta_{E0} - (\frac{5}{18}R)\Delta\theta - \frac{\theta_0\Omega^2(a\phi)^4}{2gHa^2} \tag{2.26}$$

The result of this lengthy derivation is, that even in a very simple model of the Earth's atmosphere, the Hadley cell is limited to a latitude ϕ_H. Figure 2.5a shows the solution of Equations 2.23 and 2.26 for earth-like conditions. In this case, the Hadley cell's boundary lies around 20°.

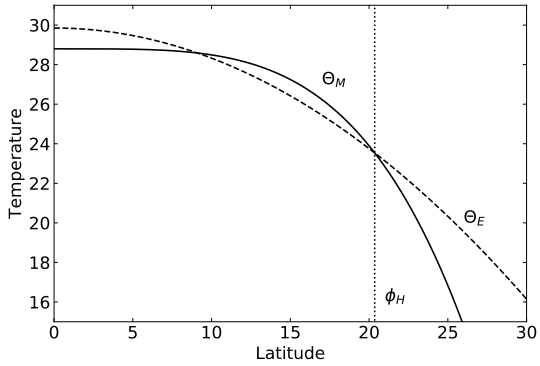

(a) Zonal and vertical mean temperatures from the Held and Hou model

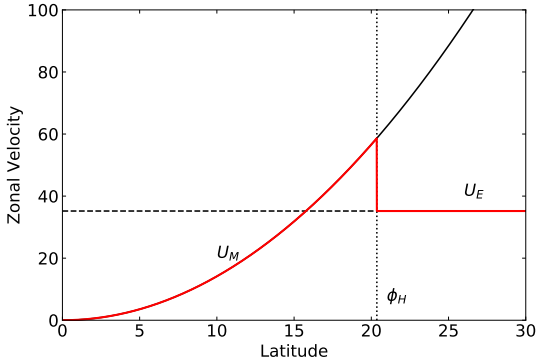

(b) Zonal and vertical mean wind from the Held and Hou model

Figure 2.5: (a) Zonal and vertical mean temperature calculated from Equation 2.22 for θ_E and Equation 2.26 for θ_M in Celsius. (b) Zonal wind in the upper branch of the Held and Hou model U_M from Equation 2.21 and the radiative equilibrium wind U_E from Equation 2.27. The models follows along the red line. Calculated with parameters: $\theta_{E0} = 303K$, $\Delta_{theta} = 50K$, $\theta_0 = 300K$, $\Omega = 7.272x10^{-5}s^{-1}$, $g = 9.81ms^{-1}$ and $H = 10km$. Adapted from Vallis (2006, Chap. 14, Fig. 11.6 and Fig. 11.7)

In a similar manner as θ_M has been derived, an expression for a wind at $z = H$ can be inferred from the radiative equilibrium temperature, using the thermal wind balance (Eq. 2.41). Therefore, a simplified version of Equation 2.22 is inserted to derive Equation 2.27, wherein R remains the thermal Rossby number and a the Earth's radius (cf. Fig. 2.5b).

$$U_E = \Omega a R \tag{2.27}$$

Held and Hou (1980) show that the Hadley cell on an earth-like planet terminates in the subtropics even without baroclinic instability. This may play an important role on the Earth today (Vallis, 2006, cf.). The model depicts a Hadley cell which is completely zonally symmetric and has its energy maximum at the equator. Using the continuity equation and the thermodynamic equation at the equator, a scaling for the maximum strength of the mass streamfunction can be found. Depending on the literature, there are two formulations shown in Equation 2.28 (Walker and Schneider, 2006; Schneider, 2006) and Equation 2.29 (Vallis, 2006).

$$\Psi \approx \frac{R^{2/3} a^2 H \Delta_H}{\tau \Delta_V} \tag{2.28}$$

$$\Psi \approx \frac{R^{2/3} a H \Delta_H}{\tau \Delta_V} \tag{2.29}$$

The scaling from Equation 2.28 yields results which are more comparable with today's Hadley cell strength. The catch of Vallis (2006) is that the derivation of the scaling is written down step by step and is coherent in itself. However, using the parameters from Figure 2.5 and Equation 2.28, the Hadley cell is about an order of 10^2 smaller than the Earth's Hadley cell and Schneider (2006) finds parameters which are one order of magnitude smaller.

Lindzen and Hou (1988) consider the effects of displacing the maximum of thermal forcing off the equator at latitude ϕ_0. Therefore, the equation for the radiative equilibrium temperature is ad-

justed to peak there. The angular momentum conserving wind is supposed to be zero at the border between the Hadley cells ϕ_1. The flow satisfies the cyclostrophic, but not the geostrophic balance as in Held and Hou (1980), because there is meridional motion at the equator. Hence, Lindzen and Hou (1988) use a generalized thermal wind balance. Since the zonal wind u is determined by angular momentum conservation, it is symmetric about the equator, even if the maximum of thermal forcing is placed off the equator.

The border between the winter and the summer Hadley cell is closely dependent on this displacement of thermal forcing off the equator. Even small deviations cause profound changes. In this case, the temperature difference between the radiative equilibrium temperature and the potential temperature derived from angular momentum conservation is larger. This leads to a 50% stronger winter cell than in Held and Hou (1980) and a 50% weaker summer cell.

Lindzen and Hou (1988) find that the Hadley cell is non-linearly amplified by a shift of the maximum heating off the equator. They hypothesize a Hadley cell which is symmetric about the equator, as described before, does not accurately resemble the strength of the Hadley cell in the annual mean. It rather captures the behaviour of an equinoctial Hadley cell. Averaged with the a non-linearly amplified solarstic Hadley cell, the annual mean Hadley cell is much closer to the observed Hadley cell. This non-linear amplification could not be reproduced by Schneider (2006) and also does not show in observations (Dima and Wallace, 2003).

The discrepancy between the angular momentum conserving Hadley cell and Earth observations is mostly due to the influence of eddies. The upper branch of the Earth's Hadley cell departs markedly from angular momentum conservation in the upper branch of the Hadley cell most of the time. It approaches angular conservation in the cross-equatorial winter Hadley cell (Schneider, 2006).

2.5 Eddy Decomposition

The mean of a meteorological variable does not sufficiently describe the features of the atmosphere's general circulation. Deviations from the mean in space and time capture phenomena like Rossby waves and mid-latitude low pressure systems which are crucial for poleward energy transport. Following Peixoto and Oort (1992), the instantaneous value A can be decomposed into its mean $\bar{A}$ over a time period τ (Eq. 2.30) and the departure from the mean A' (Eq. 2.31).

$$\bar{A} = \frac{1}{\tau}\int_0^\tau A dt \tag{2.30}$$

$$A = \bar{A} + A' \tag{2.31}$$

When a second meteorological variable with instantaneous value B is added, Equation 2.31 expands to Equation 2.32 for the product $\overline{AB} = (A + A')(B + B')$. The covariance of the variables $A'B'$ can also be defined as the product of the correlation of AB and the standard deviations of these two variables.

$$\overline{AB} = \bar{A}\bar{B} + A'B' \tag{2.32}$$

Analogous, an expression is found for an average over all longitudes for each latitude (Eq. 2.34). $[A]$ is the zonal mean (Eq. 2.33) and A^* is the deviation from this mean.

$$[A] = \int_0^{2\pi} A \frac{d\lambda}{2\pi} \tag{2.33}$$

$$A = [A] + A^* \tag{2.34}$$

The product $[AB] = ([A] + A^*)([B] + B^*)$ simplifies to equation 2.35.

$$[AB] = [A][B] + [A^*B^*] \tag{2.35}$$

In this case, $[A^*B^*]$ is the spatial covariance and the product of its correlation coefficient and the standard deviations of A and B.

These two methods of decomposition (Eq. 2.31 and Eq. 2.34) can be combined and are mathematically permutable. However, each permutation usually holds other physical meaning (Peixoto and Oort, 1992). In this thesis, time mean is calculated first and the zonal average thereafter, yielding a decomposition as in equation 2.36.

$$\left[\overline{AB}\right] = \left[\overline{A}\right]\left[\overline{B}\right] + \left[\overline{A}^*\overline{B}^*\right] + \left[\overline{A'B'}\right] \tag{2.36}$$

$\left[\overline{A}\right]\left[\overline{B}\right]$ describes the mean flow that is strong for example in the cross-equatorial winter Hadley cell. $\left[\overline{A}^*\overline{B}^*\right]$ describes stationary and $\left[\overline{A'B'}\right]$ transient eddies.

2.6 An Eddy Driven Hadley Cell

Eddies have a profound influence on the general circulation (cf. Fig. 2.6). In the mid-latitudes, the potential vorticity changes between the surface layer, where it is determined by the temperature gradient, and the interior of the troposphere which is dominated by the planetary vorticity component. This leads to a strong generation of eddies in this area. Partly, eddies propagate upward and equatorward and dissipate at the poleward boundary of the Hadley cell. This process strengthens the meridional mass transport. In the upper troposphere, this is accompanied by eddy momentum flux divergence within the Hadley cell and eddy momentum flux convergence in the bordering Ferrel cell (Levine and Schneider, 2015).

A set of equations for the meridional mean circulation of the Hadley cell can formulated, even if the mean circulation does not transport momentum or energy. In consequence, all terms describing the transport of momentum or energy by the mean flow are neglected in the momentum and the thermodynamic budget equation. Hence, the temporal and zonal mean northward wind $[\bar{v}]$ in the momentum budget equation (Eq. 2.37) is only dependent on the Coriolis parameter f, the time tendency of momentum $\frac{\partial u}{\partial t}$ and the eddy momentum flux divergence $\mathbf{E} = -\frac{1}{a\cos^2\phi}\frac{\partial}{\partial\phi}\left(\cos^2\phi\,[\bar{u}^*\bar{v}^*] + \overline{u'v'}\right)$.

$$\frac{\partial u}{\partial t} - f\bar{v} = \mathbf{E} \tag{2.37}$$

The thermodynamic budget equation transforms into Equation 2.38. The temporal mean upward

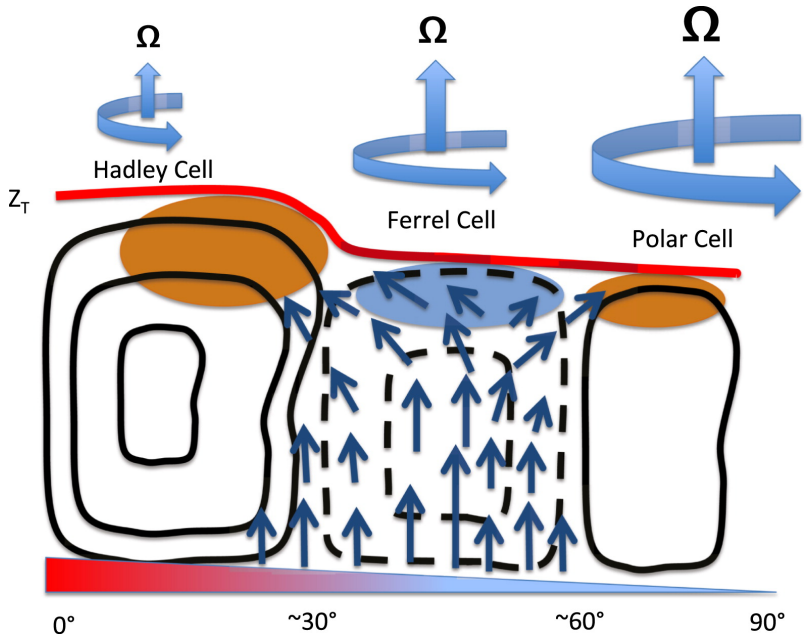

Figure 2.6: Schematic diagram: The influence of macroturbulence on the zonal mean momentum budget. Black lines signify the Hadley cell's mass transport (dashed: clockwise, solid: anticlockwise). Ω is the planetary vorticity. The red solid line is the tropopause which is determined by baroclinic activity poleward of the Hadley cell. The ellipses stand for eddy flux momentum divergence (orange) and convergence (lightblue). Baroclinc eddies originate in the mid-latitudes, where the temperature gradient at the surface is steep, and then propagate upward and equatorward (blue arrows), before they dissipate at the border of the Hadley cell. Figure adapted from Levine and Schneider (2015, Fig. 1).

wind $\bar{w}$ is dependent on the Brunt–Väisälä frequency N which characterizes, how a displaced air parcel oscillates, depending on the thermal stratification of the atmosphere, time tendency of the buoyancy $\frac{\partial \bar{b}}{\partial t}$ and the heat transport terms $\mathbf{J}$. $Q[b]$ is diabatic heating and $-\frac{1}{\cos^2\phi}\frac{\partial}{\partial\phi}\left(\cos^2\phi\overline{v'b'}\right)$ is the eddy heat flux divergence.

$$\frac{\partial \bar{b}}{\partial t} + N^2 w = Q[b] - \frac{1}{\cos^2\phi}\frac{\partial}{\partial\phi}\left(\cos^2\phi\overline{v'b'}\right) = \mathbf{J} \tag{2.38}$$

Using the temporal and zonal mean continuity equation (Eq. 2.39), a meridional mass streamfunction Ψ is formulated (Eq. 2.40). The mass streamfunction Ψ is typically used to quantify the strength of a cell in the general circulation of the atmosphere (further explained in Section 4.2.4).

$$\frac{\partial[\bar{v}]}{\partial y} + \frac{\partial[\bar{w}]}{\partial z} = 0 \tag{2.39}$$

$$[\bar{w}] = \frac{\partial\Psi}{\partial y}[\bar{v}] = -\frac{\partial\Psi}{\partial z} \tag{2.40}$$

This yields a diagnostic equation for eddy influence on the Hadley cell's strength by using the thermal wind balance (Eq. 2.41) and assuming a steady state (Eq. 2.37 and Eq. 2.38).

$$f\frac{\partial[\bar{u}]}{\partial z} = -\frac{\partial[\bar{b}]}{\partial y} \tag{2.41}$$

The resulting Equation 2.42 shows that the strength of the Hadley cell is influenced by the meridional gradient of diabatic heating and of eddy heat flux divergence, as well as by the vertical gradient of eddy momentum flux divergence.

$$f^2 \frac{\partial^2 \Psi}{\partial z^2} + N^2 \frac{\partial^2 \Psi}{\partial y^2} = f \frac{\partial \mathbf{E}}{\partial z} + \frac{\partial \mathbf{J}}{\partial y} \tag{2.42}$$

Walker and Schneider (2005) show that baroclinic eddies suppress the non-linear amplification of the Hadley cell strength through displacement of maximum thermal heating off the equator, as described in Lindzen and Hou (1988). Thus, the annually averaged Hadley cell is similar to a Hadley cell forced with annually averaged heating. Moreover, the influence of eddies on the Hadley cell varies throughout the seasons.

Bordoni and Schneider (2008) describe two regimes of the Hadley cell: a Hadley cell at the angular momentum conserving limit and an eddy driven Hadley cell. The transition between the two regimes can take months or can happen rapidly, depending on the thermal inertia of the surface.

3 Research Question

In the energetic framework, the latitudinal position of the annual mean ITCZ can be explained as an interaction between cross-equatorial energy transport and net energy input at the equator. This relationship can be consistent over very long time periods (Schneider et al., 2014) and throughout the seasonal cycle (Adam et al., 2016). However, the scope of the energetic framework is limited for some data sets (Biasutti et al., 2018; Wei and Bordoni, 2018; Biasutti and Voigt, 2019).

Biasutti et al. (2018) hypothesize that a failure of the energetic framework is connected to two of its crucial assumptions:

1. The gross moist stability has to be positive.

2. The eddy influence on the Hadley cell can be neglected away from its poleward boundary.

The first assumption is connected to the stratification of the tropical atmosphere. The energetic framework assumes that the energy in the upper troposphere exceeds energy in the lower troposphere. Therefore, the gross moist stability is positive. In some month of the year, a shallow circulation forms close to the equator that disconnects the latitudinal position of the ITCZ from the cross-equatorial energy transport. In this case, the gross moist stability becomes negative. This is investigated in connection with the energetic framework by, inter alia, Wei and Bordoni (2018). However, research investigating the second assumption could not be found.

From a dynamical point of view, the impact of eddy momentum transport on the Hadley cell strength varies throughout the seasons (Schneider, 2006). In some months, the meridional mass transport is driven by a Hadley cell that is thermally direct. That means the meridional gradient of diabatic heating determines the strength of the Hadley cell entirely which also means that eddies are negligible. This is connected to an angular momentum conserving flow in the upper branch of the Hadley cell, much like in the Held and Hou model. In other months, the eddy influence on the meridional mass transport of the Hadley cell distorts the tight relationship between the meridional gradient of diabatic heating and strength of the Hadley cell. This is connected to an influence of eddy momentum flux on the upper branch of the Hadley cell. This dynamical perspective on the Hadley cell could give further insight into the validity of the energetic framework's second assumption.

Many studies that investigate climate dynamics use aquaplanets as an idealized set-up to investigate the underlying mechanisms of the general circulation. Often a prescribed sea surface temperature gradient is used to represent the meridional gradient of heating. But this is not permissible for set-ups that should capture the core features of the energetic framework, because the latter requires at least some degree of ocean response. TRACMIP (Voigt et al., 2016) provides a data set that meets the requirements to reproduce an atmosphere that follows the energetic framework. Indeed, the aquaplanet simulations included in TRACMIP are meant to provide a set-up

in which the energetic framework should be successful, as the lack of continents and the zonally-symmetric ocean heat transport could be expected to eliminate eddy effects in the deep tropics. But as shown in Biasutti and Voigt (2019), all models of the TRACMIP ensemble a deviation from the energetic framework, in particular in the seasonal cycle. Since the simulations from TRACMIP cover a wide range of models, this is an ideal data set to investigate inhowfar the dynamical view on the Hadley cell can aid the understanding of the deviations from the energetic framework in the seasonal cycle. This leads to the following research questions:

1. How does the meridional momentum budget look like in TRACMIP AquaControl in the annual mean and throughout the seasonal cycle?

2. How strong is the influence of eddy momentum transport on the Hadley cell in the annual mean and throughout the seasonal cycle? Is the influence robust across different models?

3. When the energetic framework cannot successfully explain the position of the ITCZ, do eddies play a role?

In Chapter 4, the TRACMIP data set is described and the data used to perform the analysis in this thesis is documented. Additionally, the methods to characterize the influence of eddies for answering research question 2 are presented. The following Chapter 5 gives an overview of Hadley cells in the TRACMIP AquaControl simulations, in the annual mean and the seasonal cycle for the model median of each model. Chapter 6 describes how the momentum budget is represented in the model median of TRACMIP AquaControl and furthermore investigates its model spread. Hence, this chapter will address the 1st research question. The 2nd research question is discussed in Chapter 6. The 3rd research question is the focus of Chapter 7. Here, the influence of eddy momentum transport on the connection between cross-equatorial momentum transport and the ITCZ position is investigated. Chapter 8 summarizes the results and the answers to all of the three research questions.

4 Data and Methods

4.1 The Tropical Rain Belts with an Annual Cycle and a Continent Model Intercomparison Project

The aim of the TRACMIP dataset (Voigt et al., 2016) is to close the gap between aquaplanet simulations with prescribed sea surface temperature (AquaPlanet Experiment (APE), (Williamson et al., 2012)), which are very sensitive to changes in convection parametrizations, and full simulations as in model intercomparison projects like CMIP6 (Eyring et al., 2016).

The project set-up features a slab ocean with a parameterized ocean heat flux from the Southern to the Northern Hemisphere (q-flux). Because of the slab ocean, surface temperatures are responsive and constrain convection in contrast to the APE. Frierson et al. (2013) show that the ocean heat flux is one of the main causes for the ITCZ to shift northward from the equator. The q-flux imposes this flux onto the slab ocean. Therefore, the TRACMIP experiment includes essential elements of the Earth's tropical climate. The insolation in TRACMIP simulations has a seasonal and diurnal cycle. Accordingly, the obliquity is set to 23.5° and the vernal equinox is set to March 21st. The eccentricity is set to zero for the set-up used in this thesis. This means the distance between

Table 4.1: Five Experiments explore the Dynamics of Tropical Rainbands (Monsoons and ITCZ) from Voigt et al. (2016) [a]

Experiment	Land	CO_2(ppmv)	Eccentricity ε	Years	Initial Condition
AquaControl	No	348	0	15+30	Arbitrary initial state, 15 years of spin-up
LandControl	Yes	348	0	40	Year 45 of AquaControl
Aqua4xCO2	No	1392	0	40	Year 45 of AquaControl
Land4xCO2	Yes	1392	0	40	Year 40 of LandControl
LandOrbit	Yes	348	0.02	40	Year 40 of LandControl

[a] The control configuration is an aquaplanet coupled to a slab ocean. Insolation varies with diurnal and annual cycles. CO_2 is varied, and a tropical jello-continent and different orbital parameters are used to study tropical rainfall in present-day-like conditions and in conditions mimicking the mid-Holocene and global warming.

Table 4.2: Overview of the models used for the analysis of this thesis adapted from Voigt et al. (2016)

Nr	Model	Reference	Resolutions	Remarks
1	CALTECH	O'Gorman and Schneider (2008) Bordoni and Schneider (2008)	T42 (2.8°); 30 levels	Idealized physics: gray radiation, no radiative effects of clouds and water vapor, simplified Betts-Miller convection scheme
2	CAM3	Collins et al. (2006)	T42 (2.9°); 26 levels	Atmosphere component of CCSM3
3	CAM4	Neale et al. (2013)	1.9° lat x 2.5° lon, finite volume (nominally 2.0°); 26 levels	Atmosphere component of CCSM4, aquaplanet modifications as in Rose et al. (2014)
4	CNRM-AM5	Voldoire et al. (2013)	T127 (0.9° lat x 0.9° lon); 31 levels	Atmosphere component of CNRM-CM5
5	ECHAM 6.1	Stevens et al. (2013)	T63 (1.9° lat x 1.9° lon); 47 levels	Atmosphere component of MPI-ESM
6	ECHAM 6.3	Stevens et al. (2013)	T63 (1.9° lat x 1.9° lon); 47 levels	Update of ECHAM6.1
7	LMDZ5A	Hourdin et al. (2013)	1.9° lat x 3.8° lon; 39 levels	Atmosphere component of IPSL-CM5A-LR
8	MetUM-CTL	Walters et al. (2017)	N96 (1.9° lat x 1.3° lon); 85 levels	Standard configuration of GA6.0
9	MetUm-ENT	Walters et al. (2017)	N96 (1.9° lat x 1.3° lon); 85 levels	50% convective entrainment and detrainment compared to MetUM-CTL
10	MIROC5	Watanabe et al. (2010)	T85 (1.4° lat x 1.3° lon); 40 levels	
11	MPAS	Skamarock et al. (2012)	240km; 30 levels	

Table 4.3: Overview of the TRACMIP AquaControl data used for calculations in this thesis

Model name	ua	va	wap	tauu
CALTECH	daily	daily	daily	daily
CAM3	3-hourly	3-hourly	3-hourly	daily
CAM4	3-hourly	3-hourly	3-hourly	daily
CNRM-AM5	3-hourly	3-hourly	3-hourly	none
ECHAM61	3-hourly	3-hourly	3-hourly	daily
ECHAM63	3-hourly	3-hourly	3-hourly	daily
LMDZ5A	daily	daily	daily	none
MIROC5	3-hourly	3-hourly	3-hourly	daily
MPAS	3-hourly	3-hourly	3-hourly	daily
MetUM-CTL	3-hourly	3-hourly	3-hourly	daily
MetUM-ENT	3-hourly	3-hourly	3-hourly	daily

Earth and sun is constant. Hence, the incoming radiation on the annual mean is symmetric along the equator. This is not the case on the Earth today [1].

Fourteen models participated in TRACMIP. However, only eleven models (cf. Table 4.2) are used for this analysis. The analysis does not include GISS models E2 and CAM5Nor, because there was no wind data available for daily and for 3-hourly data. The wind fields of AM 2.1 contained implausible values, hence this model was excluded as well. Still, the eleven models used show a large variety on modelling solutions. The ensemble offers two generations of the CAM model (CAM 3 and CAM 4), two different versions of ECHAM6 (ECHAM 6.1 and ECHAM6.3) and the model MetUM with two different convection schemes (MetUM-CTL and MetUM-ENT). Apart from CALTECH, all models include a comprehensive radiation scheme and convection parametrization. CALTECH uses a gray radiation scheme and a simplified convection treatment. Therefore, it does not account for feedback from clouds or water vapor (Voigt et al., 2016).

TRACMIP offers the five set-ups listed in Table 4.1. The default set-up in this thesis is Aqua-Control. The entire surface is covered by a slab ocean. The ocean heat capacity equals a 30 m deep mixed layer. This causes a pronounced precipitation peak in the tropics, but also a seasonal delay (Donohoe et al., 2014). In the AquaControl set-up, the delay amounts to 2.5 to 3 months, reaching the poleward maxima of the ITCZ in October and April to May in the Southern and Northern Hemisphere respectively (Voigt et al., 2016). The present-day concentration of greenhouse gases, solar irradiation and ozone data are adopted from APE. Chlorofluorocarbons' and aerosols' direct radiative effects are set to zero. Using this set-up, the tropical momentum balance of the models and its impact on energetic quantities are investigated.

The data set offers aquaplanet simulations to study the influence of climate change using the set-up Aqua4xCO2. As indicated by the name, the CO_2 concentration in Aqua4xCO2 simulations is instantaneously quadrupled, from 348 ppm to 1392 ppm. The respective AquaControl simulations

[1] The effect of the elliptical orbit of today's Earth can be investigated separately using the data from the LandOrbit set-up where eccentricity is set to $\varepsilon = 0.02$ which is comparable to the Earth eccentricity today.

serve as an initial state. These are not used in this thesis. Simulations with a tropical continent are also available, but not used here. Those set-ups are LandControl, Land4xCO2 and LandOrbit (cf. Table 4.1). A full description of the data set and its features can be found in Voigt et al. (2016).

For the calculations in this thesis, the horizontal wind variables, zonal wind *ua* and meridional wind *va*, along with the model output of the westerly surface stress τ_u are included. TRACMIP offers monthly data over 30 years, daily data from the last 10 years and 3-hourly data from the last 3 years of the simulation. Whereever 3-hourly data is available, it is used to calculate mean fields and eddies of the momentum balance. If the 3-hourly data is not provided, the calculation are done with daily data. Additionally, the vertical wind in the pressure system *wap* is utilized to investigate the influence of the vertical momentum transport in Section 6.5.2. For model output of the westerly surface stress τ_u, only daily data is used to calculate the monthly means[2]. The means of each model and the eddy decomposition is calculated in the latitude coordinates of the output. For further calculations and model medians the models are interpolated to the latitude coordinates of ECHAM 6.1. In Chapter 7, this thesis includes data from Biasutti and Voigt (2019) for the ITCZ position and the atmospheric cross-equatorial energy transport calculated from monthly data of TRACMIP AquaControl simulations. All data used in this thesis is summarized in Table 4.3.

[2] 3-hourly data for τ_u was available for some of the models. The difference between the 3-hourly data and the daily data was very small. Because of this and due to the fact that the daily data was available for more models, the daily data was chosen.

4.2 Methods

This section introduces the methods to analyze the momentum budget and to quantify the influence of eddy activity on the Hadley cell.

4.2.1 Conservation of Angular Momentum

Angular momentum conservation implies that angular momentum contours cannot cross mass streamlines. This is connected to the assumption that thermodynamics directly governs the Hadley circulation like in Held and Hou (1980). This criterion is an idealized state. Even in models tailored to conserve angular momentum in the upper branch of the Hadley cell, this criterion is hard to maintain (Hill et al., 2019). Still, it is a good qualitative indicator of the eddy influence on the Hadley cell. Furthermore, using the Hide theorem, an expression for the angular momentum conserving wind u_M (Chapter 2, Eq. 2.19) can be found (Hide, 1969). The deviation of the eastward wind u in the upper branch of the Hadley cell from u_M signifies the eddy influence. Walker and Schneider (2005) find that the eastward wind u in the upper branch does not deviate more than 10% from u_M in the winter cell, but about 25% in the equinoctial cell and as much as 50% in the summer cell. In Section 6.1, the angular momentum budget of the data set is presented in the model median with a focus on the tropical upper troposphere. Additionally, the angular momentum conserving wind is calculated and compared to eastward wind u_{up} in the range 250 hPa to 150 hPa.

4.2.2 The Eddy Decomposition of the Zonal Momentum Balance

Various simplifications of the momentum budget equation are admissible for the upper branch of the Hadley cell (Schneider, 2006). In this thesis, the viscosity and the friction due to surface stress are neglected. In consequence, the time tendency of the momentum budget $\frac{\partial[\bar{u}]}{\partial t}$ is fully explained by the mean meridional transport of planetary momentum and the divergence of meridional momentum flux (Eq. 4.1).

$$\frac{\partial[\bar{u}]}{\partial t} = -f[\bar{v}] - \nabla \cdot [\overline{u\mathbf{v}}] \tag{4.1}$$

The brackets have the meaning as described in Section 2.5, u stands for the eastward and $\mathbf{v} = (u, v, \omega)$ is the three dimensional wind vector. $f = 2\sin\phi\Omega$ is the Coriolis parameter. Ω is the Earth rotation. a is the Earth's radius and ϕ the latitude.

The momentum transport $[\overline{u\mathbf{v}}]$ is decomposed into its three components by applying the Equation 2.36: the momentum transport by the mean meridional circulation $([\bar{u}][\bar{v}], [\bar{u}][\bar{\omega}])$, stationary eddy transport $\left(\left[\bar{u}^*\bar{v}^*\right], \left[\bar{u}^*\bar{\omega}^*\right]\right)$ and transient eddy transport $\left(\left[\overline{u'v'}\right], \left[\overline{u'v'}\right]\right)$. The zonal momentum transport is zero on the zonal mean $[\overline{uu}] = 0$. The simplified zonal momentum balance (Eq. 4.1) becomes Equation 4.2 by inserting the eddy decomposed momentum transport.

$$\begin{aligned}\left[\overline{\frac{\partial u}{\partial t}}\right] = -f[\bar{v}] &- \left[\frac{1}{a\cos^2\phi}\frac{\partial([\bar{u}][\bar{v}]\cos^2\phi)}{\partial\phi} + \frac{\partial[\bar{u}][\bar{\omega}]}{\partial p}\right] \\ &- \left[\frac{1}{a\cos^2\phi}\frac{\partial(([\bar{u}^*\bar{v}^*] + [\overline{u'v'}])\cos^2\phi)}{\partial\phi} + \frac{\partial([\bar{u}^*\bar{\omega}^*] + [\overline{u'\omega'}])}{\partial p}\right]\end{aligned} \tag{4.2}$$

The zonal surface stress τ_u is equivalent to the mass-weighted integral (denoted as $<>$) of the zonal momentum balance (Eq. 4.3, Peixoto and Oort (1992)).

$$\tau_u = \left\langle -\frac{1}{a\cos^2\phi}\left[\frac{\partial([\bar{u}][\bar{v}]\cos^2\phi)}{\partial\phi} + \frac{\partial\left(\left([\bar{u}^*\bar{v}^*] + [\overline{u'v'}]\right)\cos^2\phi\right)}{\partial\phi}\right] - f[\bar{v}]\right\rangle \tag{4.3}$$

The vertical integral of the vertical momentum transport is zero $< [\overline{u\omega}] >= 0$. Additionally, steady state is assumed ${}^{\partial u}/_{\partial t} = 0$.

Since the easterly surface stress τ_u is a separate output variable of many models (cf. Table 4.3), this relationship is used to test how well the eddy decomposition represents the momentum budget of the model. Differences can occur when the temporal resolution of the output is too coarse to resolve eddies. The method was applied e.g. for a similar analysis on CMIP5 data in Simpson et al. (2014).

In this thesis, the method is implemented by using daily data of τ_u to calculate zonally averaged multi-year monthly means. The zonally averaged multi-year monthly means of τ_u are compared to zonally averaged multi-year monthly means of the mass-weighted integral of the zonal momentum balance. In Figure 4.1, the seasonal model median of both quantities is shown for the 8 models that provide τ_u (cf. Table 4.3). Especially in the tropics, where the influence of the mean meridional circulation is comparatively large, the integral shows good agreement with τ_u. In the seasons DJF (December, January and February) and MAM (March, April and May), this analysis suggest that the eddy decomposition does not fully represent the momentum balance in the extra-tropics of the Northern Hemisphere.

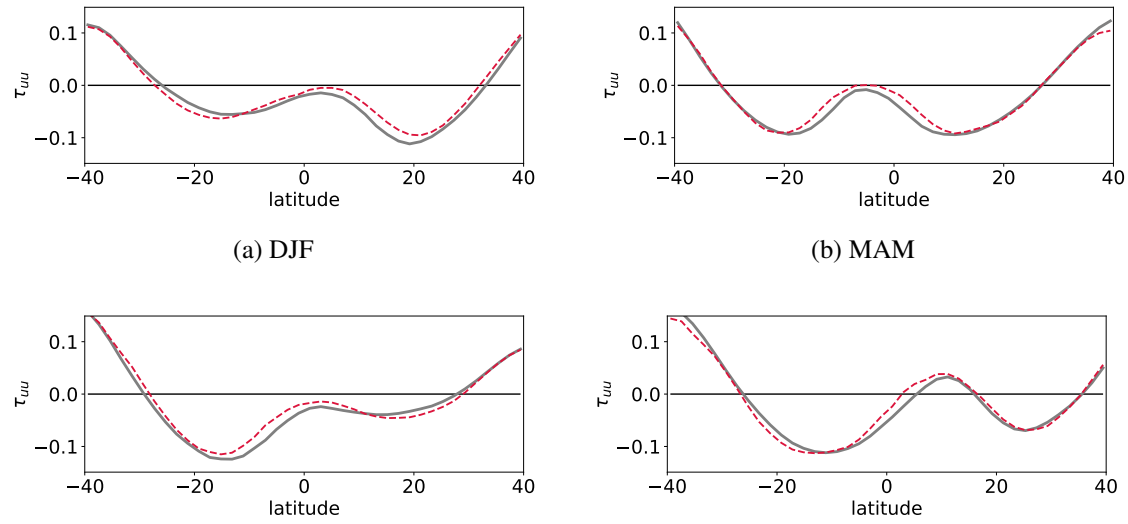

(a) DJF (b) MAM

(c) JJA (d) SON

Figure 4.1: Displayed is the easterly surface stress τ_u from the model output (solid grey) and from calculations (dashed red) for the seasons (a) December, January, February (DJF), (b) March, April, May (MAM), (c) June, July and August (JJA) and (d) September, October, November (SON). The dashed red line stands for median of all simulations for which τ_u was also available (cf. Table 4.3).

4.2.3 The Local Rossby Number *Ro*

The local Rossby number *Ro* is defined as in Equation 4.4.

$$Ro = -\frac{[\bar{\zeta}]}{f} \tag{4.4}$$

Ro is the negative ratio of the zonally averaged relative vorticity $[\bar{\zeta}]$ and the Coriolis parameter $f = 2\sin\phi\Omega$. But this does not explain the meaning it holds in the upper branch of the Hadley cell. To understand this, the Equation 4.2 is rewritten. To yield a meaningful momentum balance, we assume steady state $\partial u/\partial t = 0$. Using the continuity equation, the momentum flux divergence by the mean meridional circulation simplifies to the advection of relative vorticity (Eq. 4.5).

$$\left[\frac{1}{a\cos^2\phi}\frac{\partial([\bar{u}][\bar{v}]\cos^2\phi)}{\partial\phi} + \frac{\partial[\bar{u}][\bar{\omega}]}{\partial p}\right] = [\bar{\zeta}][\bar{v}] \tag{4.5}$$

Furthermore, all terms that are connected to eddy momentum flux divergence are summerized under **E** (Eq. 4.6).

$$\mathbf{E} = \left[\frac{1}{a\cos^2\phi}\frac{\partial(([\bar{u}^*\bar{v}^*] + [\overline{u'v'}])\cos^2\phi)}{\partial\phi} + \frac{\partial([\bar{u}^*\bar{\omega}^*] + [\overline{u'\omega'}])}{\partial p}\right] \tag{4.6}$$

This is how the easy to read Equation 4.7 is found.

$$(f + [\bar{\zeta}])[\bar{v}] = -\mathbf{E} \tag{4.7}$$

In this form, the meridional advection of absolute vorticity $f + \zeta$ is balanced by divergence of eddy momentum transport **E**. The absolute vorticity is the sum of the Coriolis parameter f and the relative vorticity ζ.

Now, the definition of the local Rossby number *Ro* (Eq. 4.4) is used to replace the sum of absolute vorticity in Equation 4.7. This yields a zonal momentum balance in the form of Equation 4.8.

$$f(1 - Ro)[\bar{v}] = -\mathbf{E} \tag{4.8}$$

In this context (Eq. 4.8), *Ro* describes how closely the meridional advection of momentum is coupled to the divergence of eddy momentum transport. Hence, it is a measure of the influence of eddies on the Hadley circulation (Bordoni and Schneider, 2008). In case of $Ro \to 0$, the meridional advection of momentum is entirely due to eddies. Opposed to this, the meridional advection of momentum is decoupled from eddies in case of $Ro \to 1$. Another way to view the meaning of the local Rossby number is that the absolute angular momentum is correlated to the meridional gradient of angular momentum $f + \zeta = -(a^2\cos\phi)^{-1}\partial_\phi M$ in which M denotes the angular momentum. Hence, for $Ro \to 1$ the gradient of angular momentum must be small (Schneider, 2006).

The local Rossby number can be $Ro \geq 0.9$ in the upper branch of the strong winter Hadley cell for models without macro turbulence, but only $Ro \geq 0.7$ and $Ro \geq 0.5$ in the weaker equinoctial and the summer cell, respectively. If marcoturbulence is permitted in the simulations, the local Rossby number can be as small as $Ro \approx 0.1$ on the poleward edge of the Hadley cell. In this case,

$Ro \geq 0.5$ in the winter cell and $Ro \geq 0.3$ for the summer and the equinocturnal cell (Schneider, 2006).

In this thesis, the values given for the Ro are its maxima in the upper branch of the respective Hadley cell (400 hPa to 150 hPa). The border between the Hadley cells and the poleward borders in the Southern and Northern Hemisphere serve as latitudinal limits of the upper branch of the Hadley cell. The calculations are unstable close to the equator because $f \to 0$. Hence, values between 5° S/N are deleted.

4.2.4 The Decomposition of the Mass Streamfunction

For equations that have the form of the zonally averaged continuity equation of an incompressible fluid (cf. Eq. 2.39), a stream function can be found (Peixoto and Oort, 1992) in the form of Equation 2.40). The mass streamfunction Ψ (Eq. 4.9) gives the northward transport of mass through the area $2\pi a \Delta p$ per second. a is the radius of the Earth, Δp is the thickness of the pressure layer. g is the gravitational acceleration, $[\bar{v}]$ is the zonally averaged northward wind.

$$\Psi = \frac{2\pi a \cos\phi}{g} \int_p^{p_s} [\bar{v}] dp \tag{4.9}$$

Bordoni and Schneider (2008) propose that the meridional wind $[\bar{v}]$ in Eq. 4.9 can be replaced by an expression from the momentum budget. For this, the decomposed zonal momentum balance in the upper branch of the Hadley cell (Eq. 4.2) in a steady state $\frac{\partial [\bar{u}]}{\partial t} = 0$ (Eq. 4.10) is used in this thesis.

$$\begin{aligned} f[\bar{v}] = &- \left[\frac{1}{a\cos^2\phi} \frac{\partial([\bar{u}][\bar{v}]\cos^2\phi)}{\partial\phi} + \frac{\partial[\bar{u}][\bar{\omega}]}{\partial p} \right] \\ &- \left[\frac{1}{a\cos^2\phi} \frac{\partial(([\bar{u}^*\bar{v}^*] + [\overline{u'v'}])\cos^2\phi)}{\partial\phi} + \frac{\partial([\bar{u}^*\bar{\omega}^*] + [\overline{u'\omega'}])}{\partial p} \right] \end{aligned} \tag{4.10}$$

Bordoni and Schneider (2008) further group the decomposition in the divergence of momentum transport by the mean meridional circulation $\mathbf{M}$ (Eq. 4.11) and the divergence of eddy momentum transport $\mathbf{E}$ (Eq. 4.12). In first instance, this is done for the meridional momentum budget only. Later, the influence of vertical momentum on the Hadley cell is investigated separately (Section 4.2.6 and Section 6.5.2).

$$\mathbf{M} = -\frac{1}{a\cos^2\phi} \frac{\partial([\bar{u}][\bar{v}]\cos^2\phi)}{\partial\phi} \tag{4.11}$$

$$\mathbf{E} = -\frac{1}{a\cos^2\phi} \frac{\partial(([\bar{u}^*\bar{v}^*] + [\overline{u'v'}])\cos^2\phi)}{\partial\phi} \tag{4.12}$$

Thus, a decomposition of the mass streamfunction in the form of Equation 4.13 can be defined.

$$\Psi = \Psi_M + \Psi_E \tag{4.13}$$

The streamfunction of the mass transport by the mean meridional circulation is denoted as Ψ_M (Eq. 4.14) and the streamfunction of the mass transport by eddies is denoted as Ψ_E (Eq. 4.15).

$$\Psi_M = \frac{2\pi a \cos\phi}{fg} \int_p^{p_s} \frac{1}{a\cos^2\phi} \frac{\partial([\bar{u}][\bar{v}]\cos^2\phi)}{\partial\phi} dp \tag{4.14}$$

$$\Psi_E = \frac{2\pi a \cos\phi}{fg} \int_p^{p_s} \frac{1}{a\cos^2\phi} \frac{\partial(([\bar{u}^*\bar{v}^*] + [\overline{u'v'}])\cos^2\phi)}{\partial\phi} dp \tag{4.15}$$

The variables have their usual meaning: ϕ is the latitude, u the eastward wind, v the northward wind, $f = 2\Omega\sin\phi$ is the Coriolis parameter that includes the angular velocity of the Earth Ω and a its radius. For the notations of bars and brackets see Section 2.5.

For this analysis, the results from the calculation following Section 4.2.2 are used that are presented in Section 6.2 and Section 6.3. The results from this analysis can be found in Section 6.5. The calculations are unstable close to the equator because $f \to 0$. Hence, values between 5° S/N are deleted. Also, a maximum of the mass streamfunction has to be found outside of 5° S/N to take the composition from this location. This is also the reason why the maximum of the mass streamfunctions strength presented in Chapter 5 may deviated from those in Section 6.5.

Furthermore, an index Ind_Ψ is defined that is similar to Ro.

$$Ind_\Psi = \frac{\Psi_M}{\Psi_M + \Psi_E} \tag{4.16}$$

Ind_Ψ compares the mass streamfunction driven by the mean flow with total mass streamfunction from the decomposition. The values used for this index is retrieved from the maximum of the mass streamfunction outside of 5° S/N for each month and each model. In Section 6.4.1 and Section 6.5.1 the influence of the time tendency $\Psi_{\frac{\partial u}{\partial t}}$ and the vertical momentum flux divergence $\mathbf{V}$ on the decomposition is investigated. As a consequence, Ψ_M and Ψ_E include the vertical momentum flux divergence by the mean circulation $\mathbf{V_M}$ and by eddies $\mathbf{V_E}$ as defined in Section 4.2.6 of this Chapter.

4.2.5 Investigating the Influence of the Time Tendency

The local Rossby number Ro in the zonal momentum balance (cf. Eq. 4.8) and the definition of the decomposition of the mass streamfunction (cf. Eq. 4.15 and Eq. 4.14) assume a steady state, in which the time tendency vanishes $\partial u/\partial t = 0$. This assumption is correct in the annual mean, but it can be inadequate for seasonal and monthly means for which quantities in this thesis are calculated. Therefore, the influence of the momentum time tendency $\frac{\partial[\bar{u}]}{\partial t}$ is investigated in Section 6.4.1 using the methods of the section. For this, the definition of the local Rossby number (Eq. 4.4) and decomposition of the mass streamfunction (Eq. 4.13) are expanded to include an expression of time tendency.

To find a local Rossby number corrected by the time tendency $R_{\frac{\partial u}{\partial t}}$, the decomposed zonal momentum balance (Eq. 4.2) is rewritten as the decomposed zonal momentum balance in steady state (Eq. 4.10) in Section 4.2.3. A similar equation can be defined without assuming steady state (Eq. 4.17).

$$\frac{\partial[\bar{u}]}{\partial t} + (f+\zeta)[\bar{v}] = \mathbf{E} \tag{4.17}$$

Furthermore, the definition of *Ro* (Eq. 4.4) is inserted in Equation 4.17. This yields the Equation 4.18.

$$f[\bar{v}](1-(Ro-\frac{1}{f[\bar{v}]}\frac{\partial u}{\partial t})=\mathbf{E} \tag{4.18}$$

Now it is possible to define a local Rossby number corrected by the time tendency $R_{\frac{\partial u}{\partial t}}$ as in Equation 4.19.

$$R_{\frac{\partial u}{\partial t}}=Ro-\frac{1}{f[\bar{v}]}\frac{\partial u}{\partial t} \tag{4.19}$$

In this form, it is possible to discuss the local Rossby number *Ro* directly against the influence of the time tendency on this quantity $-\frac{1}{f[\bar{v}]}\frac{\partial u}{\partial t}$. This is done in Section 6.4.1.

The decomposed zonal momentum balance (Eq. 4.2) can be written as Equation 4.20.

$$f[\bar{v}]=\mathbf{M}+\mathbf{E}-\frac{\partial[\bar{u}]}{\partial t} \tag{4.20}$$

Analogous to Section 4.2.4, an expression is formulated to described the mass streamfunction due to the time tendency (Eq. 4.21). Equation 4.21, Equation 4.15 and Equation 4.14 should add up to the total strength of the mass streamfunction.

$$\Psi_{\frac{\partial u}{\partial t}}=-\frac{2\pi a\cos\phi}{fg}\int_p^{p_s}\frac{\partial u}{\partial t}dp \tag{4.21}$$

The values of $\Psi_{\frac{\partial u}{\partial t}}$ displayed in Section 6.4.1 are taken at the maximum of the mass streamfunction outside of 5° S/N as Ψ_M, Ψ_E and $\Psi_{\mathbf{V}}$.

To calculate the time tendency $\frac{\partial u}{\partial t}$ the difference of the first u_{first} and last day of a month u_{last} is divided by the time (Eq. 4.22). The time is the number of day the respective month N_{days} multiplied by the seconds of one day $N_{\text{sec}}=86400$. The number of days of one month varies among models because they use different calendars. Hence, a year in a model can have 360, 365 or 366 days and month can have $N_{\text{days}}=28$ to $N_{\text{days}}=31$.

$$\frac{\partial u}{\partial t}=\frac{u_{\text{first}}-u_{\text{last}}}{N_{\text{sec}}N_{\text{days}}} \tag{4.22}$$

4.2.6 Investigating the Influence of Vertical Momentum Transport

In Section 6.5.2, the assumption that the vertical momentum transport does not have a large influence on the maximum strength of the Hadley cell is investigated. For this the zonal vertical momentum transport $[u\omega]$ and divergence of the vertical momentum transport $\mathbf{V}$ (Eq. 4.23) is calculated for each month of the year. The vertical velocity in the pressure system is ω and p is the pressure.

$$\mathbf{V}=-\frac{\partial[\overline{u\omega}]}{\partial p} \tag{4.23}$$

Furthermore, $\mathbf{V}$ can be included in the decomposition of the mass streamfunction. For this, the decomposed zonal momentum balance (Eq. 4.10) is amended to include the vertical momentum transport following Peixoto and Oort (1992). The resulting sum (Eq. 4.24 is used to define a

streamfunction of mass transport driven by vertical momentum transport $\Psi_{\mathbf{V}}$ (Eq. 4.25) that adds up with $\Psi_{\mathbf{M}}$ and $\Psi_{\mathbf{E}}$ to the total mass streamfunction Ψ.

$$f[\bar{v}] = \mathbf{M} + \mathbf{E} + \mathbf{V} \tag{4.24}$$

$$\Psi_{\mathbf{V}} = -\frac{2\pi a \cos\phi}{fg} \int_{p}^{p_s} \frac{\partial \overline{[u\omega]}}{\partial p} dp \tag{4.25}$$

The values displayed in Section 6.5.2 are taken at the maximum of the mass streamfunction outside of 5° S/N as Ψ_M, Ψ_E and $\Psi_{\frac{\partial u}{\partial t}}$.

5 Mass Transport of the Hadley Cell in TRACMIP AquaControl

5.1 Mass Transport in the Annual Mean

The mass streamfunction describes the northward transport of air mass above a given level and latitude (cf. Section 4.2.4). It quantifies the strength of the zonally averaged Hadley cell. In the upper branch of the Northern Hemisphere Hadley cell, the mass is transported northward in the upper troposphere. Hence, the mass streamfunction is positive. Accordingly, the mass streamfunction of the Southern Hemisphere Hadley cell is negative. The Hadley cells of both hemispheres are situated in the tropics. On the annual mean, they border on each other in vicinity to the equator, at 7° N in the model median (Figure 5.1). The shift off the equator is linked to the q-flux implemented through the slab ocean of the TRACMIP set-up (cf. Chapter 4). The border between the Hadley cell of each hemisphere is shifted toward the Northern Hemisphere in every model (Table 5.1, column ITCZ). Moreover, the border is farther north than the ITCZ calculated based on the precipitation centeroid (Voigt et al., 2016).

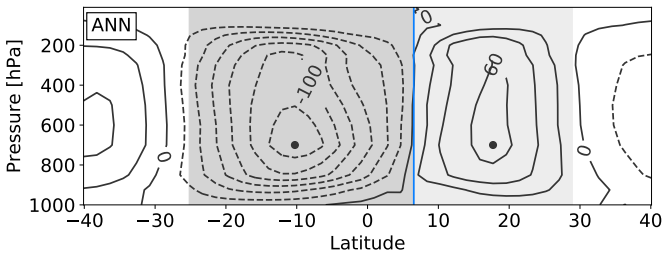

Figure 5.1: Displayed is the model median of the annual mean mass steamfunction (contour steps $20 \times 10^9\,\mathrm{kg\,s^{-1}}$). Solid and dashed contours represent positive and negative values, respectively. The grey areas mark the latitudinal extent of the Hadley cells according to the definition from Schneider (2006) in which the poleward edge is defined as the latitude of 10% of the maximum strength.

The poleward extent of the Hadley cell is defined as that latitude at which the mass streamfunction has only 10% of its maximum strength (Schneider, 2006). The poleward extent of the Hadley cell is mostly defined by the geometry and the angular velocity of the Earth. To some extent, the pole to equator temperature difference (Held and Hou, 1980; Levine and Schneider, 2015) also plays a role in width and placement of the Hadley cell. It emerges that the poleward borders of the Hadley cell are expected to be similar among models, because the geometry and angular velocity of the Earth is prescribed and constant. Furthermore, the equator to pole temperature difference is expected to be similar among models, since the radiative input into the models is the same. The data set precisely displays these assumptions. Even though the strength of the Hadley cell differs between the hemispheres, the poleward borders are similar. The Southern Hemisphere Hadley

Table 5.1: Annual mean Hadley cell extent and strength of the model ensemble

Model	SH Max Strength	NH Max Strength	SH boundary	ITCZ[1]	NH boundary
Median	**-129.48**	**71.95**	**-27**	**7**	**29**
CALTECH	-52.43	42.13	-25	7	25
CAM 3	-120.84	63.93	-27	7	27
CAM 4	-128.99	71.95	-29	7	31
CNRM-AM5	-110.17	75.23	-27	5	27
ECHAM 6.1	-154.62	73.39	-27	10	29
ECHAM 6.3	-145.87	83.46	-27	8	29
LMDZ5A	-158.49	99.20	-25	7	27
MetUM-CTL	-142.93	62.05	-27	10	29
MetUM-ENT	-153.11	66.12	-27	10	29
MIROC 5	-129.48	81.30	-27	5	27
MPAS	-104.19	60.69	-29	7	29

cell terminates at 27° S (+/- 2°) and the Northern Hemisphere Hadley cell at 29° N (+/- 2°) (cf. Table 5.1).

The Northern Hemisphere Hadley cell is markedly smaller in the latitudinal extent than the Southern Hemisphere Hadley cell. It is also a lot weaker than its counterpart in the Southern Hemisphere. Its maximum strength only accounts for about 55% of the Southern Hemisphere maximum strength in the model median. The difference in strength is more pronounced in models in which the border between the Hadley cell is situated farther in the Northern Hemisphere. The simple physics used in CALTECH show a stunning effect on the strength of the Hadley circulation. Even if the extent of the Hadley cell is only slightly smaller than in the other models, the maximum strength of the Southern Hemisphere Hadley cell is only about half as strong as in MPAS, which simulates the second weakest Southern Hemisphere Hadley cell of the ensemble. Furthermore, the Northern Hemisphere Hadley cell accounts for about 80% of the Southern Hemisphere Hadley cell strength. In short, CALTECH produces the weakest Hadley circulation with the smallest extent of the ensemble, but the difference in maximum strength between the Hadley cells of the hemispheres is the smallest.

The modified convection scheme in MetUM-ENT appears to slightly intensify the circulation in comparison with MetUM-CTL. Both models show a stark discrepancy between the maximum strength of the Southern and the Northern Hemisphere Hadley cell (45% of the strength). The model spread of the maximum Hadley cell strength is considerable, regardless of the hemisphere.

The annual mean of the TRACMIP AquaControl ensemble shows robust results as concerns the extent of the Hadley cell and the border between the circulation of both hemispheres. The maximum of the Hadley cell strength is a less reliable quantity. The model spread is considerable, regardless of the hemisphere, ranging from $-52\,\mathrm{kg\,s^{-1}}$ to $-158\,\mathrm{kg\,s^{-1}}$ in the Southern Hemisphere and from $42\,\mathrm{kg\,s^{-1}}$ to $99\,\mathrm{kg\,s^{-1}}$ in the Northern Hemisphere. The simulations solely

[1] In this case the ITCZ stands for the common boundary of the two Hadley cells in the deep tropics.

agree on the fact that the Southern Hemisphere Hadley cell is stronger than the Northern Hemisphere Hadley cell. However, they do not agree on how much weaker the Northern Hemisphere should be, ranging between 42% and 80% of the strength of the Southern Hemisphere Hadley cell.

5.2 The Seasonal Cycle of Mass Transport

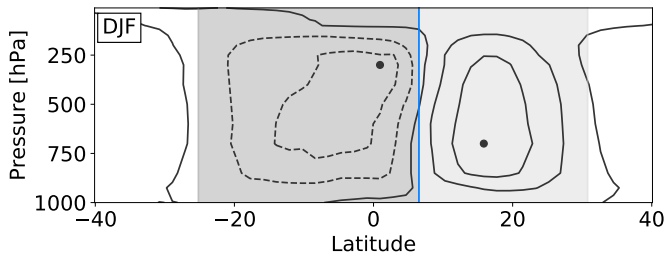

(a) DJF

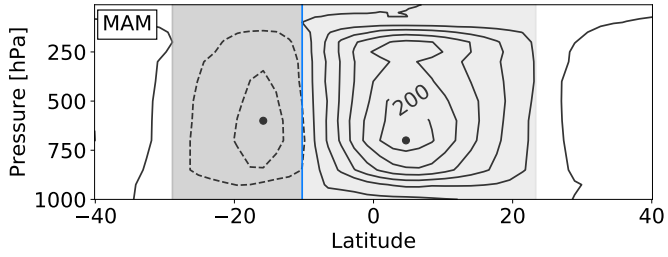

(b) MAM

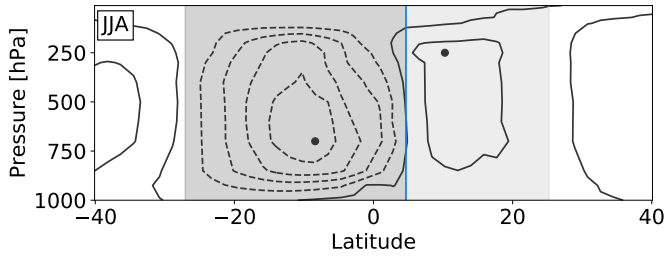

(c) JJA

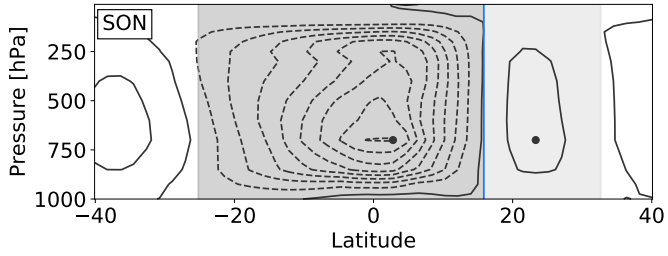

(d) SON

Figure 5.2: Displayed is the model median mass steamfunction (contour steps $40 \times 10^9\,\mathrm{kg\,s^{-1}}$) for the seasons (a) DJF (December, November, January), (b) MAM (March, April, May), (c) JJA (June, July, August), (d) SON (September, October, November). Solid and dashed contours represent positive and negative values, respectively. The grey areas mark the latitudinal extent of the Hadley cells according to the definition from Schneider (2006) in which the poleward edge is defined as the latitude of 10% of the maximum strength.

In TRACMIP AquaControl, the atmospheric response to temperature forcing is delayed due to the implementation of a slab ocean (Donohoe et al., 2014). In today's climate, the mass streamfunction peaks in JJA (June, July and August) and DJF (December, January and February) in the Southern and the Northern Hemisphere Hadley cell respectively. This peak is accompanied by a shift of their common border off the equator far into the summer hemisphere. The winter hemisphere Hadley cell transports energy into the low-energy winter hemisphere to balance the energy budget of the Earth. Due to the delay caused by the slab ocean, the seasons SON (September, October and November) and MAM (March, April and May) in TRACMIP resemble the seasons JJA and DJF of today's climate.

The common border of the Hadley cells migrates from 8° S in MAM (Figure 5.2b) to 16° N SON (Figure 5.2d). Meanwhile, the edges of the respective Hadley cells move very little in comparison: $\Delta 4°$ in the Southern Hemisphere and $\Delta 8°$ in the Northern Hemisphere (Figure 5.2). The migration of the common border is accompanied by massive changes in the strength of the mass streamfunction. The mass transport of the Northern Hemisphere Hadley cell strengthens in DJF and peaks in MAM when the border between the Hadley cells is farthest South. The Hadley circulation in the Northern Hemisphere weakens in JJA. Its mass streamfunction maximum only amounts to a quarter of its maximum in the previous season and the values remain low in SON. This pattern is analogous for its Southern counterpart. The Southern Hemisphere Hadley cell's mass streamfunction reaches the highest values during SON. More precisely, the Southern Hemisphere Hadley cell is strongest in September (Figure 5.4a) and the Northern Hemisphere Hadley cell is strongest in April (Figure 5.4b). The boxplots in Figure 5.3 give an orientation as to where the maxima of Figure 5.4 are located.

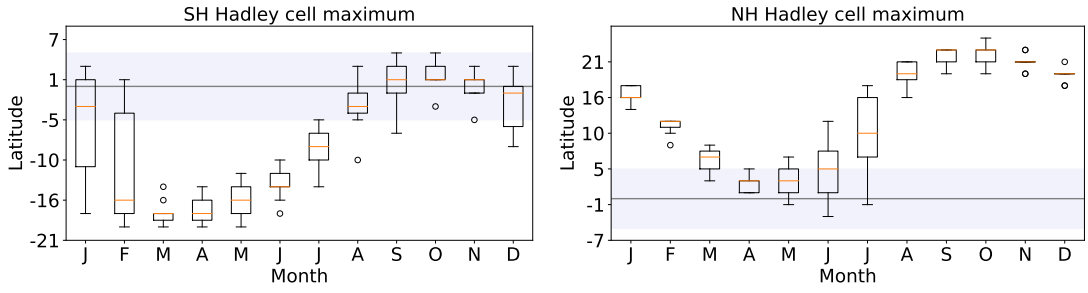

(a) Southern Hemisphere Hadley cell (b) Northern Hemisphere Hadley cell

Figure 5.3: Boxplot of the latitudinal position of the mass streamfunction maximum strength $\phi\Psi_{max}$ for the TRACMIP AquaControl models in the Southern Hemisphere (Fig. 5.3a) and Northern Hemisphere (Fig. 5.3b). The orange line denotes the model median, the box signifies the boundary to the upper and lower quartile, whiskers extent to 1.5 IQR. The circles are the outliers of the ensemble.

The mass streamfunction reaches its absolute peak in September for the Southern Hemisphere Hadley cell. The agreement is weaker in the Northern Hemisphere where some models show an absolute peak in March (CNRM-AM 5) or May (CAM 3 and ECHAM 6.3). While there is high agreement of the seasonal pattern. The absolute values of the mass streamfunction also differ in the seasonal cycle as well as in the annual mean, especially when the Hadley cell is strong. The Southern Hemisphere Hadley cells MIROC 5 and ECHAM 6.1 are about more than $100 \times 10^9\,\mathrm{kg\,s^{-1}}$ stronger than the model median in September and October. These models also

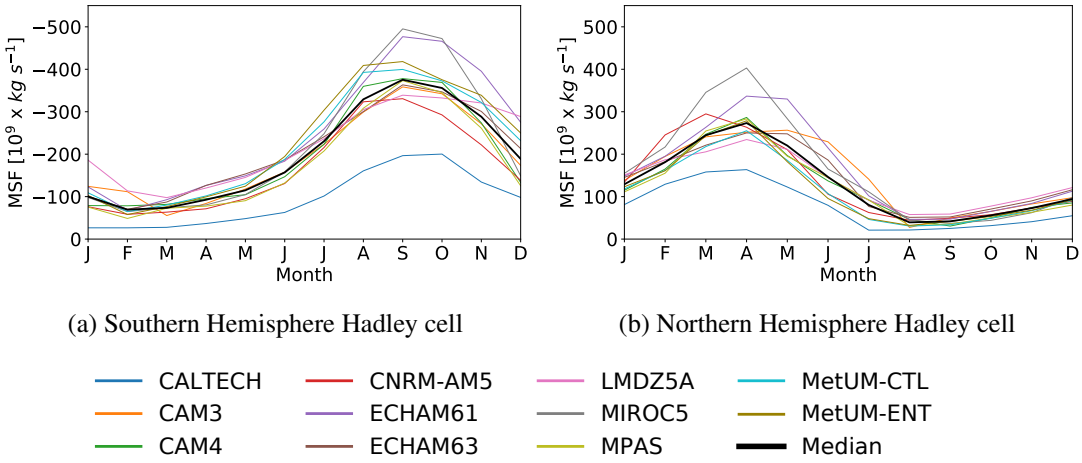

(a) Southern Hemisphere Hadley cell

(b) Northern Hemisphere Hadley cell

Figure 5.4: The evolution of the mass streamfunction maximum strength in the models and their median (Fig. 5.4a) in the Southern Hemisphere and (Fig. 5.4b) Northern Hemisphere throughout the year. The black line denotes the model median, individual simulations are displayed in colors according to the models used.

show a stronger peak of the Northern Hemisphere Hadley cell during MAM. Interestingly, the peak in MIROC 5 is very distinct in the Southern Hemisphere so that the model represents the model median in the annual mean (Table 5.1). For the Southern Hemisphere Hadley cell, the months March to July and August to February for the Northern Hemisphere show reasonable agreement in their mass streamfunction strength.

The seasonal patterns of the Hadley cells' migration show good agreement. These patterns reflect the delayed response, as described by Donohoe et al. (2014). In SON, and most specifically in September, all models simulate the strongest mass streamfunction of the seasonal cycle for the Southern Hemisphere Hadley cell. The agreement among models is not as good for the Northern Hemisphere Hadley cell. In the model median, the mass streamfunction in this hemisphere peaks in April and all models display the maximum strength during MAM. The agreement of the magnitude of the maximum mass streamfunction is good from March to July and August to February for the Southern Hemisphere and the Northern Hemisphere, respectively. But the agreement among models is weaker in months in which the mass transport is strong in both hemispheres. The models ECHAM 6.1 and MIROC 5 exceed the model median in those months dramatically while the maximum mass streamfunction in CALTECH consistently stays below the model median in both hemispheres.

6 The Momentum Budget in TRACMIP

This chapter aims to give an in depth analysis of the momentum budget in TRACMIP AquaControl. From Section 6.1 to Section 6.3, the focus lies on an accurate description of the momentum budget in the data set. This includes a description of the meridional momentum budget in the annual mean and throughout the seasonal cycle in Section 6.2 and Section 6.3. Nonetheless, some of the described quantities aid a better understanding of the influence of eddy momentum transport on the Hadley cell.

In Section 6.4 and Section 6.5, the results for the local Rossby number Ro and the fraction of the mass streamfunction driven by the mean meridional circulation Ind_Ψ as a result of decomposition of the mass streamfunction are presented as two ways to quantify the eddy influence on the Hadley cell in only one number. Therefore, the focus of these two sections is to quantify influence of eddies on the Hadley cell in the annual mean and throughout the seasonal cycle. Furthermore, these sections discuss the model spread of this influence.

6.1 Angular Momentum

The zonally averaged angular momentum (Eq. 2.16) depends on the Earth's angular velocity Ω, the latitude ϕ and the eastward wind u. The Earth's radius is denoted as a. As described in

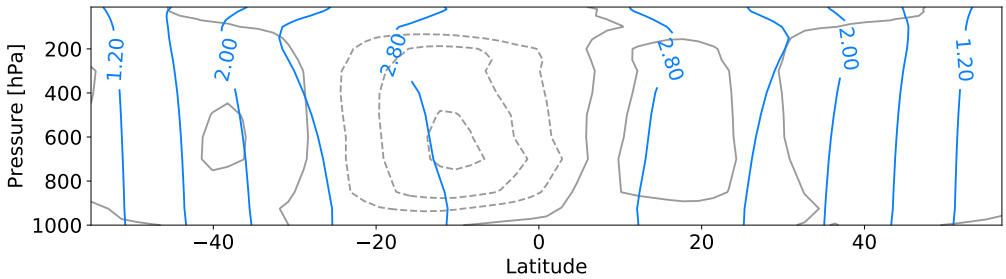

Figure 6.1: TRACMIP AquaControl annual mean model median of angular momentum (blue, contour intervals $0.4 \times 10^9\,\mathrm{kg\,m^2\,s^{-1}}$) and the mass steam function (grey, contour intervals $40 \times 10^9\,\mathrm{kg\,s^{-1}}$). Solid and dashed contours represent positive and negative values, respectively.

Chapter 2, the angular momentum consists of two components: the planetary angular momentum M_Ω (Eq. 2.17) and the relative angular momentum M_R (Eq. 2.18). M_Ω is much larger than the relative angular momentum in today's atmosphere and in TRACMIP AquaControl (Figure 6.1). This mostly stems from the velocity on the Earth's surface which due to the rotation of the Earth $a\cos\phi\Omega$ is much larger than u, at least in the lower latitudes. The latitudinal structure of the angular momentum is proportional to $\cos^2\phi$. Accordingly, the angular momentum maximum of the model median is at the equator and amounts to $3 \times 10^9\,\mathrm{kg\,m^2\,s^{-1}}$ in the annual mean and in every season.

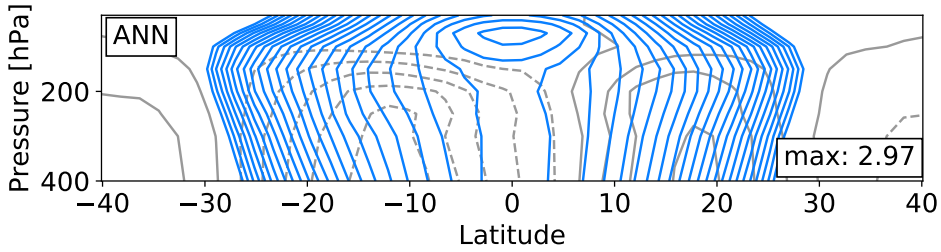

(a) Annual mean

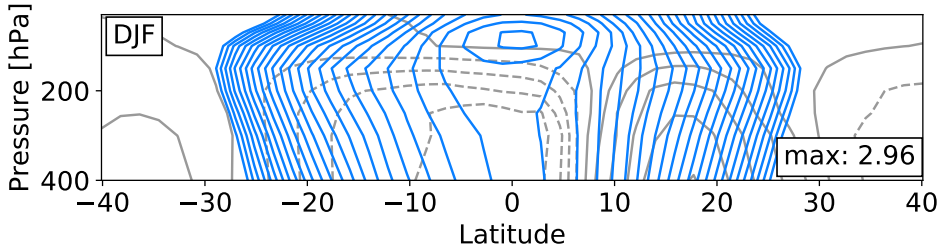

(b) DJF

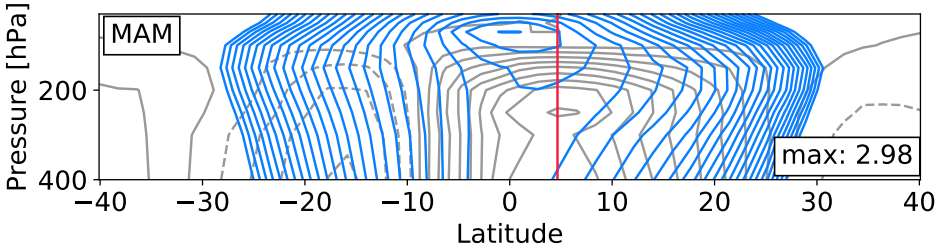

(c) MAM

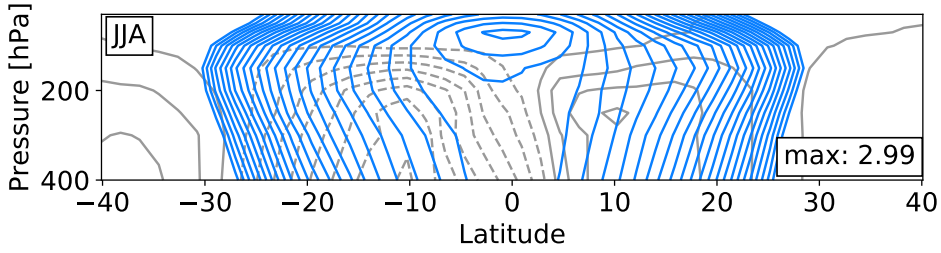

(d) JJA

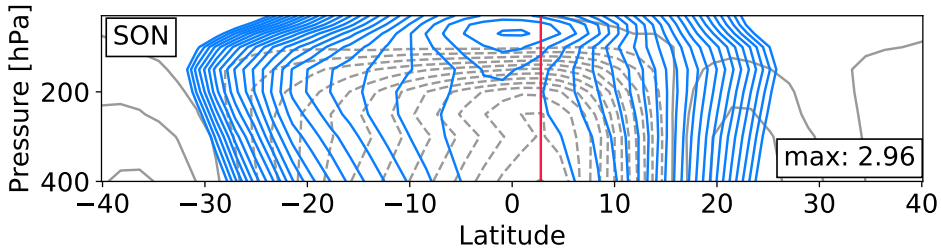

(e) SON

Figure 6.2: TRACMIP AquaControl model median of angular momentum (blue, contour interval $0.01 \times 10^9\,\mathrm{kg\,m^2\,s^{-1}}$) and mass steam function (grey, contour interval $20 \times 10^9\,\mathrm{kg\,s^{-1}}$) of the upper troposphere for (a) the annual mean (ANN) and seasons (b) DJF (December, January, February), (c) MAM (March, April, May), (d) JJA (June, July, August), (e) SON (September, October, November). Solid and dashed contours represent positive and negative values, respectively. The red line denotes the latitude of mass streamfunction's maximum.

Within the energetic framework, angular momentum is assumed to be conserved in the upper branch of the Hadley cell (i.e. between 400 hPa and 150 hPa). The angular momentum conservation implies that angular momentum contours cannot cross streamlines of the mass streamfunction. This condition is not met in today's atmosphere (Schneider, 2006). Even for models which aim at simulating an angular momentum conserving atmosphere, it is hard to attain this pattern (cf. Hill et al. (2019)). In the annual mean, TRACMIP AquaControl does not meet this strict criterion (Figure 6.1 and in detail Figure 6.2a). However, angular momentum is more homogeneous within the Hadley cell than in the mid latitudes. In the upper branch of the Hadley cell, angular momentum contours are bent, indicating that the upper troposphere is approaching a state which is closer to angular momentum conservation.

The planetary angular momentum M_Ω is constant throughout the seasons. Hence, Figure 6.2 zooms in on the upper branch of the Hadley cell and the lower stratosphere where the seasonally varying relative angular momentum M_R has a greater influence.

During the seasonal cycle, the maximum of angular momentum stays at the equator. Its magnitude varies very little throughout the seasons. The angular momentum contours in the upper branch of the Hadley cell are bent in all seasons. This pattern is especially pronounced in SON and MAM above the maximum of mass transport in the Southern and the Northern Hemisphere Hadley cell, respectively. The assumption of angular momentum conservation is plausible in these seasons for the upper branch of the Hadley cell away from the poleward edge.

Figure 6.3 shows the eastward wind in the upper troposphere u_{up} in comparison to the angular momentum conserving wind u_M for the seasons SON and MAM. u_{up} is relatively close to u_M in MAM at the equator and in the tropics of the Northern Hemisphere. This indicates that the influence of eddies is weak during this season in the Northern Hemisphere Hadley cell. On the other hand, u_{up} shows a greater distance from u_M in the Southern Hemisphere Hadley cell in SON, indicating a stronger influence of eddies on the Southern Hemisphere than on the Northern Hemisphere winter cell. However, the model median in both months is still far away from the 10% deviation from u_M that Walker and Schneider (2005) found for u_{up} in these season in the respective hemispheres (Figure 6.3).

Figure 6.2 shows furthermore that the Hide's theorem is not met in TRACMIP AquaControl simulations, as the model median and all models individually show a closed contour of angular momentum away from the boundary (Figure 6.2a and Table 6.1) in the annual mean at the tropopause and in the lower stratosphere. Such closed angular momentum contours can also be found in all seasons of the ensemble median (Figure 6.2b to Figure 6.2e). Due to the viscous term of the momentum budget equation, this requires the downward gradient of momentum to be compensated by upward eddy momentum. This could also explain small variations of angular momentum maximum during the seasons. When the ascending branch of the Hadley cell is beneath the angular momentum maximum, the maximum gets slightly stronger. This angular momentum maximum in the equatorial upper troposphere is also found in observational data (cf. Chapter 2 or Schneider (2006)).

In conclusion, angular momentum is dominated by the planetary component M_Ω. However, angular momentum as a whole is influenced by the Hadley cell, especially during seasons SON and MAM. In these seasons, the upper branch of the Hadley cell apart from its poleward edges can to some extent be regarded as angular momentum conserving. Comparison of the angular

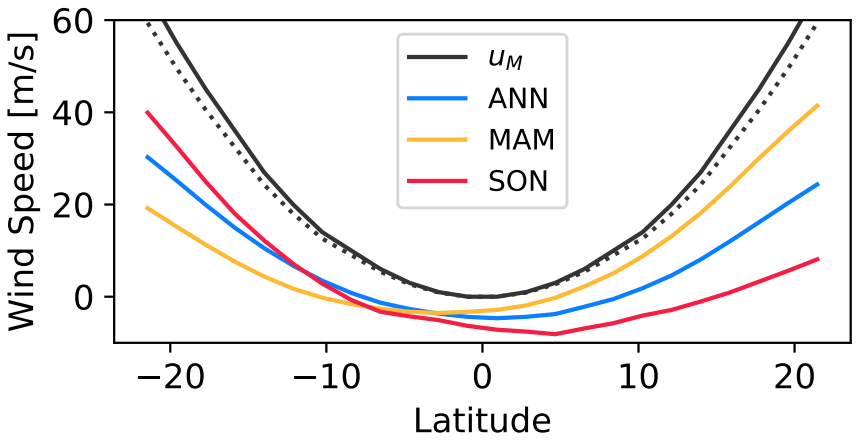

Figure 6.3: Angular momentum conserving wind u_M (black solid) and the 10% deviation that should be characteristic for a winter cell according to Walker and Schneider (2005) (black dotted). The model median eastward wind in the upper troposphere u_{up} (in colors) of TRACMIP AquaControl for the season MAM (March, April, May, boreal winter) and in SON (September, October, November, boreal summer).

Table 6.1: Angular momentum maxima in the upper troposphere and lower stratosphere in the annual mean

Level [hPa]	Model	Maximum [$m^2 s^{-1}$]	Latitude [°]
30	MIROC5	2.97	-1
70	CAM 3	2.97	-1
	ECHAM 6.1	2.97	1
	ECHAM 6.3	2.99	1
	LMDZ5A	3.02	1
	Median	**2.97**	**1**
	MetUM-CTL	3.00	1
	MetUM-ENT	2.99	1
100	MPAS	2.97	-1
	CAM 4	3.00	1
150	CALTECH	2.93	1
	CNRM-AM 5	2.97	-1

momentum conserving wind u_M to the median wind in the upper troposphere u_{up} in the seasons MAM and SON indicates that the winter cell of the Northern Hemisphere is closer to the angular momentum conserving limit than the winter cell of the Southern Hemisphere.

6.2 Meridional Momentum Transport

In the temporal-zonal mean, meridional momentum advection is caused by the divergence of momentum transport, if friction and viscosity are negligible (cf. Chap. 4, Eq. eq:szonmom). In the atmosphere, momentum is transported by the eastward wind u. Since the Hadley cell is a meridional circulation, the eddy decomposition of the meridional momentum transport $[\overline{uv}]$ gives an insight on the predominant modes of transport within the Hadley cell. In accordance with the thermally direct Hadley cell of Held and Hou (1980), momentum transport by mean meridional circulation $\mathbf{M_t} = [\bar{u}][\bar{v}]$ would be assumed to be the only source of momentum transport in the upper branch of the Hadley cell. However, observations show that eddy momentum transport $\left[\overline{u'v'}\right] + \left[\bar{u}^*\bar{v}^*\right]$ exists at least the poleward boundary of the Hadley cell (Dima and Wallace, 2003). Furthermore, there are theoretical considerations about eddy momentum transport's influence on the Hadley cell strength (Walker and Schneider, 2005).

6.2.1 Meridional Momentum Transport in the Annual Mean

Figure 6.4b to Figure 6.4d show the different modes of momentum transport in the temporal-zonal mean that can be obtained by applying the eddy decomposition on the meridional momentum transport $[\overline{uv}]$ of the data set (cf. Chapter 4, Eq. 2.36). In addition to the mean meridional circulation $\mathbf{M_t} = [u][v]$ (Figure 6.4b), the eddy decomposition differentiates between transient $\mathbf{E_t} = \left[\overline{u'v'}\right]$ (Figure 6.4c) and stationary eddy momentum transport $\mathbf{E_s} = \left[\bar{u}^*\bar{v}^*\right]$ (Figure 6.4d) as sources of momentum transport. Since stationary eddies are an order of magnitude smaller, the eddy momentum transport in this thesis is considered to be fully represented by the transient eddy momentum transport $\mathbf{E_t}$. However, the stationary eddy momentum transport $\mathbf{E_s}$ is shortly discussed in context of Figure 6.4.

Strong meridional momentum transport occurs between 20° S and 20° N where the Hadley circulation is strong in the upper branch of the cell and near its surface. This corresponds with the results of the eddy decomposition which identify the momentum transport to be dominated by the mean meridional circulation in these regions.

In the lower branch of the Hadley cell, the maximum momentum transport coincides with the latitude of maximum mass transport (Fig 6.4a). In this region, the direction of momentum transport is uniform for each Hadley cell, because the direction of the mean zonal wind $[\bar{u}]$ due to surface friction is constantly westward. Transient eddy momentum transport $\mathbf{E_t}$ is negligibly small here.

The momentum transport in the upper troposphere is stronger and more difficult to describe. For example, the momentum transport by the mean meridional circulation M_t (Fig 6.4b) changes its direction between the Hadley cells' equatorward border and poleward edges. This is because $\mathbf{M_t}$ consists of the mean northward wind $[\bar{v}]$ and the mean eastward wind $[\bar{u}]$. The direction of $[\bar{v}]$ stays constant in the upper branch of each Hadley cell. But the direction of $[\bar{u}]$ changes from the deep tropics where westward wind prevails[1] to the subtropics with a strong eastward subtropical jet. Hence, the direction of $\mathbf{M_t}$ changes close to the equator from a northward to a southward transport of momentum in the annual mean. $\mathbf{M_t}$ peaks where the mean zonal wind freshens rapidly,

[1] The zonal wind in the upper branch of the Hadley cell adheres to the Hide's theorem in TRACMIP AquaControl, because it stays within the limit set by u_M. Aquaplanet simulations need a seasonal cycle to reproduce this feature correctly even in the upper troposphere close to the equator (Lee, 1999)

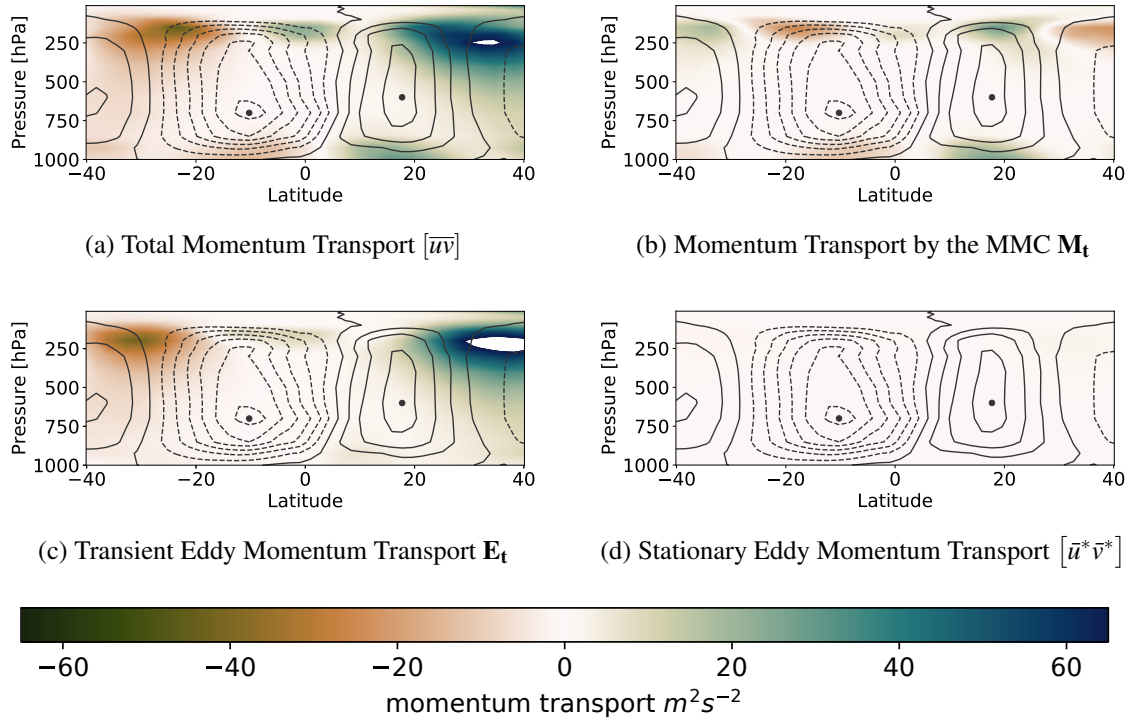

(a) Total Momentum Transport $[\overline{uv}]$

(b) Momentum Transport by the MMC $\mathbf{M_t}$

(c) Transient Eddy Momentum Transport $\mathbf{E_t}$

(d) Stationary Eddy Momentum Transport $\left[\bar{u}^*\bar{v}^*\right]$

Figure 6.4: The model median modes of annual mean meridional momentum transport. Displayed are the zonal mean of the total momentum transport $[\overline{uv}]$ (Fig. 6.4a), the momentum transport by the mean meridional circulation (MMC) $\mathbf{M_t} = [\bar{u}][\bar{v}]$ (Fig. 6.4b), the transient eddy momentum transport $\mathbf{E_t} = \left[\overline{u'v'}\right]$ (Fig. 6.4c) and the stationary eddy momentum transport $\left[\bar{u}^*\bar{v}^*\right]$ (Fig. 6.4d) in $\mathrm{m^2\,s^{-2}}$. Additionally, the respective mass streamfunction (black contours, contour intervals $40 \times 10^9\,\mathrm{kg\,s^{-1}}$) is given for orientation. Solid and dashed contours represent positive and negative values, respectively.

equatorward of the total momentum transport but poleward of the maximum mass transport's latitude (Figure 6.4b in the upper troposphere, Table 6.2). $\mathbf{M_t}$ in the Northern Hemisphere is slightly weaker than in the Ferrel cell of the Southern Hemisphere where it amounts to $27.74\,\mathrm{m^2\,s^{-2}}$.

The peak of $\mathbf{E_t}$ is situated poleward of the Hadley cell edge (Fig. 6.4c). Increased eddy activity is connected to the terminus of the Hadley cell as described in the following: Horizontal transient eddies in the upper troposphere become more frequent, as baroclinic eddies, deep enough to reach the upper troposphere, propagate horizontally from there (Levine and Schneider, 2015). Simultaneously, the Coriolis parameter f increases toward the pole and the near-surface meridional temperature gradient becomes stronger due to weaker Hadley circulation. The Hadley circulation homogenizes the near surface temperature in the tropics. As a result, increasing wave activity towards the poles acts as a terminus for the Hadley circulation. Hence, the extrema of $\mathbf{E_t}$ and the subtropical jets of both hemispheres are collocated (Figure 6.4c and Table 6.2). Extrema of $\mathbf{E_t}$ in both hemispheres are comparable (Table 6.2). Yet the strongest $\mathbf{E_t}$ occurs in the Northern Hemisphere.

The meridional momentum transport $[\overline{uv}]$ in the upper troposphere peaks poleward of $\mathbf{M_t}$ and equatorward of $\mathbf{E_t}$ (Fig, 6.4a) where $\mathbf{M_t}$ and $\mathbf{E_t}$ overlap. There is a local maximum of momentum transport $[\overline{uv}]$ around the equator above the ascending branch of the Southern Hemisphere Hadley cell in the deep tropics. The usual conditions for transient eddy production as stated before are not given in the deep tropics. Hence, it seems unusual that the peak is not only sustained by $\mathbf{M_t}$,

Table 6.2: Transport Modes in TRACMIP AquaControl: Extrema in Both Hemispheres in the Annual Mean

	SH			NH		
	Strength [$m^2 s^{-2}$]	Latitude [° S]	Level [hPa]	Strength [$m^2 s^{-2}$]	Latitude [° N]	Level [hPa]
Total	-61.00	-25	150	50.95	25	150
MMC	-42.96	-20	150	28.32	20	150
Transient	-56.86	35	200	51.73	35	200
Stationary	-1.80	33	200	2.72	31	200

but is also caused by transient eddy transport. The superposition of $\mathbf{E_t}$ creates the distinct local maximum in the meridional momentum transport (cf. Figures 6.4a - 6.4c).

Stationary eddy transport $\left[\bar{u}^*\bar{v}^*\right]$ (Fig. 6.4d) arises from time-constant perturbations of the atmosphere, e.g. land-sea contrast or mountain chains. Since such permanent causes of perturbation do not exist on an aquaplanet, $\left[\bar{u}^*\bar{v}^*\right]$ is the weakest mode of momentum transport (Figure 6.4d). It is one order of magnitude smaller than the other modes of momentum transport. In the model median of the annual mean, stationary eddy transport is strong where transient eddy transport is strong as well: at the equatorward edge of the Southern Hemisphere Hadley cell and within the subtropical jet. Here it reaches its total maximum (Table 6.2).

The meridional momentum transport $[\overline{uv}]$ is strongest between 250 hPa and 150 hPa. In this altitude, the upper branch of the Hadley cells as well as the subtropical jet are located. Furthermore, it is the area in which the influence of $\mathbf{E_t}$ is strongly opposed to the near-surface return flow of the Hadley cell. This is where $\mathbf{E_t}$ influences the strength of the Hadley cell (Walker and Schneider, 2005; Singh et al., 2017). It is also an area of strong mass and energy transport. Therefore, this area is further investigated in the following.

Figure 6.5 shows the vertical average in this pressure range in the model median and for each model of the TRACMIP AquaControl ensemble in the tropics between 40° S and 40° N. This allows an for investigating not only the model median, but the entire model spread.

As stated before, the strongest meridional momentum transport $[\overline{uv}]$ occurs at the poleward edges of the Hadley cell (cf. Figure 6.5a). The deep tropics are dominated by southward transport of negative momentum. Since the southward transport of negative momentum is equivalent to the northward transport of momentum, there is a net northward momentum transport across the equator in the upper branch of the Southern Hemisphere Hadley cell.

In the model median, the meridional momentum transport $[\overline{uv}]$ displayed in Figure 6.5a shows three extrema concordant with Figure 6.4a. There is one distinct minimum at the poleward edge of the Southern Hemisphere Hadley cell (SH), a local maximum around the equator (EQ) and a plateau of momentum transport from the poleward edge of the Northern Hemisphere Hadley cell (NH) to well into the subtropical jet which is weaker than the minimum in the Southern Hemisphere. These features can be found in simulations of all models. However, the peaks' magnitude in CALTECH are a lot and the peaks of MetUM-ENT are somewhat weaker than the median. The momentum transport at the EQ peak has only about 30% of the strength of the other two peaks. This local maximum is very weak in CALTECH, CNRM-AM 5 and MIROC 5. In the Northern Hemisphere, the area of strong momentum transport spans from 23° N to 35° N and does not show a distinct peak. The overall agreement among models is acceptable. Besides deviations

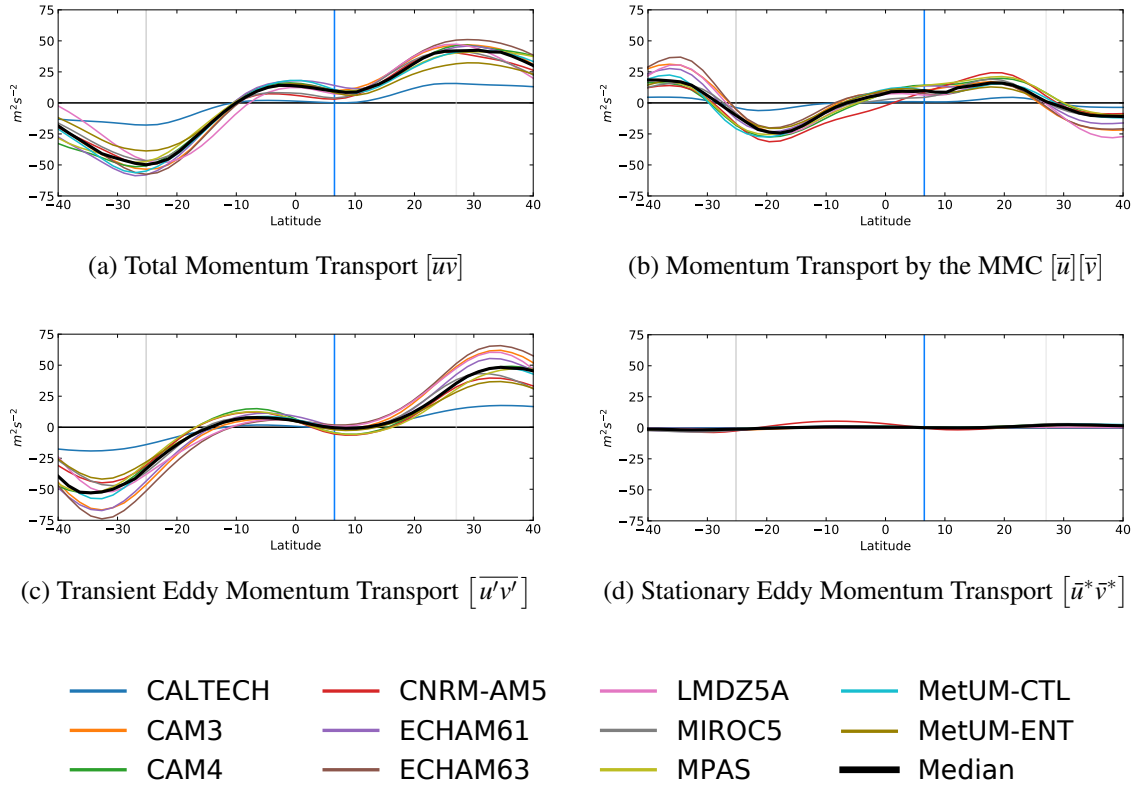

(a) Total Momentum Transport $[\overline{uv}]$

(b) Momentum Transport by the MMC $[\bar{u}][\bar{v}]$

(c) Transient Eddy Momentum Transport $\left[\overline{u'v'}\right]$

(d) Stationary Eddy Momentum Transport $\left[\bar{u}^*\bar{v}^*\right]$

Figure 6.5: The modes of annual mean meridional momentum transport in the tropical upper troposphere. The momentum transport in $m^2\,s^{-2}$ between 250 hPa and 150 hPa is vertically averaged for the zonal mean of the total momentum transport $[\overline{uv}]$ (Fig. 6.5a), the momentum transport by the mean meridional circulation (MMC) $\mathbf{M_t} = [\bar{u}][\bar{v}]$ (Fig. 6.5b), the transient eddy momentum transport $\mathbf{E_t} = \left[\overline{u'v'}\right]$ (Fig. 6.5c) and the stationary eddy momentum transport $\left[\bar{u}^*\bar{v}^*\right]$ (Fig. 6.5d). Bold black lines show the model median and simulations in colors according to the model used. Vertical blue lines represent the latitude of the common boundary of the two Hadley cells in the model median. Vertical grey lines indicate the poleward boundary of the respective Hadley cell in the model median.

in CALTECH, MetUM-ENT stands out as the model with the least momentum transport in the upper branch of the Hadley cell, while ECHAM 6.3 shows the strongest momentum transport in the tropics.

Fig. 6.5b shows the mean meridional circulation $\mathbf{M_t}$ to be the prevalent mode of momentum transport within the Hadley cell, away from its poleward edges. The maximum of $\mathbf{M_t}$ is in the model median in both hemispheres at 18°(+/- 1°) S/N and at 18°(+/- 2°) S/N for all models but CALTECH. Yet in the Northern Hemisphere, the peak is slightly farther to the pole. Here, the peak is weaker in the median, at about $^2/_3$ of the minimum $\mathbf{M_t}$ in the Southern Hemisphere, and in all models. The models with the highest $\mathbf{M_t}$ values is MPAS. In contrast to MPAS, MetUM-CTL shows one of the strongest $\mathbf{M_t}$ in the Southern Hemisphere and a response in the weaker half of the ensemble in the Northern Hemisphere. This is an interesting feature, keeping in mind that they both produce a Northern Hemisphere Hadley cell of very similar strength. Yet MetUM-CTL shows a much stronger Southern Hemisphere Hadley cell. In the CALTECH model, $\mathbf{M_t}$ is very small compared to the other models and peaks poleward of them at 22° S/N. Another surprising fact is that a group of models find very strong $\mathbf{M_t}$ in the Ferrel cell (CAM 3, ECHAM 6.1, ECHAM 6.3,

LMDZ5A). For example, in ECHAM 6.3, $\mathbf{M_t}$ in the Ferrel cell exceeds the same transport in the Hadley cell of the opposite hemisphere. At least in CAM 3, ECHAM 6.1 and ECHAM 6.3, this is accompanied by strong $\mathbf{E_t}$ in the subtropics.

The equatorial domain (EQ) is dominated by positive $\mathbf{M_t}$ in all models but CNRM-AM 5 and MIROC 5. In these models, only positive transient eddy momentum $\mathbf{E_t}$ contributes to the northward momentum transport at the equator (cf. Fig. 6.5c). The $\mathbf{M_t}$ peaks somewhere between 5° N and 10° N in this domain and amounts to 1/4 to 1/2 of $\mathbf{M_t}$ in the Southern Hemisphere Hadley cell, depending on the model. This feature is associated with the stronger cross-equatorial Southern Hemisphere Hadley cell which imposes southward wind above the equator in the annual mean. In an atmosphere in which both Hadley cells are equally strong and therefore the border between the mass stream function would be located at the equator, such a transport would not exist.

$\mathbf{E_t}$ changes its sign between the latitude of maximum mass transport and the latitude of the maximum $\mathbf{M_t}$ in all models (Fig. 6.5c). From there on, it increases rapidly and reaches an extremum outside of the respective Hadley cell. Even though the models' solutions diverge markedly as $\mathbf{E_t}$ grows stronger, it is possible to draw some general observations from the model ensemble. $\mathbf{E_t}$-extrema exceed the extrema of both the total momentum transport and $\mathbf{M_t}$. This is especially true for ECHAM 6.1, ECHAM 6.3 and CAM 3 which show the largest contribution from $\mathbf{E_t}$ and for the Northern Hemisphere in which the Hadley cell is weaker for all models. There is also a northward momentum transport within the equatorial domain which is small but robust among models. The stationary eddies are very small in all models. CNRM-AM 5 stands apart from the other models in this regard. In this model, the contribution of stationary eddies is also small but four to five times larger than in the rest of the ensemble, especially within the winter Hadley cell in MAM and SON.

In summary, both the mean meridional circulation momentum $\mathbf{M_t}$ and the transient eddy momentum $\mathbf{E_t}$ contribute to the total momentum transport in the annual mean in the TRACMIP AquaControl ensemble. Stationary eddies are negligible, as expected in an aquaplanet set-up, except for CNRM-AM 5 where it shows a slight amplitude well below $10\,\mathrm{m^2\,s^{-2}}$ between 20° S and the equator. The influence of each component, $\mathbf{M_t}$ and $\mathbf{E_t}$, depends on latitude and altitude. While they counteract each other at the latitude of maximum mass stream function in all models but CALTECH, they aid each other at the maximum of the total momentum transport. Different solutions of these two momentum quantities in the different simulations cancel each other out in the upper troposphere. Therefore, the agreement among models in the total meridional momentum transport $[\overline{uv}]$ in the upper troposphere is good.

6.2.2 The Seasonal Cycle of Meridional Momentum Transport

In the season cycle, the thermal forcing of the Hadley cell fluctuates substantially. In response to this, not only the mass transport varies (cf. Chapter 5) but also the momentum transport. This section describes these resulting variantions the in momentum transport.

Figure 6.6 shows the model median of the meridional momentum transport $[\overline{uv}]$ (column Total) and its components $\mathbf{M_t}$ (column MMC) and $\mathbf{E_t}$ (column Transient) for each season (DFJ, MAM, JJA, SON). In this context, first the seasonal cycle of the model median Southern Hemisphere Hadley cell is described as an example for the whole ensemble. Secondly, the differences in the

seasonal cycle of the Northern Hemisphere Hadley cell are stated. Finally, some generalizations are made based on the seasonal cycle. Figure 6.7 is used to describe the model spread in the upper troposphere. In connection with this figure, the seasonal cycle of the three peaks of momentum transport identified in Subsection 6.2.1 are discussed. This figure also allows to further observe the model spread.

To facilitate a deeper understanding of momentum transport's role in the seasonal migration of the Hadley cell, seasonal variations of the Southern Hemisphere momentum transport in the model median (Figure 6.6) are exemplary described in the following: The seasonal cycle of the Southern Hemisphere Hadley cell begins in MAM. In this season, due to the simulations' temporary delay, it is summer in the Southern Hemisphere. The zonal mean momentum transport $\mathbf{M_t}$ is at its weakest point in the seasonal cycle, both near the surface and in the upper troposphere (Figure 6.6, Column MMC, row MAM). On the other hand, transient eddy momentum transport $\mathbf{E_t}$ is strong south of the poleward edge of the Hadley cell. Moreover, $\mathbf{E_t}$ is the stronger mode of transport in the upper branch of the Southern Hemisphere Hadley cell. This corresponds well with the overall picture that the summer cell is dominated by eddies (Schneider, 2006; Bordoni and Schneider, 2008).

From MAM to JJA, $\mathbf{M_t}$ strengthens in the Southern Hemisphere Hadley cell, as the Northern Hemisphere Hadley cell retreats polewards. $\mathbf{M_t}$ transports momentum southward, both near the surface and in the upper troposphere. $\mathbf{E_t}$ reaches its maximum in the seasonal cycle at the equatorward edge of the Southern Hemisphere Ferrel cell. At the same time, the influence of $\mathbf{E_t}$ on momentum transport in the upper branch of the Hadley cell declines. Now, it only reaches the poleward edge of the upper branch instead of dominating the entire upper branch as in MAM.

SON is the winter season in the Southern Hemisphere. Balancing the global energy budget, the winter cell transports energy from the summer to the winter hemisphere. The common border of the Hadley cells shifts northward far off the equator (cf. Chapter 5). The near surface southward $\mathbf{M_t}$ strengthens further. But in the upper branch of the Hadley cell, the $\mathbf{M_t}$ is now split into two sections like in the annual mean but more extreme. One part of the Southern Hemisphere Hadley cell is right above the equator and transports momentum northward because it is now under the influence of the equatorial westward wind in the upper troposphere. Away from the deep tropics, it transports momentum southward like in JJA. Poleward of the Hadley cell, $\mathbf{E_t}$ weakens. Nevertheless, a northward $\mathbf{E_t}$ develops in the upper branch of the Hadley cell. In consequence, the upper branch in SON transports momentum rather northward than southward, unlike in JJA (Figure 6.6, Column TOTAL, row SON).

In DJF, the equatorial edge of the Southern Hemisphere Hadley cell migrates southward. $\mathbf{M_t}$ declines rapidly from SON to DJF. $\mathbf{M_t}$ in the upper branch of the Hadley cell is still split in the two parts. Mostly, because the southward meridional wind across the equator is still strong in the upper troposphere. Additionally, there is a weak northward $\mathbf{E_t}$ component. Poleward of the Hadley cell, $\mathbf{E_t}$ drops to its minimum in the seasonal cycle. From DJF to MAM, $\mathbf{M_t}$ decreases to its lowest point in the seasonal cycle, while $\mathbf{E_t}$ increases at the poleward edge of the Hadley cell.

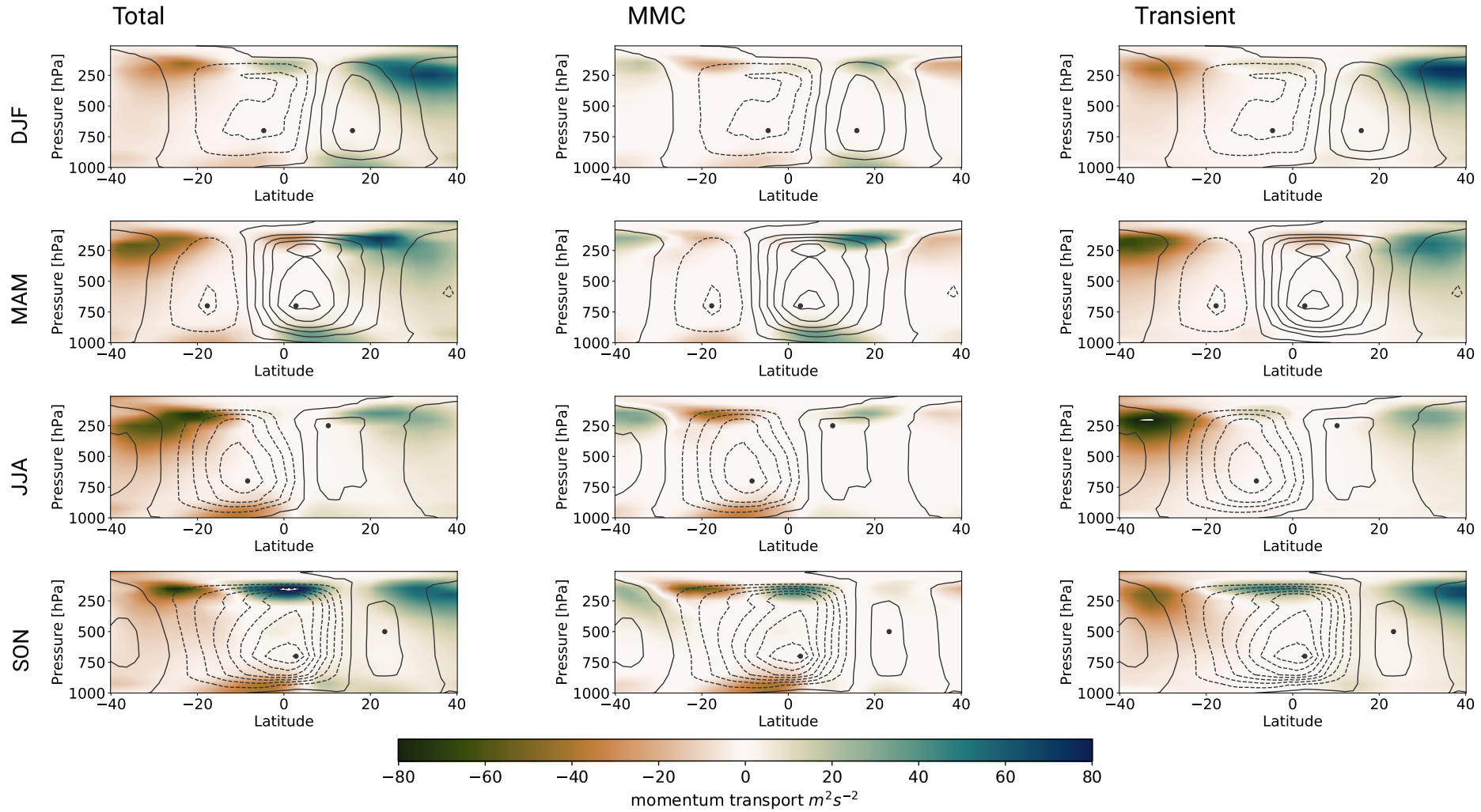

Figure 6.6: Model median of meridional momentum transport (Column TOTAL), momentum transport by the mean meridional circulation $\mathbf{M_t}$ (Column MMC) and transient eddy momentum transport $\mathbf{E_t}$ (Column Transient) for the seasons December, January and February (Row DJF), March, April, May (Row MAM), June, July and August (Row JJA) and September, October and November (Row SON). Model median of the respective seasonal mean of the mass steamfunction in steps of 40×10^9 kg s^{-1} (contours). Solid and dashed contours represent positive and negative values, respectively.

The Northern Hemisphere Hadley cell goes through a very similar seasonal pattern but shifted by two seasons. Since it is generally the weaker Hadley cell, $\mathbf{M_t}$ almost vanishes in the summer cell in SON and the southward momentum transport in the winter cell is not as strong because both $\mathbf{M_t}$ and $\mathbf{E_t}$ are not as pronounced in the deep tropics.

Figure 6.6 (column TOTAL) highlights that the annual mean in the tropical upper troposphere is dominated by strong momentum transport in the Southern Hemisphere's winter cell. The annual mean on the poleward edges of the Hadley cell is strongly influenced by the transitional seasons DJF and JJA where momentum transport in the upper troposphere, poleward of the Hadley cell, is strongest in the Southern and the Northern Hemisphere, respectively. Near the surface, the seasons more equally contribute to the annual mean. This leads to an annual mean which is nearly symmetric about the equator. The seasonal migration of the Hadley cell seems to follow the rule: Near surface flow leads, the upper troposphere follows. Such a pattern would agree well with the slanted common borders of the Hadley cells leaning against the strengthening Hadley cell.

In the following paragraphs, the seasonal cycle of momentum transport is discussed among the model ensemble in the upper troposphere throughout the seasonal cycle (cf. Figure 6.7). The annual mean of the model median momentum transport $[\overline{uv}]$ (Fig. 6.5) shows extrema in three domains: a minimum at the poleward edge of the Southern Hemisphere Hadley cell (SH), a local extremum around the equator (EQ) and a maximum of momentum transport at the poleward edge of the Northern Hemisphere Hadley cell (NH). The seasonal cycle of these three domains will therefore be described separately to facilitate comparability with the annual mean.

The distinct SH peak is located around 23° S in all seasons but MAM. In MAM, the Southern Hemisphere Hadley cell is a summer cell. In its upper branch, eddies have a strong influence on momentum transport in total. This leads to a poleward shift of the minimum meridional momentum transport in most models. As a result, the minimum in the Southern Hemisphere (SH) is not as distinct in MAM as in the other seasons. Models' agreement on the position of SH improves in JJA compared to MAM. Yet the strength strongly differs among models, especially for $\mathbf{E_t}$. In SON, agreement improves particularly in $\mathbf{E_t}$ which weakens from JJA to SON. Season DJF shows the best agreement among models. Only CALTECH which has a much weaker overall mass transport than the other models shows far lower momentum transport and no distinct peak in this season.

The strength of the maximum in the Northern Hemisphere Hadley cell (NH) is fairly constant throughout the seasons but opposed to the SH minimum. The position shifts from approximately 23° N in MAM to about 30° S in SON. This reflects how $\mathbf{M_t}$ and $\mathbf{E_t}$ interact with each other in the different seasons. In MAM, there is strong $\mathbf{M_t}$, while $\mathbf{E_t}$ is weak. Therefore, the peak is shifted equatorward. Opposed to this, $\mathbf{M_t}$ is almost non-existent in SON, when $\mathbf{E_t}$ is strong. Models' agreement in NH is comparable to SH. Yet in contrast to the SH minimum in SON, agreement on the NH maximum is high, because the difference between models in the modes of transport cancel each other out.

In DJF, agreement on strength and position of the EQ maximum of northward momentum transport is good. Only CNRM-AM 5 and CALTECH do not show an extremum. In other models, $\mathbf{M_t}$ and $\mathbf{E_t}$ add up. From DJF to MAM, total momentum transport on EQ reaches a minimum with a strong southward trend, since the equatorial domain is now governed by the Northern Hemisphere Hadley cell. Agreement on the peak strength is low. In JJA, the sign of EQ hints at which Hadley cell governs the equatorial domain in each model.

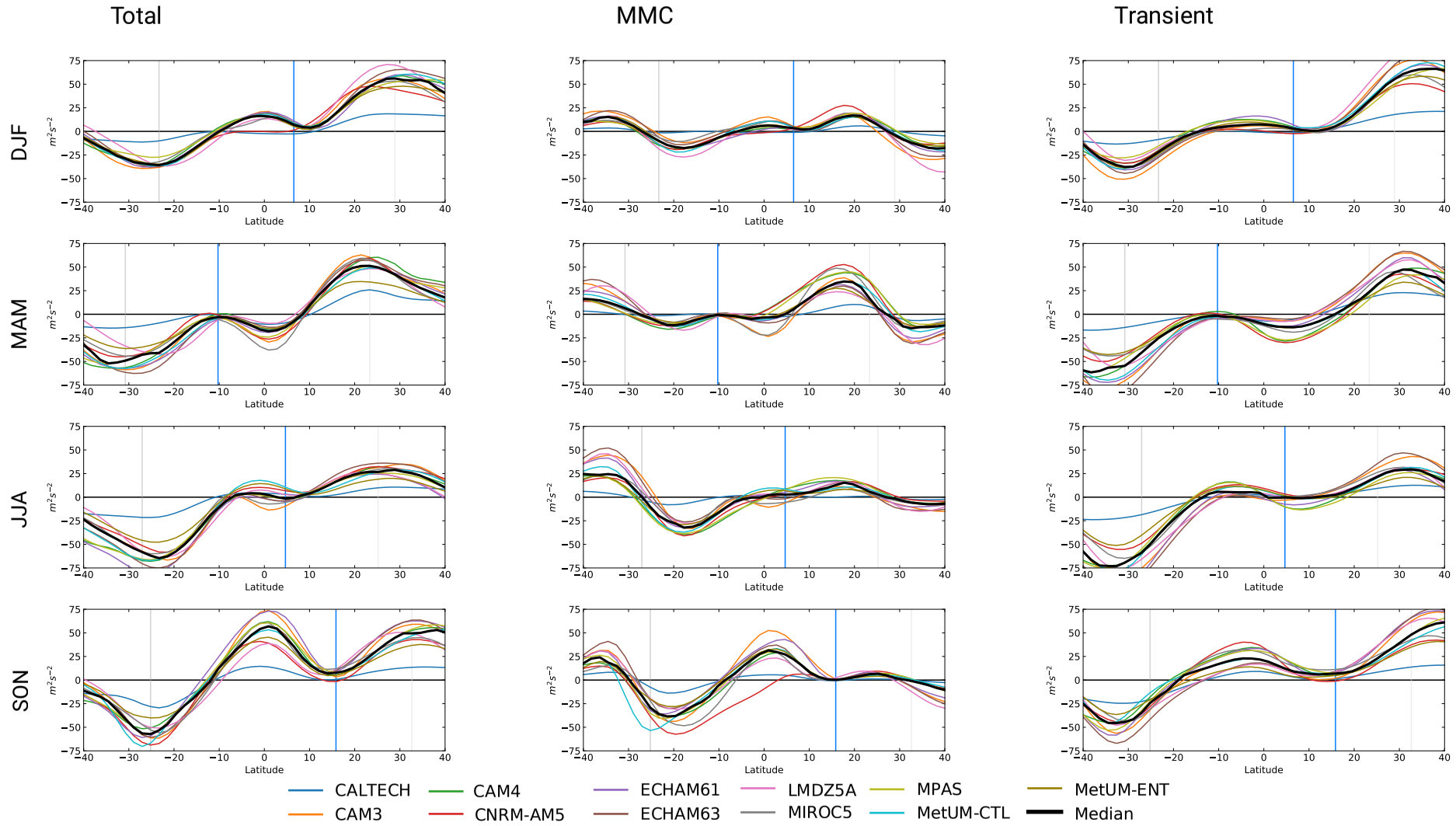

Figure 6.7: Meridional momentum transport (Column TOTAL), momentum transport by the mean meridional circulation $\mathbf{M_t}$ (Column MMC) and transient eddy momentum transport $\mathbf{E_t}$ (Column Transient) in the upper troposphere (averaged between 250 hPa and 150 hPa) in $m^2\,s^{-2}$ for the each season: DJF, MAM, JJA, SON. Colored lines according to the legend. Vertical blue lines represent the latitude of the common boundary of the two Hadley cells in the model median. Vertical grey lines indicate the poleward boundary of the respective Hadley cell in the model median.

While NH still dominates the domain in CAM 3 and MIROC 5, in accordance with the findings in Chapter 5, SH already governs the equatorial domain in the MetUM models. In SON, the EQ maximum is very pronounced in all models. In ECHAM 6.1 and CAM 3, this peak even exceeds the poleward SH minimum in scale. In these models, $\mathbf{M_t}$ is the main contributor to the EQ maximum. In contrast, CNRM-AM 5 does not show a maximum in $\mathbf{M_t}$. The EQ maximum in momentum transport is solely dependent on $\mathbf{E_t}$ in this model. For most models, $\mathbf{M_t}$ and $\mathbf{E_t}$ contribute to total momentum transport in a roughly similar degree.

Figure 6.7 allows for emphasizing differences that occur due to the implementation of an entrainment parametrization. The meridional momentum transport in the season MAM serves as an extreme case. Results from the MetUM models are provided in two modes. MetUM-ENT (olive) parametrizes entrainment in its convection scheme, while MetUM-CTL (aqua) does not. Through the entrainment parametrization, $\mathbf{E_t}$ drops by more than $1/3$ at the poleward edge of SH. Since M_t is similar in both models, a stark difference occurs in the meridional momentum transport $[\overline{uv}]$. To sum this chapter up, the seasonal cycle of the model median momentum transport $[\overline{uv}]$ shows extrema in three domains: a minimum at the poleward edge of the Southern Hemisphere Hadley cell (SH), a local extremum around the equator (EQ) which changes its sign depending of the season, and a maximum of momentum transport at the poleward edge of the Northern Hemisphere Hadley cell (NH) which is weaker than the minimum in the Southern Hemisphere in every season but DJF. The models show the most robust pattern in DJF (Figure 6.7) in the Southern Hemisphere and in MAM in the Northern Hemisphere, except for MetUM-ENT and CALTECH. In JJA, models are inconclusive about the sign of momentum transport close to the equator (EQ), because in some models the equator is still dominated by Northern Hemisphere Hadley cells and others are already on the influence of the Southern Hemisphere Hadley cell. Most models predict the strongest momentum transport in JJA, because $\mathbf{E_t}$ in the extratropics is very strong, even though the agreement is low on the magnitude of the transport. In SON, overall agreement among models is medium. The models' solutions for the positive momentum transport at the equator are unequal. Differences between the models from $\mathbf{M_t}$ and $\mathbf{E_t}$ rather add up than cancel each other out. In the ensemble, momentum transport by the mean meridional circulation $\mathbf{M_t}$ is curiously more uncertain in the prediction of the magnitude of meridional momentum transport$[\overline{uv}]$ above the descending branch of the Hadley cell. This effect is even more pronounced in the Northern Hemisphere winter cell than in the Southern Hemisphere one. Surprisingly, in both cases $\mathbf{M_t}$ and $\mathbf{E_t}$ cancel each other out. Models CAM 3 and ECHAM 6.1 show the strongest momentum transport at the equator, whereas CNRM-AM5 shows none. Overall, the patterns of meridional momentum transport are comparable between the models.

6.2.3 Examples for transient eddies in the deep tropics of TRACMIP AquaControl

When describing the general circulation, eddies dissipate at the poleward border of the Hadley cell (cf. Chapter 2). Stationary eddy momentum transport is the dominant mode of eddy momentum transport in today's atmosphere in the tropics (Dima and Wallace, 2003). Additionally, it has been found to be an important source of uncertainty in model output for the tropics in the past (Ca-

ballero, 2008). Meridional eddy momentum transport in the tropics arises mostly from stationary eddies (Zurita-Gotor, 2019) that are mostly absent in TRACMIP AquaControl.

As an in depth study of said phenomenon is beyond the scope of this thesis, this section merely gives a first insight of the wave structure associated with $\mathbf{E_t}$. Herefore, deviations u' in the 3-hourly data from the monthly mean of the eastward wind u were calculated. Furthermore, three models were selected which showed strong transient eddy momentum transport in the deep tropics for the chosen months: CAM 3, CAM 4 and MPAS. The altitude (150 hPa) and longitude chosen for the Hovmöller plots show the strongest eddy activity for the selected months.

For March of the second year in the data set, the model MPAS was chosen. It shows strong $\mathbf{E_t}$ during MAM in the equatorial domain EQ (Figure 6.7). The sign of u' changes every 10 days in Figure 6.8. CAM 4 shows a similar pattern during March.

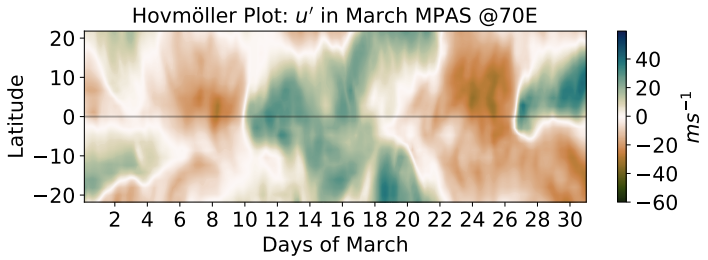

Figure 6.8: Hovmöller plot of March in MPAS with AquaControl set-up in 150 hPa at 70° E for the deep tropics. Shown are deviations of the zonal wind from its monthly mean u' for the second year of the 3-hourly output.

A few months later, the pattern of u' changes. Here, CAM 4 was chosen to represent u' in June (Figure 6.9), when the model shows weaker southward $\mathbf{E_t}$ than in March. Interestingly, the magnitude of u' does not change significantly in this time span. Thus, the decrease in $\mathbf{E_t}$ must be caused by weaker temporal variation of the northward wind v'. However, the structure of u' in June is very different from u' in March. Here, the sign of u' changes only once over the time span in the deep tropics.

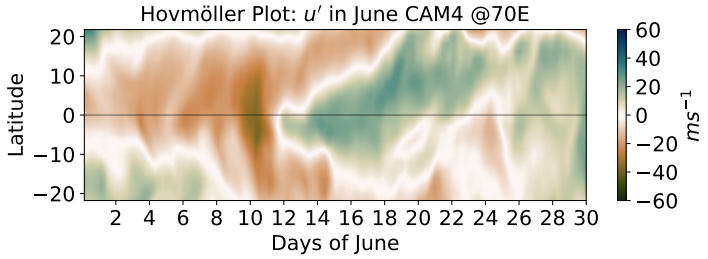

Figure 6.9: Hovmöller plot of June in CAM 4 with AquaControl set-up in 150 hPa at 70° E for the deep tropics. Shown are deviations of the zonal wind from its monthly mean u' for the second year of the 3-hourly output.

In SON, the deep tropical $\mathbf{E_t}$ in the model median peaks in the seasonal cycle. CAM 3 has the strongest deep tropical $\mathbf{E_t}$ of the ensemble in this season, and more specifically in September. Therefore, Figure 6.10 displays u' in CAM 3 for September. It is somewhat surprising that u' is weaker than in March and June in MPAS and CAM 4, as $\mathbf{E_t}$ is strong here. Consequently, $\mathbf{E_t}$ must be stronger, because v' amplifies even small deviations from the mean zonal wind. Moreover, the

structure of u' is obscure compared to March and June. The sign of u' changes several times during the course of this month. In animations, the signal of the deviation appears to originate from the poleward edge of the Hadley cell and propagate through the tropics, much like the negative u' signal which emerges at day 16 on the southern edge of the plot and reaches the northern edge at day 24.

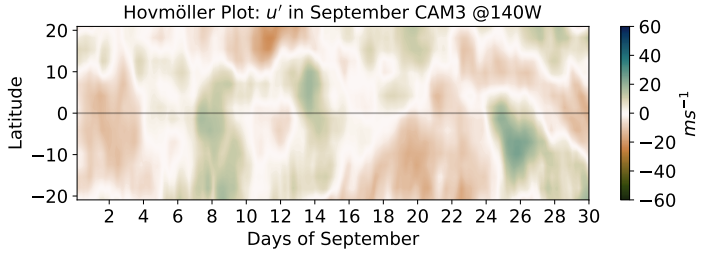

Figure 6.10: Hovmöller plot of September in CAM 3 with AquaControl set-up in 150 hPa at 140° W for the deep tropics. Shown are deviations of the zonal wind from its monthly mean u' for the second year of the 3-hourly output.

In conclusion, the TRACMIP AquaControl ensemble shows interesting features of eddy activity. The strength and shape of the eddies depends on both month and model. They can take the shape of stationary eddies which seem to originate in the tropics, like in March and June of MPAS and CAM 4, or transient eddies from the extratropics which propagate through the deep tropics like in September of CAM 3. A more comprehensive wave analysis would give further insight on the waves' properties and would ultimately help to classify them.

6.3 Divergence of Meridional Momentum Flux

The divergence of meridional momentum transport describes the sources and sinks of momentum transport. As such, it constitutes a part of the momentum budget equation. This section presents the annual mean and the seasonal cycle of the quantity. Here, divergence is directly calculated from the decomposed meridional momentum transport for each month and model. Therefore, the total momentum flux divergence is comprised of divergence of the meridional momentum flux by the mean meridional circulation $\mathbf{M} = -\frac{1}{a\cos^2\phi}\frac{\partial}{\partial\phi}\left([\overline{u}][\overline{v}]\cos^2\phi\right)$ and eddy momentum flux divergence $\mathbf{E} = -\frac{1}{a\cos^2\phi}\frac{\partial}{\partial\phi}\left(\left[\overline{u'v'}\right]\cos^2\phi\right)$. In the following section, the influence of stationary eddy momentum flux divergence will be discussed as well in order to justify why it can be neglected in further considerations.

6.3.1 The Divergence of Meridional Momentum Flux in the Annual Mean

This section is split in two parts. First, the zonal mean meridional momentum flux divergence and its components is described using the model median in Figure 6.11. Secondly, the model spread in the upper troposphere is discussed (Fig. 6.12).

The meridional momentum flux divergence shown in Figure 6.11a is implicated in the upper branch and the near-surface return flow of the Hadley cell. The surface meridional momentum flux converges at approximately 20° S/N. Near the equator, meridional momentum flux diverges.

Yet the maximum momentum flux divergence occurs in the upper branch of the Southern Hemisphere Hadley cell. This maximum is collocated with the latitude of maximum mass transport. The upper branch of the Northern Hemisphere Hadley cell is also dominated by momentum flux divergence but not as strongly. In vicinity of the equator and above the strong near-surface meridonal momentum divergence is a weak convergence in the upper troposphere. Total meridional momentum flux divergence is comprised of momentum flux divergence by the mean meridional circulation **M** (Fig. 6.11b) transient eddy momentum flux divergence (Fig. 6.11c). Just like the stationary eddy transport (Fig. 6.11d), stationary eddy momentum flux divergence is weak compared to the other two components. The stationary eddy momentum flux convergence in the upper branch of the Hadley cell is very small in the annual mean[2]. Therefore, stationary eddy momentum flux divergence is negligible and it is assumed that eddy momentum flux divergence is fully represented by the transient eddy momentum flux divergence $\mathbf{E} = -\frac{1}{a\cos^2\phi}\frac{\partial}{\partial\phi}\left(\overline{u'v'}\cos^2\phi\right)$.

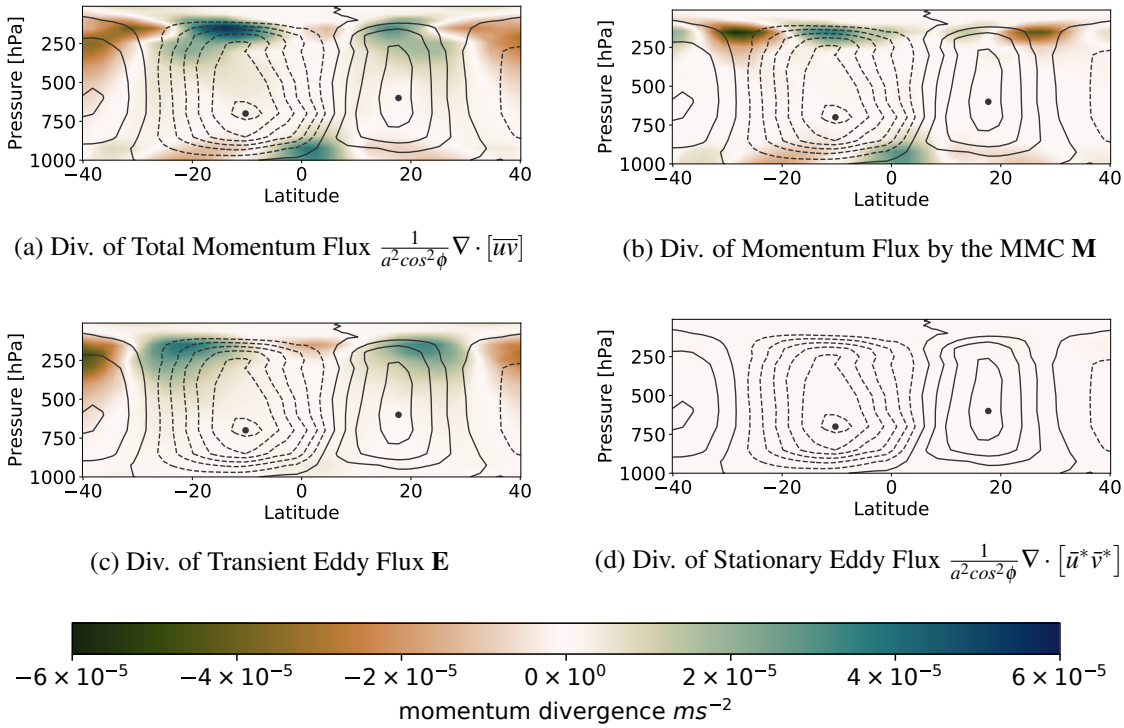

(a) Div. of Total Momentum Flux $\frac{1}{a^2cos^2\phi}\nabla\cdot[\overline{uv}]$

(b) Div. of Momentum Flux by the MMC **M**

(c) Div. of Transient Eddy Flux **E**

(d) Div. of Stationary Eddy Flux $\frac{1}{a^2cos^2\phi}\nabla\cdot\left[\bar{u}^*\bar{v}^*\right]$

Figure 6.11: The model median modes of annual mean divergence of meridional momentum flux. Displayed are (a) the zonal mean of the total divergence of meridional momentum flux $\frac{1}{a^2cos^2\phi}\nabla\cdot[\overline{uv}]$, (b) divergence of momentum flux by the mean meridional circulation (MMC) **M**, (c) divergence of transient eddy momentum flux **E** and (d) divergence of the stationary eddy momentum flux $\frac{1}{a^2cos^2\phi}\nabla\cdot\left[\bar{u}^*\bar{v}^*\right]$ (Fig. 6.11d) in $\mathrm{m\,s^{-2}}$. Additionally, the respective mass streamfunction (black contours, contour intervals $40\times10^9\,\mathrm{kg\,s^{-1}}$) is given for orientation. Solid and dashed contours represent positive and negative values, respectively.

Near the surface, divergence of momentum transport is dominated by **M**. Therefore, it is due to the mean meridional circulation that divergence of momentum transport occurs near the equator and convergence poleward of the latitude of maximum mass transport. The convergence is more pronounced in the Southern Hemisphere Hadley cell than in its northern counterpart. But

[2] Only CNRM-AM 5 shows values apart from zero. It can therefore be easily neglected in the annual mean. But especially in SON, this quantity cannot be neglected when looking at the momentum budget of CNRM-AM 5. There, the stationary momentum flux divergence amounts to $1.5\times10^{-5}\,\mathrm{m\,s^{-2}}$.

all extrema near the surface are weaker than extrema in the upper troposphere, for meridional momentum flux divergence and all its components.

In the upper troposphere, **M** colludes with **E**. **M** is confined to the upper branch of the Hadley cell. The strongest divergence occurs either above the maximum of mass transport, in the Southern Hemisphere Hadley cell, or equatorward of it, in the Northern Hemisphere Hadley cell. Convergence is collocated with the subtropical jet in both hemispheres. **E** reaches much further into the mid troposphere down to 500 hPa. It shows convergence close to the tropopause at the equator. At the poleward edges of the Hadley cell **E** dampens the effect of convergence from **M**, but strengths the divergence from **M** where they overlap. Therefore, the area of momentum flux convergence shifts toward the Ferrell cell due to transient eddies.

Figure 6.12 gives insight on the momentum convergence between 250 hPa and 150 hPa. The maxima of momentum divergence and its components lie within these pressure levels. It is therefore considered representative for divergence in the upper troposphere.

Momentum flux divergence shows a peak at 12° S in the Southern Hemisphere and a smaller peak of 18° N in the Northern Hemisphere. The agreement among models is poor: Magnitude and position of the peaks vary. In the Southern Hemisphere, the peaks of MetUM-CTL and LMDZ5A are more than 10° apart from each other. It seems like the reason why peaks are in closer vicinity in the Northern Hemisphere is because the Hadley cell is narrower there. Still MIROC 5 and MetUM-CTL peak about 10° apart. This is mainly due to low agreement in **M**. MetUM-CTL, for example, shows low **M** throughout the Hadley cell. Therefore, **E** dominates the meridional momentum flux divergence. The peak of **E** is situated at the poleward edge of the Hadley cell. This shifts the peak to 22° N. On the other hand, the models MIROC 5 and LMDZ5A show pronounced peaks of **M** within the Hadley cell. In contrast to the other models, CNRM-AM 5 computes momentum convergence from **M** throughout the deep tropics from 15° S to 15° N .

In contrast to the picture given Fig. 6.12b, **E** shows a more coherent pattern. This might by due to the fact that the **E** maximum is associated with the poleward edge of the Hadley cell. There is high agreement between the models about the latitude of this poleward border. However, some models compute **E** peaks that are considerably weaker than the model median (CALTECH, MetUM-ENT and LMDZ5A). In most models, **E** shifts rapidly from divergence to convergence at the poleward border of the Hadley cell. All models show the ascending branch of the Southern Hemisphere Hadley cell to be accompanied by negative **E** in the upper troposphere. In general, **E** is stronger than **M** outside of the Hadley cell.

In conclusion, meridional momentum flux divergence plays a role in the upper branch and the near-surface return flow of the Hadley cell. While divergence in momentum flux of the near-surface return flow is only comprised of **M**, the merdional momentum flux in the upper troposphere is comprised of **M** and **E**. The strongest divergence is reached in the upper branch of the Southern Hemisphere Hadley cell. The strongest convergence is poleward of the strongest divergence, in the Ferrell cell. For both extrema, **M** and **E** overlap. The robustness of this pattern is questionable, since agreement on the strength of **M** among models is poor. Yet the agreement of **E** is high among models. Hence, deviations in this quantity are not compensated by deviations in **E** to give a more coherent picture of the total meridioal momentum flux divergence.

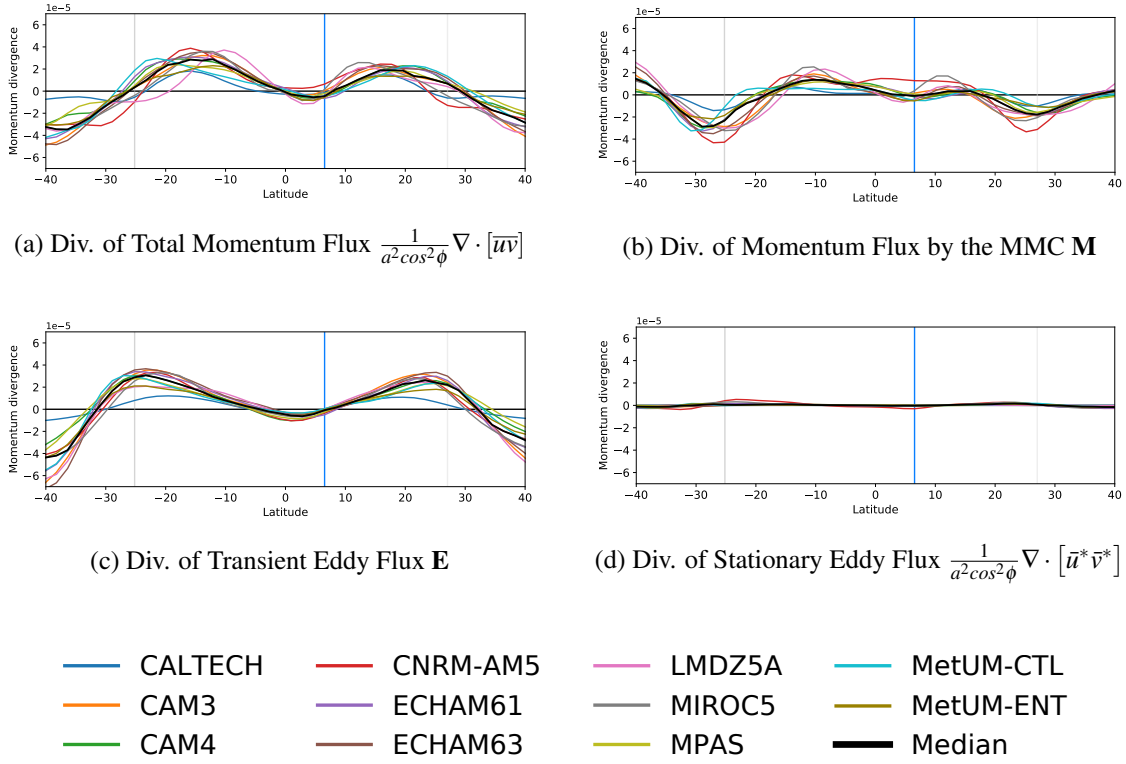

(a) Div. of Total Momentum Flux $\frac{1}{a^2 cos^2\phi}\nabla\cdot[\overline{uv}]$

(b) Div. of Momentum Flux by the MMC **M**

(c) Div. of Transient Eddy Flux **E**

(d) Div. of Stationary Eddy Flux $\frac{1}{a^2 cos^2\phi}\nabla\cdot\left[\bar{u}^*\bar{v}^*\right]$

Figure 6.12: Modes of annual mean divergence of meridional momentum flux in upper troposphere.(a) Zonal mean of divergence of total momentum transport, (b) momentum flux by the mean meridional circulation **M**, (c) transient eddy momentum flux **E** and (d) stationary eddy momentum flux $\frac{1}{a^2 cos^2\phi}\nabla\cdot\left[\bar{u}^*\bar{v}^*\right]$ are vertically averaged between 250 hPa and 150 hPa. Bold black lines show the model median and colors individual simulations. Vertical blue lines represent the latitude of the common boundary of the two Hadley cells and vertical grey lines indicate their poleward boundary in the model median.

6.3.2 Seasonal Cycle of Meridional Momentum Divergence

In the previous section, extrema of momentum flux divergence were identified in the annual mean of the model median (Fig. 6.11). In this section, their seasonal cycle is these extrema are discussed using Figure 6.13. Thereafter, the robustness of upper troposphere momentum flux divergence is discussed in light of Figure 6.14. Meridional momentum flux divergence is the weighted derivative of the meridional momentum transport. Hence as the meridional momentum transport, the meridional momentum flux divergence thus follows a pronounced seasonal cycle (Fig. 6.13, column Total).

Starting with the near-surface return flow of the Hadley cell in Figure 6.13 and column Total, the model median shows a local peak of momentum flux divergence around the equator in all seasons. The peak shifts towards the summer hemisphere in seasons with a cross-equatorial Hadley cell (column Total, rows MAM and SON) and remains in the respective hemisphere throughout the transitional seasons (column Total, rows DJF and JJA) until the next cross-equatorial Hadley cell has built up.

Near-surface momentum flux converges poleward of the maximum mass transport (denoted as black dot in Fig. 6.13). In the Southern Hemisphere Hadley cell, momentum flux convergence

persists throughout the year. In the Northern Hemisphere, momentum flux convergence is very weak in SON and JJA when the Hadley cell almost vanishes.

In the tropical upper troposphere, **M** and **E** both contribute to the total meridional momentum flux divergence (Fig. 6.13, column Transient). As in the annual mean, around the equator the upper troposphere is dominated by momentum flux convergence fostered by both **M** and **E**. The convergence is latitudinally collocated with the ascending area of the stronger Hadley cell and the near-surface momentum divergence discussed in one of the previous paragraphs. The momentum convergence in the equatorial upper troposphere is much stronger in SON and MAM, the seasons that show a cross-equatorial Hadley cell.

Away from the equator, momentum flux diverges in the upper branch of the Hadley cell. Closer to the equator, this is due to **M** but in the poleward half of the Hadley cell it is because of **E** in most seasons. The summer cell is an exception from this as positive **E** spans the entire upper branch of the Hadley cell.

Total momentum flux divergence reaches its maximum in the upper troposphere in SON when the Southern Hemisphere Hadley cell is strongest. In general, meridional momentum flux divergence shows the largest values in the upper branch of the strengthening or the cross-equatorial Hadley cell. Yet models find very different solutions for the seasonal evolution of meridional momentum flux divergence in each model (cf. Figure 6.14). This model spread is described for the cross-equatorial Hadley cell in the following paragraphs, dividing the model behaviours into three patterns.

For example in cross-equatorial Hadley cells, MIROC 5 (grey, Fig. 6.14, column Total, rows MAM and SON) computes very high values of momentum flux divergence compared to the rest of the ensemble and shows only one peak of momentum flux divergence in this region regardless of the hemisphere. A similar pattern can be found in CAM 3 (orange) and CNRM-AM 5 (red).

As opposed to this, MetUM-CTL produces two maxima within cross-equatorial Hadley cells (aqua, in Fig. 6.14, for example SON). One is at the poleward edge of the Hadley cell and one closer to the equator which is plateau-like and has only $1/3$ of the strength of the poleward peak. Both peaks are induced by both **E** and **M**. This pattern is also found in MPAS (lightgreen) for the Northern Hemisphere Hadley cell in MAM.

Many other models compute the absolute maximum of meridional momentum divergence close to the equator and a plateau-like local maximum at the poleward edge, for example MetUM-ENT. But this pattern is also present in the cross-equatorial Hadley cells of CAM 4, ECHAM 6.1, ECHAM 6.3, MPAS (for SH/SON) and LMDZ5A. The different patterns are mostly shaped by different behaviours of the models when it comes to **M**. Compared to **M** the agreement is good in **E**. Even though **E** shows variations in the strength and position of its peaks the models follow a similar shape.

In conclusion, the momentum flux divergence in the near-surface return flow is brought about by to **M**. Therefore, momentum flux divergence varies strongly throughout the seasons. It is weakest in DJF and strongest in SON. There are five peaks of tropical meridional momentum flux divergence in the upper troposphere throughout the seasons. Peaks in the Southern Hemisphere are present in SON including the convergence, peaks in the Northern Hemisphere are located in MAM. Due to the low agreement among models, the model median may not adequately represent the whole ensemble.

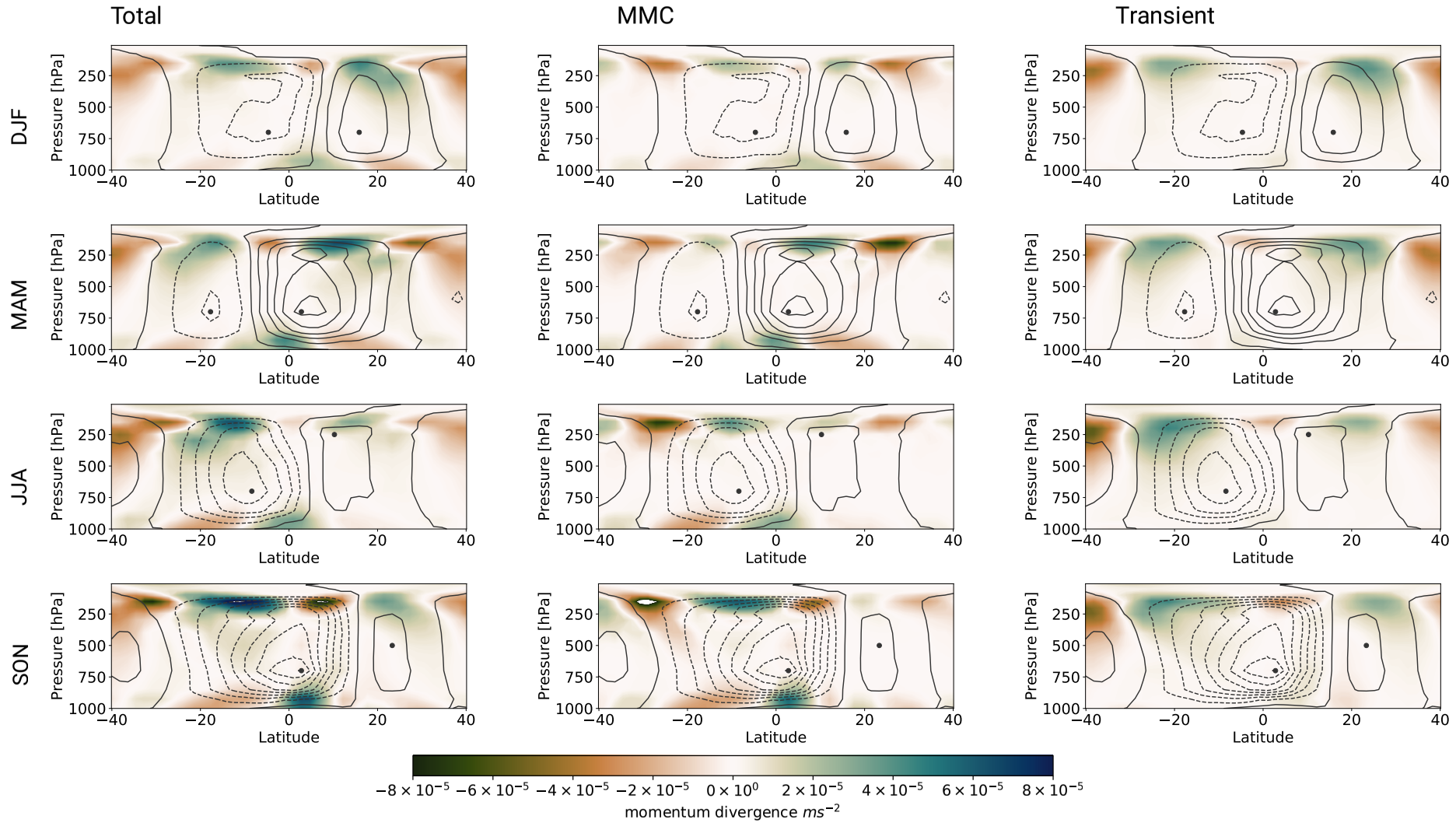

Figure 6.13: Model median of meridional momentum flux divergence (column TOTAL), momentum flux divergence by the mean meridional circulation $\mathbf{M}$ (column MMC) and transient eddy momentum flux divergence $\mathbf{E}$ (column Transient) for the seasons December, January and February (row DJF), March, April, May (row MAM), June, July and August (row JJA) and September, October and November (row SON). Model median of the respective seasonal mean of the mass steamfunction in steps of $40\times10^{9}\,\mathrm{kg\,s^{-1}}$ (contours). Solid and dashed contours represent positive and negative values, respectively.

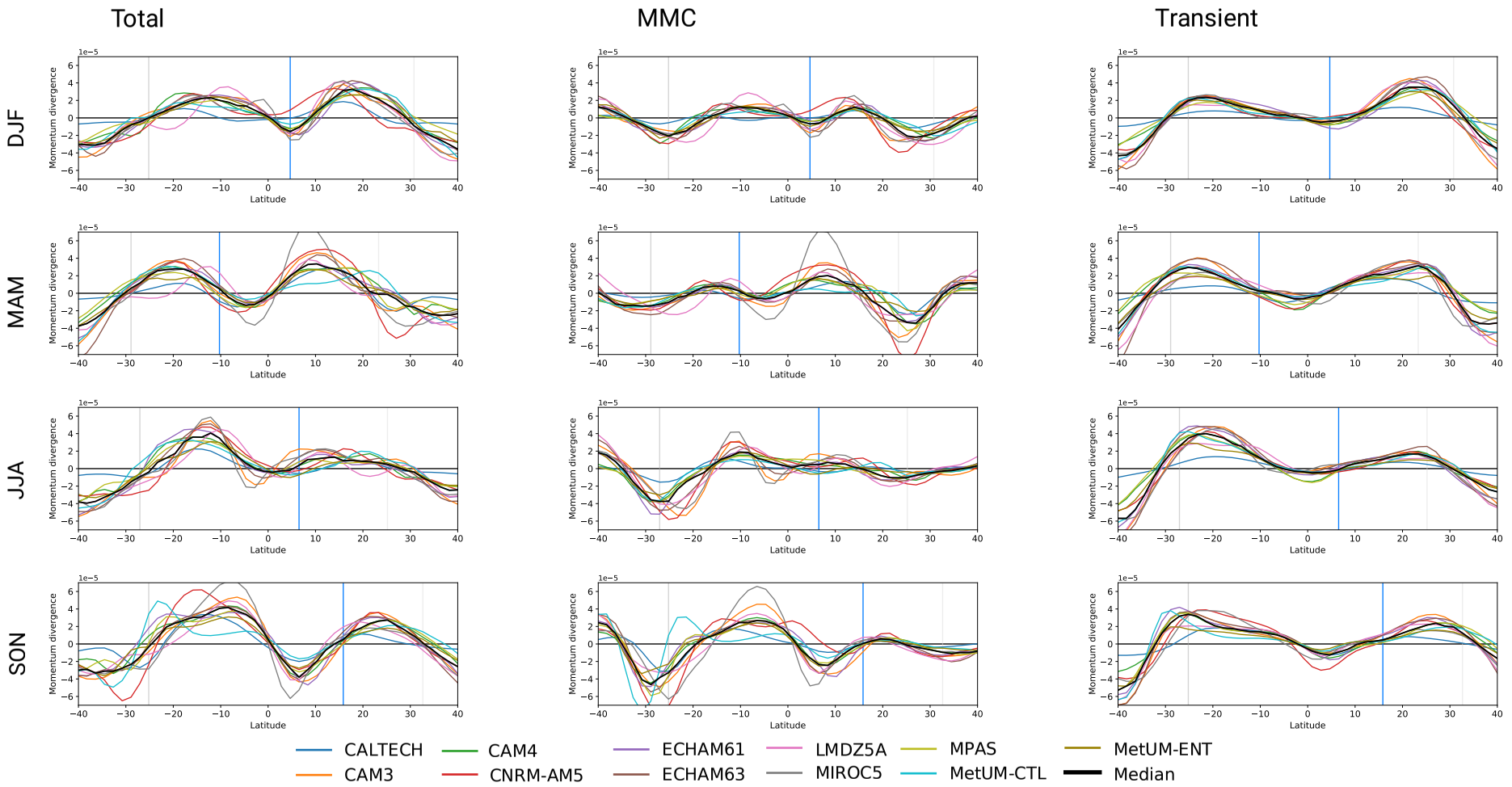

Figure 6.14: Meridional momentum flux divergence (column TOTAL), momentum flux divergence by the mean meridional circulation **M** (column MMC) and transient eddy momentum flux divergence **E** (column Transient) in the upper troposphere (averaged between 250 hPa and 150 hPa) in $m^2\,s^{-2}$ for the each season: DJF, MAM, JJA, SON. Colored lines indicate the individual models according to the legend. Vertical blue lines represent the latitude of the common boundary of the two Hadley cells in the model median. Vertical grey lines indicate the poleward boundary of the respective Hadley cell in the model median.

6.4 The Local Rossby Number *Ro*

The local Rossby number *Ro* quantifies the influence of eddies in the upper branch of the Hadley cell. In the absence of eddies, the local Rossby number is $Ro = 1$. A local Rossby number of $Ro = 0$ indicates that the mean meridional circulation does not contribute to the total momentum flux and eddies thus accomplish the meridional advection of planetary momentum (cf. Chapter 4). The values of *Ro* between 5° S/N are deleted, because the calculations are unstable as the Coriolis parameter f approaches zero close to the equator, $f \to 0$ for $\phi \to 0$ (cf. Eq. 4.4).

The local Rossby number of the model median is markedly higher in the upper branch of the

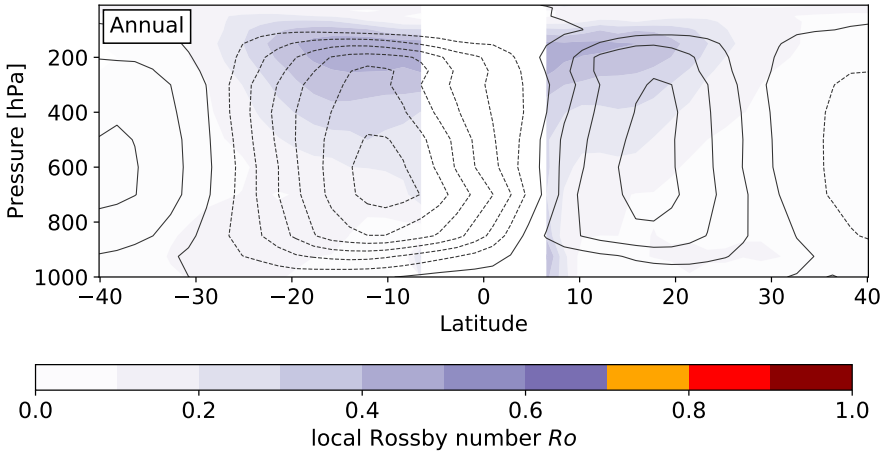

Figure 6.15: Model median of the local Rossby number *Ro* (filled contours) and the mass steam function (grey, $20 \times 10^9\,\mathrm{kg\,s^{-1}}$) in the annual mean (Annual). Solid and dashed contours represent positive and negative values, respectively.

Hadley cell compared to the mean tropical troposphere in the annual mean (Figure 6.15). Accordingly, **M** is high (cf. Figure 6.11b) and the Coriolis parameter f is still small close to the equator. *Ro* exceeds $Ro = 0.5$ in this region, in line with Schneider (2006). Nevertheless, the influence of **M** is weaker in the upper branch of the Northern Hemisphere Hadley cell than in the Southern Hemisphere. Therefore, the local Rossby number is smaller in the upper branch of the Northern Hemisphere Hadley cell.

As the other quantities analyzed in this thesis from Chapter 5 to Section 6.3, the magnitude of *Ro* fluctuates throughout the seasons (Figure 6.16). In the transitional season DJF, the influence of eddies in the upper branch of the Southern and Northern Hemisphere Hadley cell are at comparable levels with $Ro \leq 0.6$ and $Ro \leq 0.5$, respectively. From DJF to MAM, the Northern Hemisphere Hadley cell transitions into a cross-equatorial winter cell. Hence, the influence of eddies close to the latitude of the maximum mass transport increases to $Ro \geq 0.8$. In contrast, eddies have a substantial influence on the Southern Hemisphere summer cell in these months. Therefore, *Ro* must be small. The pattern in JJA is comparable to the pattern in DJF, only with slightly larger *Ro*. Correspondingly, the pattern in SON is reverse to MAM, only with smaller *Ro* in both hemispheres.

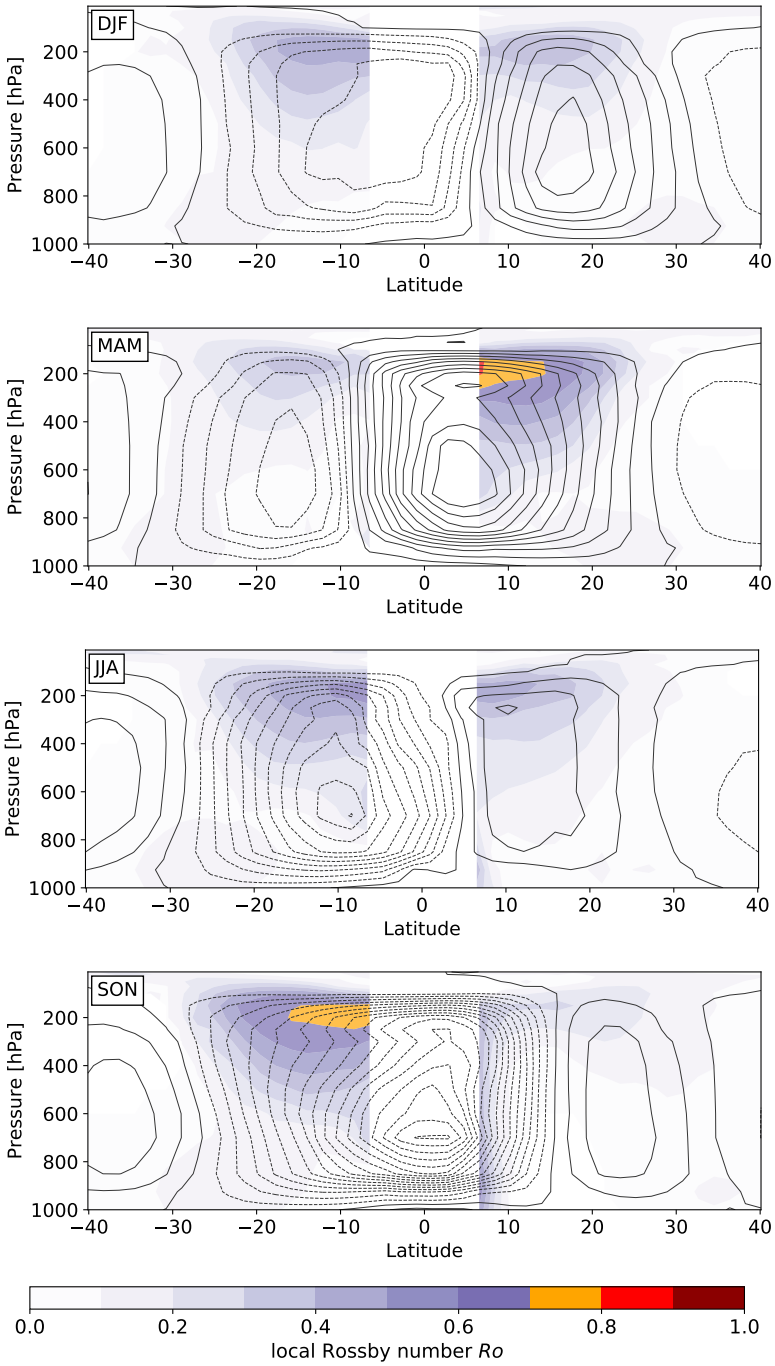

Figure 6.16: Model median of the local Rossby number *Ro* (filled contours) and the mass steam function (grey, $20 \times 10^9\,\mathrm{kg\,s^{-1}}$) for the seasons (DJF, MAM, JJA, SON). Solid and dashed contours represent positive and negative values, respectively.

The Northern Hemisphere Hadley cell in SON has the strongest influence of eddies with $R_0 \leq 0.3$ in the upper branch of the Hadley cell. In turn, it also has the highest local Rossby number in MAM. One might assume at first that *Ro* would be higher in a stronger Hadley cell. In this rationale, the Southern Hemisphere winter cell should have higher local Rossby number *Ro* than its northern counterpart. But the relationship is not as straightforward. The model median gradient of u in the Northern Hemisphere winter cell is slightly stronger close to the equator than in the

Southern Hemisphere winter cell. Yet two other factors may add to the difference. Firstly, there is less transient eddy activity in the upper branch of the Northern Hemisphere winter cell than in its southern counterpart. Secondly, in the other seasons and the annual mean, it seems, as if larger *Ro*-values occur closer to the border between the two Hadley cells and above the maximum of the Hadley cell. In SON, the corresponding area in the upper branch of the Southern Hemisphere Hadley cell lies within 5° S/N, where *Ro* cannot be calculated.

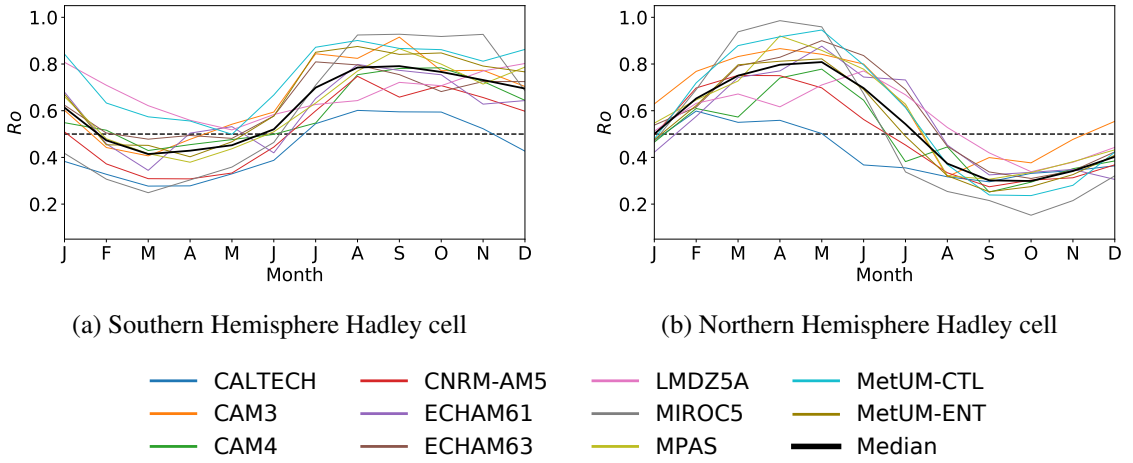

(a) Southern Hemisphere Hadley cell

(b) Northern Hemisphere Hadley cell

Figure 6.17: The evolution of the local Rossby number *Ro* in models and their median in the upper branch of (a) the Southern Hemisphere and (b) Northern Hemisphere Hadley cell. Schneider (2006) finds that eddy permitting simulations of the Hadley cell show values $R_0 \geq 0.5$ for cross-equatorial Hadley cells (dashed line).

Figure 6.17 shows the maximum values of *Ro* in the upper branch, between 400 hPa and 150 hPa in the Southern Hemisphere (Fig. 6.17a) and the Northern Hemisphere Hadley cell (Fig. 6.17b) for each month of the average year in the data set. The model median in this figure is not the same as in Figure 6.15 and Figure 6.16 because it is the median of the *Ro* maxima and not the maximum of the median.

In the Southern Hemisphere Hadley cell, the influence of **M** remains somewhat important over the seasons with $Ro \geq 0.4$ throughout the year in many models. The influences of the mean meridional circulation on the upper branch of the Hadley cell decreases slowly until January and more rapid in the two consecutive month. In contrast, it increases rapidly from June to August.These are also the months in which the Hadley cell gains most of its strength. The influence reaches its maximum in August. One month before the Hadley cell reaches its maximum strength (Figure 5.4a).

From April to January, CALTECH computes the smallest *Ro* indicating that **E** might play an important role in the upper branch of the Hadley cell over all seasons. MIROC 5, which produces very strong Hadley cells compared to the model median, also shows a distinct seasonal cycle with the smallest *Ro* in February and March and the largest from August to November. In contrast, *Ro* is fairly close to the model median in ECHAM 6.1, which produces the second strongest Hadley cell, indicating that the local Rossby number does not directly influence the mass transport of the Hadley cell. *Ro* from MetUM-CTL and MetUM-ENT diverge from November to February. This suggests that entrainment and detrainment seemingly are of importance for eddy influence in the upper branch of the Hadley cell during its decay.

In the Northern Hemisphere Hadley cell, the local Rossby number shows the opposite pattern to the Southern Hemisphere Hadley cell. Influence of the mean meridional circulation increases slowly from September to January, then more rapidly in February and March, followed by a steep decline from June to August. The local Rossby number peaks after the mass streamfunction. For most models, the amplitude of the seasonal cycle is larger here than in the Southern Hemisphere Hadley cell. As in the Southern Hemisphere, MIROC 5 produces the largest and the smallest *Ro* in the seasonal cycle for the Northern Hemisphere Hadley cell. Also, CALTECH has the smallest *Ro* peak, indicating a strong eddy influence in the winter cell.

In most models, the local Rossby number exceeds $Ro \geq 0.5$ from July to January and from February to June in the upper branch of the Southern and Northern Hemisphere Hadley cell, respectively, indicating a comparatively weak influence of eddies during theses months. Accordingly, the model median peaks in this period. In Figure 6.17b, the peak is found towards the end of the period in May, while in Figure 6.17a it occurs in the beginning of the season when **M** is already strong but the eddy influence is still small.

In conclusion, high *Ro* occur in the upper branch of the Hadley cell towards its ascending branch, where **M** is strong. Seasonally, the highest *Ro*-values are reached in SON (MAM) in the upper branch of the Southern (Northern) Hemisphere Hadley cell, when a strong cross-equatorial circulation exists. More precisely, the model median peaks in May and August for the Northern and Southern Hemisphere Hadley cell, respectively. In most models, the local Rossby number stays above $Ro = 0.5$ during February to June (Northern Hemisphere Hadley cell) and July to January (Southern Hemisphere Hadley cell), indicating a weak influence of eddies during these periods. Furthermore, the model median *Ro* exceeds the values cited in literature (Walker and Schneider, 2005, 2006; Schneider, 2006). The model used in these studies is similar to CALTECH. The latter model shows **M** below the median in the annual mean and for every season in Section 6.3. Therefore, *Ro* in CALTECH is smaller than the model median.

6.4.1 The Role of Time Tendency within Seasons and Months and its Impact on the Local Rossby number *Ro*

In the derivation of the local Rossby number and the decomposition of the mass stream function, it is implied that the atmosphere is in a steady state. Therefore, its time tendency must vanish, $\frac{\partial u}{\partial t} = 0$. This is the case in the annual mean in all simulations of TRACMIP AquaControl. The time tendency is positive, when the zonal wind strengthens, and negative, when it weakens over time periods at a particular position.

In the seasonal cycle, the data set shows this expected pattern. In MAM and SON, the general circulation is fairly invariant. Hence, the time tendency is small. As opposed to these seasons, the circulation transitions from one cross-equatorial Hadley cell to another in seasons DJF and JJA. Therefore, the time tendency is more pronounced in these seasons. The time tendency is one order of magnitude smaller in the upper branch of the Hadley cell and therefore slightly stronger than the divergence of stationary eddies $\left[\bar{u}^* \bar{v}^*\right]$ in this data set.

Especially at the poleward edges of the Hadley cell, the changes in strength and position of the subtropical jet combined with the transitioning Hadley cell give a comparatively strong signal. During seasons DJF and JJA, two different patterns can be found. In DJF, the time tendency is

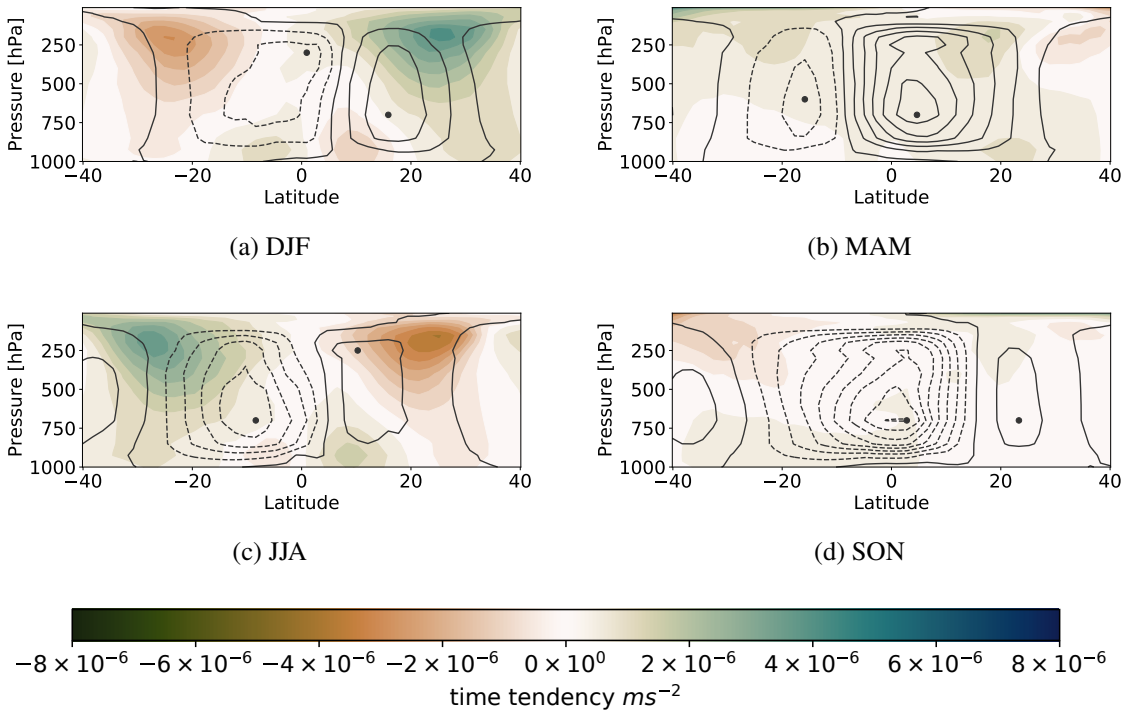

Figure 6.18: Model median of time tendency displayed filled contours and the mass steam function (grey contours, $40 \times 10^9\,\mathrm{kg\,s^{-1}}$) in each season (DJF, MAM, JJA, SON). Solid and dashed contours represent positive and negative values, respectively.

strong in November and January while the time tendency in the Northern Hemisphere stays very weak in December and only emerges in January. From there on the time tendency decreases until March. In contrast, shifts in JJA happen more concurrently in both hemisphere. The strongest time tendency is reached in July for both hemispheres. Moreover, July is the month of the strongest time tendency not only in JJA but over the entire year. Figure 6.19 shows the distribution of the time tendency in seasons DJF and JJA in the upper branch of the Hadley cell. Seasons SON and MAM are not shown because as Figure 6.18 suggests that there are no interesting features to be seen. As expected time tendency $\frac{\partial u}{\partial t}$ in the annual mean for all models is also zero in the upper branch of the Hadley cell. The pattern of time tendency is mirror inverted. While it is positive in the Northern Hemisphere in DJF, it is negative there in JJA, corresponding to the strengthening and weakening of the Northern Hemisphere Hadley cell. It is noteworthy that the time tendency is very similar among the models compared to other quantities analyzed in this thesis. But the agreement in the strengthening cell is better than in the weakening one. Moreover, it is better for the Northern than for the Southern Hemisphere Hadley cell.

To illustrate the influence of time tendency on the momentum balance, Figure 6.20 shows the model median in the upper troposphere for the time tendency and the momentum flux divergence for DJF and JJA, respectively. It shows that time tendency is in general much smaller than momentum divergence. Interestingly, time tendency is strong where momentum divergence changes sign. In these regions, at the poleward edge of the Hadley cell, time tendency becomes more relevant. This is especially true for DJF, but might be important for the Northern Hemisphere in JJA too.

To investigate the influence of time tendency onto *Ro* and the decomposition of the mass streamfunction, Equation 4.18 and Equation 4.21 have been defined in Chapter 4. Time tendency has no

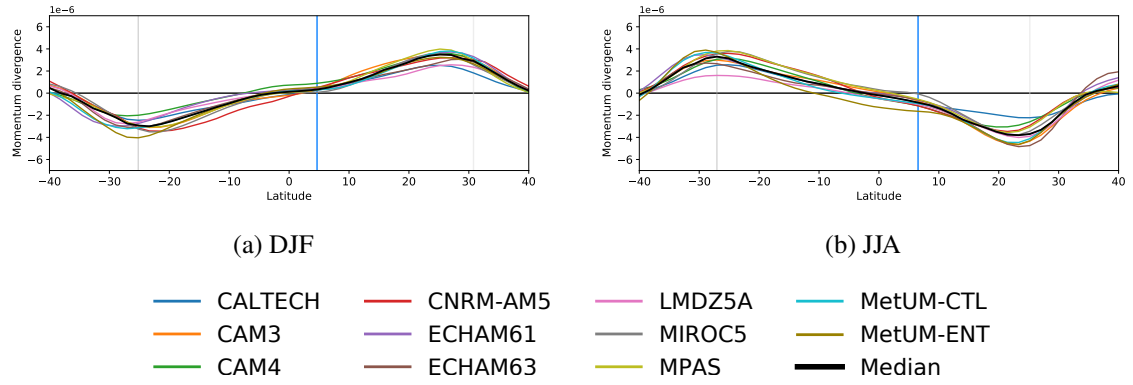

(a) DJF (b) JJA

Figure 6.19: Time tendency $\frac{\partial u}{\partial t}$ in the upper branch of the Hadley cell between 250 hPa and 150 hPa in $\mathrm{m\,s^{-2}}$ in seasons (a) December, January, February and (b) June, July, August. Bold black lines show the model median and simulations in colors according to the model used. Vertical blue lines represent the latitude of the common boundary of the two Hadley cells in the model median. Vertical grey lines indicate the poleward boundary of the respective Hadley cell in the model median. Note that the quantities on the y-axis are to the factor of 10^6 not 10^5 as the momentum flux divergence in Section 6.3.

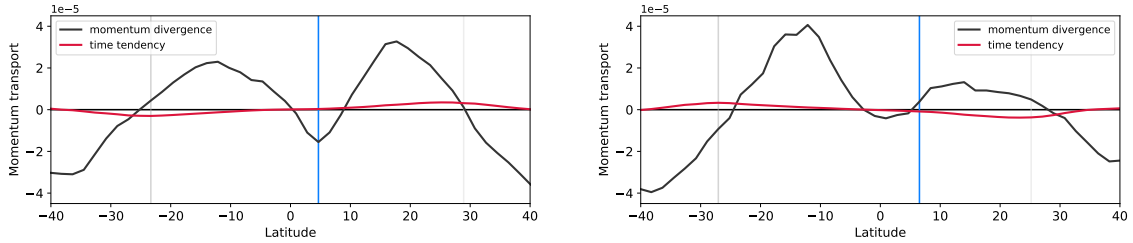

(a) DJF (b) JJA

Figure 6.20: Time tendency $\frac{\partial u}{\partial t}$ (red) in comparison to the total momentum flux divergence (black) in the model median.

significant impact on the Rossby number over the year but in August in the Northern Hemisphere. In August, the Northern Hemisphere Hadley cell mostly vanishes in many models. Thus, time tendency $\frac{\partial u}{\partial t}$ in the upper branch is strong. Furthermore, the minimum of time tendency coincides with the location of the maximum Rossby number. To illustrate this coincidence, Figure 6.21b shows the mass streamfunction and time tendency for the August in CAM 3, the model with the strongest influence of $\frac{\partial u}{\partial t}$ on the upper branch of the Hadley cell.

The influence of time tendency on *Ro* in the Northern Hemisphere is uncertain. In any case, time tendency takes away from the eddy influence in every model. Yet the assumption that time tendency is not important in regards to *Ro* is valid. Therefore, the influence of time tendency on *Ro* is assumed to be zero in both hemispheres for all months.

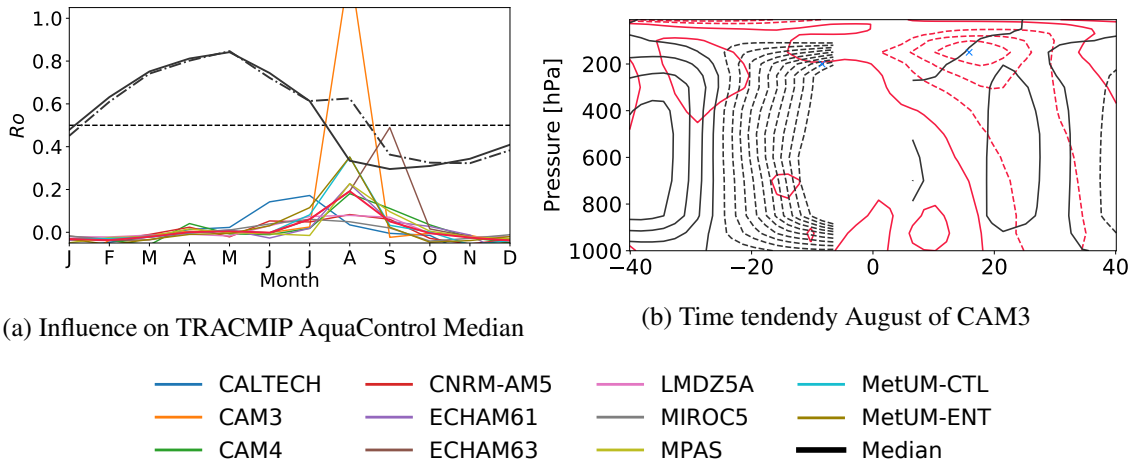

(a) Influence on TRACMIP AquaControl Median

(b) Time tendendy August of CAM3

Figure 6.21: The influence of time tendency $\frac{\partial u}{\partial t}$ on *Ro*. (a) the *Ro* median (solid black), the median of local Rossby number corrected for the time tendency (dotted black), the median of time tendency contribution (red solid) and the time tendency contribution for each model (other colors solid) . (b) The mass streamfunction (black contours) and time tendency (red contours) in August of CAM 3. Solid and dashed contours represent positive and negative values, respectively. This plot aims to give a qualitative understanding of the peak in Figure 6.21a.

6.5 Decomposition of the Mass Streamfunction Ψ

The mass streamfunction can be decomposed into a component that is connected to **E** and one that is connected to **M** (Figure 6.22). As discussed in previous sections (Sec. 6.2 to Sec.6.4), eddy influence is stronger at the poleward edges of the Hadley cell, while the divergence of momentum flux by the mean meridional circulation is more relevant towards the common border of both Hadley cells. Accordingly, the maximum of the mass streamfunction due to **E** is poleward of the total mass streamfunction's maximum, while the maximum of the mass streamfunction due to **M** is closer to the equator (Figure 6.22b). The solution of the decomposition becomes inaccurate in proximity to the surface, where friction plays an important role in the momentum balance which is neglected in this decomposition. Consequently, the contours of the decomposed mass streamfunction do not close (Figure 6.22b), as opposed to the native mass streamfunction 6.22a.

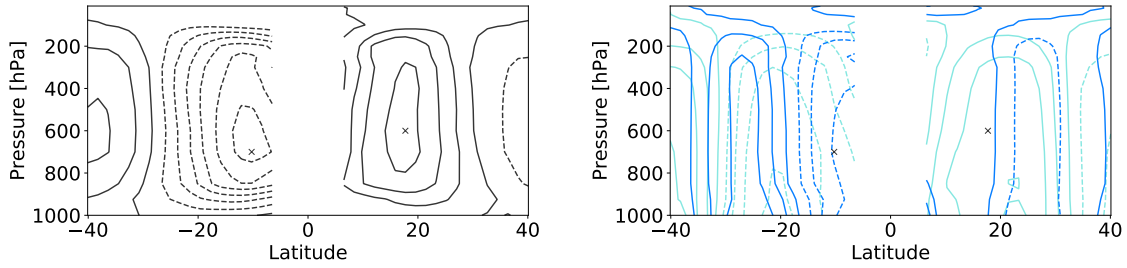

(a) Mass streamfunction Ψ

(b) Decomposition Ψ_M and Ψ_E

Figure 6.22: Model median of the annual mean for the maximum of the mass streamfunction (left) and the corresponding fractions of the mass streamfunction driven by eddies (turquoise) and by the mean meridional circulation (blue) in contour steps 20×10^9 kg s^{-1} (right). Solid and dashed contours represent positive and negative values, respectively. Black crosses mark the positions of the mass streamfunction's maximum shown in Figure 6.22a. Values within 5° S/N cannot be calculated, because solutions become unstable within this range.

Additionally, the solution becomes unstable close to the equator, where the Coriolis parameter approaches zero $f \to 0$. Therefore, values within 5° S/N are deleted.

Over the year, the decompositon works reasonably well (Fig. 6.23). Thus, the sum of both components resembles the main features of native mass streamfunction. The contribution of eddies to the mass transport stays roughly constant throughout the year, compared to pronounced changes in the contribution of $\mathbf{M}$ in SON in the Southern or MAM in the Northern Hemisphere Hadley cell.

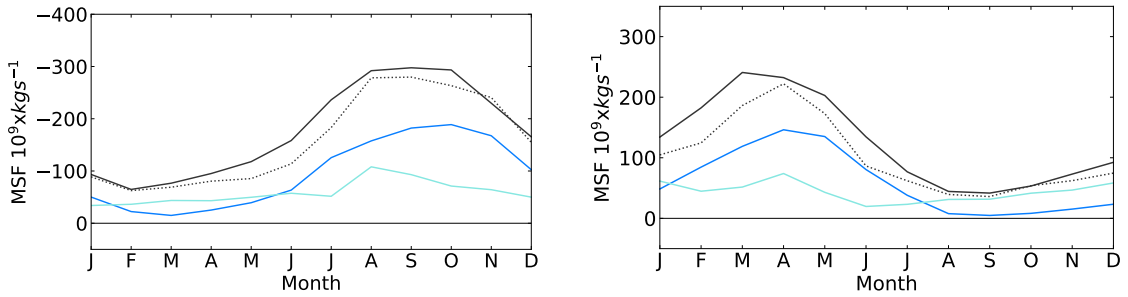

(a) Southern Hemisphere Hadley cell

(b) Northern Hemisphere Hadley cell

Figure 6.23: The evolution of the mass streamfunctions' strength (black) in 10^9 kg s^{-1} and its decomposition into a mass streamfunction driven by eddies (turquoise) and by the mean meridional circulation (blue) for the model median in (a) the Southern and (b) Northern Hemisphere Hadley cell (Fig. 6.23b). The black dotted line is the sum of the two components and indicated, inhowfar the decomposition represents the mass streamfunction as a whole.

In the Southern Hemisphere Hadley cell (Fig. 6.23a), the eddy driven component contributes more to the total mass streamfunction from February until May. In June and in January, the model median shows that the two components are equally strong. Yet from July to December, the Southern Hemisphere Hadley cell is driven by $\mathbf{M}$, since $\Psi_\mathbf{M}$ is much stronger than the eddy contribution $\Psi_\mathbf{E}$. The opposite pattern can be obtained for the Northern Hemisphere (Fig. 6.23b). The months August to December are eddy-driven and from February to June, the circulation is driven by the mean meridional circulation. The Southern Hemisphere Hadley cell is driven by the mean meridional circulation for one month longer (6 months), while the Northern Hemisphere Hadley cell is driven by eddies for one additional month.

The decomposition also successfully reproduces the seasonal cycle of the mass streamfunction's maximum for all models. However, this ranges from models representing the full strength of the mass streamfunction like MPAS (cf. Figure 6.24a and Figure 6.24b) to models like MetUM-ENT (cf. Figure 6.24c and Figure 6.24d) which only reproduce the shape but not the strength of the mass streamfunction. Since values are taken at only one point, local disturbances can severely influence the analysis. While all fields of $\Psi_\mathbf{M}$ and $\Psi_\mathbf{E}$ are smooth in CALTECH, MPAS produces an inhomogeneous $\Psi_\mathbf{E}$ field near the equator. Negative values are a local signal in June in the Northern Hemisphere Hadley cell. Only one 2° (one data step) poleward, the values turn positive. To test, whether or not the misfit in some models is caused by assumptions taken in this study, the following two subsections focus on two potential error sources: the assumption of a steady state (Section 6.5.1) and the assumption that vertical momentum transport is negligible (Section 6.5.2).

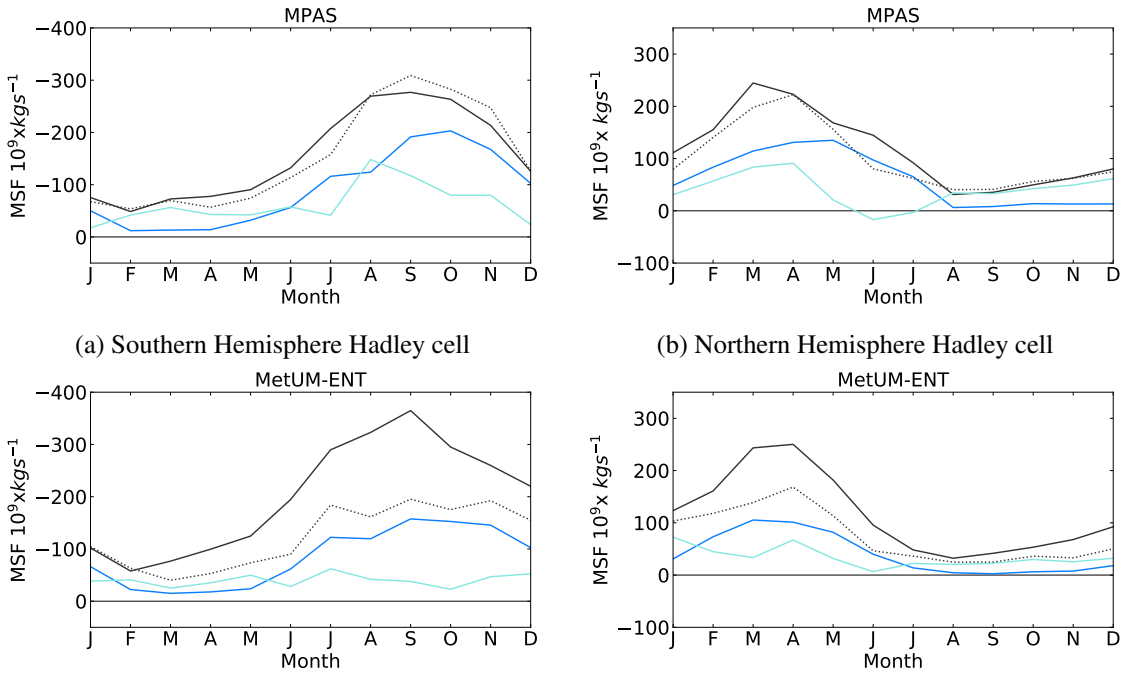

(a) Southern Hemisphere Hadley cell

(b) Northern Hemisphere Hadley cell

(c) Southern Hemisphere Hadley cell

(d) Northern Hemisphere Hadley cell

Figure 6.24: The evolution of the mass streamfunctions' strength (black) in $10^9\,\mathrm{kg\,s^{-1}}$ and its decomposition into a mass streamfunction driven by eddies (turquoise) and by the mean meridional circulation (blue) for MPAS (upper row) and MetUM-ENT (lower row) in the Southern (left column) and Northern Hemisphere Hadley cell (right column). The black dotted line is the sum of the two mass streamfunction's components and indicates, inhowfar the decomposition represents the mass streamfunction as a whole.

6.5.1 The Influence of Time Tendency on the Decomposition of the Mass Streamfunction within Seasons and Months

This subsection is dedicated to the influence of time tendency on the decomposition of the mass streamfunction, or in short, on whether or not the assumption of a steady state is valid for this method. The general properties of time tendency $\frac{\partial u}{\partial t}$ have already been presented in Section 6.4.1. To investigate the influence of time tendency on the decomposition of the mass streamfunction, Equation 4.21 has been defined in Chapter 4 as a component of the mass streamfunction which is driven by time tendency $\Psi_{\frac{\partial u}{\partial t}}$.

The decomposition of the mass streamfunction is not as sensible to $\frac{\partial u}{\partial t}$ as Ro. There is a very small contribution of time tendency $\Psi_{\frac{\partial u}{\partial t}}$ in the transitional season JJA in the Southern Hemisphere Hadley cell in the model median, as well as in all models individually. In the Northern Hemisphere, time tendency has the strongest influence in March and August in the model median and in many individual models.

MPAS (cf. Figure 6.25c and Figure 6.25d) and CAM 4 show the largest contribution of $\Psi_{\frac{\partial u}{\partial t}}$ and behave very similar. The influence is especially strong in the months in which the respective cell is strengthening. In a strengthening Hadley cell (e.g. July for the Southern Hemisphere Hadley cell), the influence of the time tendency additionally strengthens the Hadley cell. But as the cell reaches its maximum strength (e.g. September for the Southern Hemisphere Hadley cell), time tendency weakens the circulation. In line with the results for the influence of time tendency on the local

Rossby number, $\Psi_{\frac{\partial u}{\partial t}}$ weakens the Northern Hemisphere Hadley cell model median in August, but the influence is far less dramatic here.

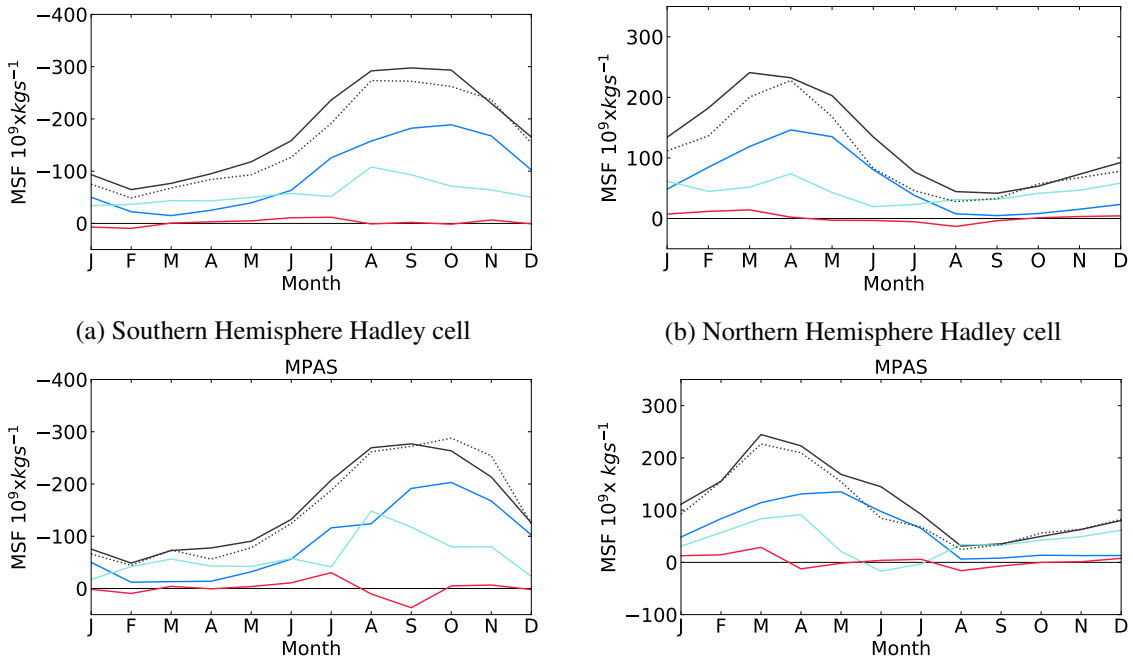

(a) Southern Hemisphere Hadley cell

(b) Northern Hemisphere Hadley cell

(c) SH Hadley cell in MPAS

(d) NH Hadley cell in MPAS

Figure 6.25: Decomposition of the mass streamfunction including time tendency $\frac{\partial u}{\partial t}$ (red). The other colors are chosen as in Figure 6.23

The role of time tendency is small compared to other terms of the zonal momentum budget. It contributes minimally during the strengthening of both Hadley cells respectively, and when the Northern Hemisphere Hadley cell vanishes almost completely, in most models in August. Since the influence of the tendency $\Psi_{\frac{\partial u}{\partial t}}$ is relatively weak, for the purpose of this thesis it is considered negligible.

6.5.2 The Role Vertical Momentum Transport and its Divergence

The decomposition of the mass streamfunction as defined in Equation 4.13 in Chapter 4 neglects the influence of vertical momentum flux divergence. It is assumed that the circulation is meridional above the maximum of the mass streamfunction. Therefore, vertical momentum flux divergence must be much smaller than the meridional momentum divergence. To investigate this assumption, the vertical momentum transport $[\overline{u\omega}]$ and its divergence $\mathbf{V}$ are calculated for each months.

In the model median, vertical momentum transport is smaller by one order of magnitude than meridional momentum transport $[\overline{uv}]$. In the annual mean, the strongest vertical momentum transport in the tropics occurs at the common border of the two Hadley cells and at their poleward edge (c.f. Figure 6.26). While vertical momentum transport in the deep tropics is positive and homogeneous throughout the atmospheric column, at the poleward edges of the respective Hadley cell $[\overline{u\omega}]$ reaches only from the upper to the mid-troposphere.

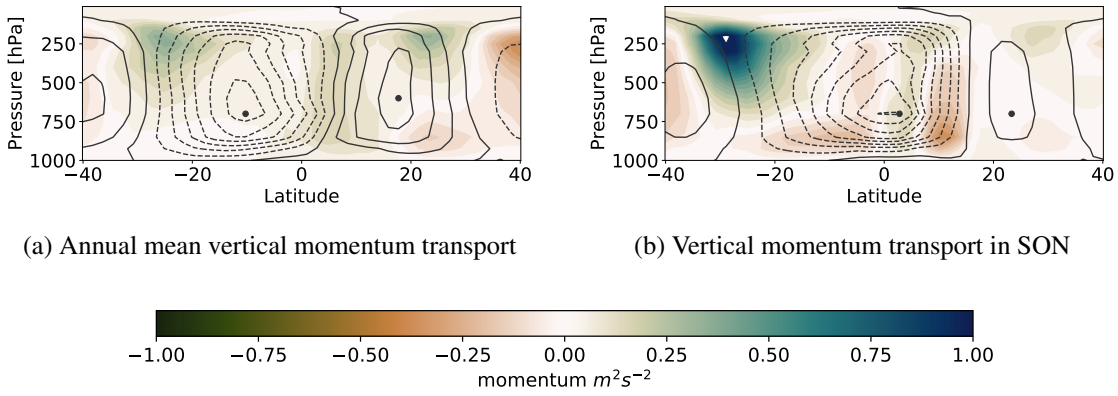

(a) Annual mean vertical momentum transport

(b) Vertical momentum transport in SON

Figure 6.26: Model median of vertical momentum transport in (a) the annual mean (left) and (b) months September, October and November (SON). The black contours show the mass streamfunction in $20 \times 10^9\,\mathrm{kg\,s^{-1}}$ in (a) and $40 \times 10^9\,\mathrm{kg\,s^{-1}}$ in (b). Dashed and solid lines represent negative and positive values, respectively.

Over the seasonal cycle, $[\overline{u\omega}]$ fluctuates strongly at the poleward edge changes of the Hadley cell. Moreover, $[\overline{u\omega}]$ seems to scale with the strength of the Hadley cell.

It is noteworthy, that the vertical momentum transport $[\overline{u\omega}]$ in the ascending branch of the Southern Hemisphere Hadley cell in SON stands apart from $[\overline{u\omega}]$ in the other seasons. As the Hadley cell's ascending branch migrates farther poleward, it leaves the region of westward wind. Therefore, the $[\overline{u\omega}]$ in this branch is split in a southern part with positive $[\overline{u\omega}]$ and a northern part with negative $[\overline{u\omega}]$ (c.f. Figure 6.26b). This would have no impact on vertical momentum flux divergence $\mathbf{V}$, if the line of zero momentum transport was not slanted. But since this is the case, $\mathbf{V}$ is amplified. In the other seasons, there is only one branch of positive $[\overline{u\omega}]$.

The contribution of vertical momentum to the momentum budget is accurately quantified by the divergence of vertical momentum flux $\mathbf{V}$ compared to its meridional counterpart. The meridional momentum flux divergence in the model median is of the same order of magnitude as $\mathbf{V}$ at the poleward edges of the Hadley cells and near the surface (c.f. Figure 6.27a in comparison with

Figure 6.11a). Additionally, **V** cannot be neglected in the Southern Hemispheric Hadley cell's ascending area in SON for the same reason stated in the previous paragraph (Figure 6.27b).

V is especially strong near the surface in SON. Another local peak can be found at the top of the ascending branch which could counteract the convergence of meridional momentum flux (cf. Figure 6.27b in comparison with the meridional momentum flux divergence in SON from Figure 6.13, Column Total).

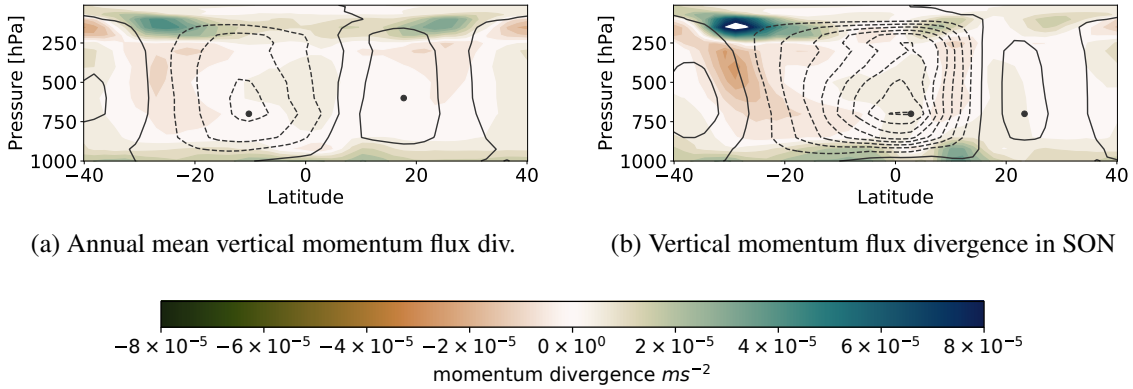

(a) Annual mean vertical momentum flux div.

(b) Vertical momentum flux divergence in SON

Figure 6.27: Model median of vertical momentum flux divergence in (a) the annual mean and (b) September, October, November (SON). The black contours show the mass streamfunction in $40\times10^{9}\,\mathrm{kg\,s^{-1}}$. Dashed and solid lines represent negative and positive values, respectively.

To quantify the influence of **V** on the mass transport, a decomposition of the mass streamfunction including a term of vertical momentum transport $\Psi_{\mathbf{V}}$ was defined as Equation 4.25. The contribution of **V** to the mass transport of the Hadley cell is the strongest, while the Hadley cell is cross-equatorial (cf. Figure 6.28a and Figure 6.28b). In the model median, $\Psi_{\mathbf{V}}$ slows the mass transport down in the Southern Hemisphere Hadley cell during the months in which the Hadley cell is strong. In the Northern Hemisphere Hadley cell the peak of the mass streamfunction is more distinct. Thus, the same effect as in the Southern Hemisphere occurs in April only. As opposed to the pattern in the Southern Hemisphere, **V** intensifies the Northern Hemisphere Hadley cell in June (Figure 6.28b).

The models MPAS and CAM 4 not only show the largest influence of time tendency on the mass streamfunction $\Psi_{\frac{\partial u}{\partial t}}$ but also the largest influence of **V** in both hemispheres. The budget of MPAS is shown again in Figure 6.28c and Figure 6.28d. In the Southern Hemisphere Hadley cell of MPAS, **V** strengthens the Hadley cell only in January, when the strength of this Hadley cell rapidly decreases. From August to November when the mass transport of the Southern Hemisphere Hadley cell is intense, **V** weakens the Hadley cell. The influence of **V** on the Northern Hemispheric Hadley cell in MPAS decelerates the mass transport in March and slightly in April. Yet MPAS shows the most dramatic case of mass transport intensification by **V** in the Northern Hemisphere Hadley cell. **V** starts to contribute to the mass transport in May and continues to so until July, when this contribution even surpasses the contributions from **M** and **E**.

In conclusion, vertical momentum divergence cannot be neglected in the decomposition of the mass streamfunction, when it comes to the individual models. While the contribution is small in the model median, some models show a significant contribution from vertical momentum divergence for the cross-equatorial and the decaying Hadley cell which does not always coincide in time or sign with the contribution in other models of the ensemble.

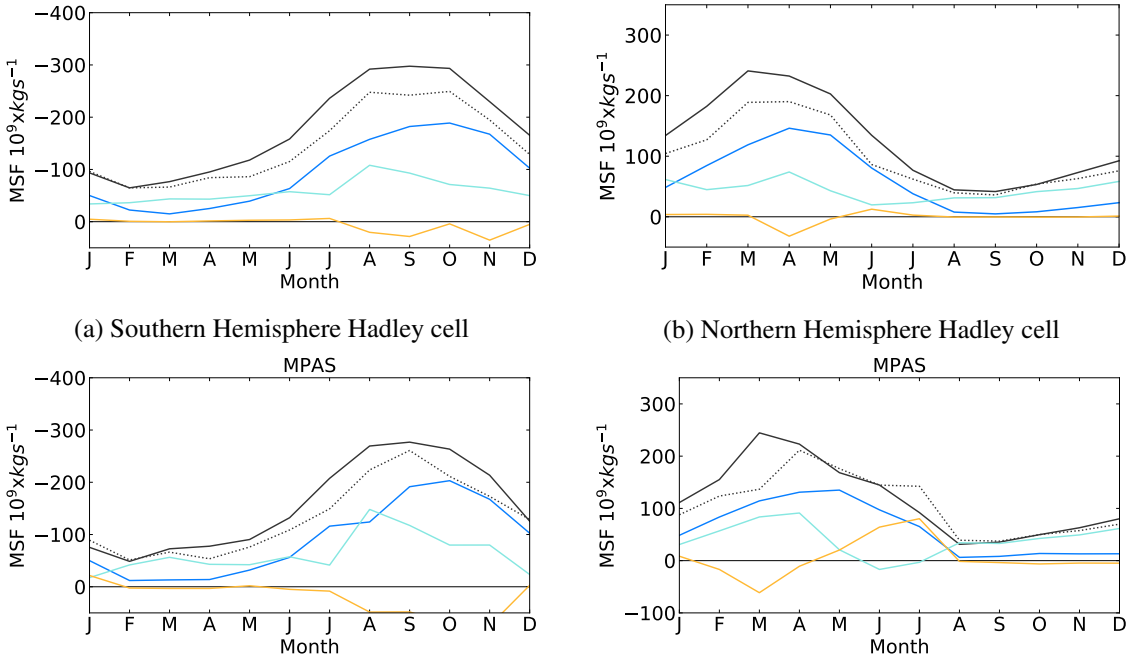

(a) Southern Hemisphere Hadley cell

(b) Northern Hemisphere Hadley cell

(c) SH Hadley cell in MPAS

(d) NH Hadley cell in MPAS

Figure 6.28: The decomposition of the mass streamfunction including vertical momentum: the contribution by the mean meridional circulation (blue), by eddies (turquoise) and by the vertical momentum (yellow) and the sum of all components(dotted black) in comparison to the mass streamfunction directly calculated from $[\bar{v}]$ (solid black).

6.5.3 An Index from the Decomposition of the Mass Streamfunction

As a consequence of the results from Section 6.5.2, decomposed **V** is included in further considerations of this chapter. In Chapter 4, a measure similar to *Ro* is derived from the decomposed mass streamfunction: Ind_Ψ. Figure 6.29 shows the model median of Ind_Ψ in TRACMIP AquaControl simulations. The black dot shows the maximum of the mass streamfunction outside the 5° S/N box, in which this value cannot be calculated. This is where the influence of $\mathbf{M} + \mathbf{V_M}$ on the Hadley cell is estimated. Again, results from this index are invalid close to the ground, as for the underlying decomposition and *Ro*.

The index shows a weak influence of eddies in the entire upper branch of the Hadley cell in almost every season. An exception can be found for the Northern Hemisphere Hadley cell in SON, where the index stays below $Ind_\Psi = 0.3$ in the model median (cf. Fig. 6.29, SON). The filled contours of Ind_Ψ are vertical, away from the upper branch of the Hadley cell and in most seasons close to the maximum mass streamfunction. This indicates that the influence of momentum flux divergence is rather small in the mid-troposphere. In the winter cells of MAM and SON, contour lines become slanted, indicating an eddy influence in the mid-troposphere which counteracts the strong influence of **M** in the upper branch of the Hadley cell. This effect is especially strong in the Southern Hemisphere Hadley cell in SON.

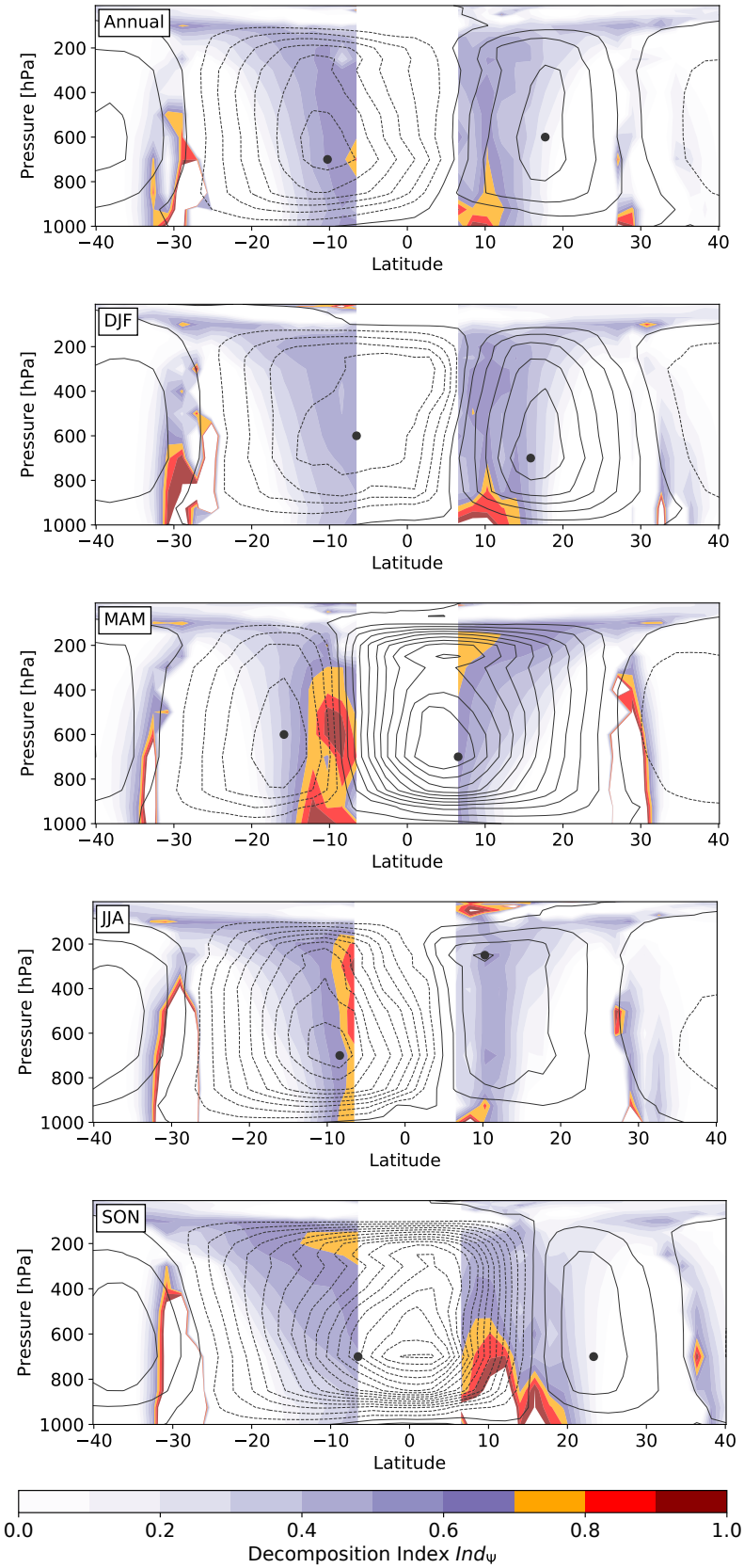

Figure 6.29: Model median of the index Ind_Ψ derived from the decomposition of the mass streamfunction (filled contours) and the mass streamfunction (grey contours, $20 \times 10^9\,\mathrm{kg\,s^{-1}}$) in the annual mean (Annual) and throughout the seasons (DJF, MAM, JJA, SON). Solid and dashed contours represent positive and negative values, respectively.

In the following, some differences between the measures R_0 and $Ind\Psi$ are discussed. The most prominent difference might be that this measure derives from vertically integrated quantities. In the annual mean, for example, the largest contribution to the mass streamfunction by **M** occurs around 300 hPa. But since there is no counteracting signal up to the point of measurement (black dot), the values stay the same. In contrast, $Ro \to 0$, when transport by the mean meridional circulation is at this height. Therefore, values from $Ind\Psi$ describe the conditions in the atmospheric column above this point, rather than the specific conditions at a certain height, as *Ro*. Secondly, values of $Ind\Psi$ are taken at another point than *Ro*. In some cases, the eddy influence in the mid-latitudes results in $Ind\Psi$ deviating from *Ro*, whereas they might have been similar if taken at the same point (cf. Fig. 6.29 in SON). Thus, $Ind\Psi$ is often a measure not only for conditions in the upper troposphere, but also includes signals from the mid-troposphere.

Figure 6.30 shows $Ind\Psi$ for every month and every model at the maximum of the mass streamfunction, apart from 5° S/N, and the model median for each month. Much like results for *Ro*, it shows a seasonal cycle with higher values, when the Hadley cell of the respective hemisphere is stronger, and lower values for weaker Hadley cells. Moreover, the seasonal cycle is more pronounced in the Northern Hemisphere in the model median. In contrast to *Ro*, the model spread of $Ind\Psi$ is much larger. While LMDZ5A generates comparable values for *Ro* and $Ind\Psi$ in both hemispheres, CNRM-AM 5 finds $Ind\Psi$ deviating strongly from *Ro* for August to November. These low values from CNRM-AM 5 are due to strong eddy influence in the mid-troposphere. Figure 6.31 shows $Ind\Psi$ in CNRM-AM 5 in September and July for comparison. In July, $Ind\Psi$ contours are vertical. This indicates that at the maximum of the mass streamfunction, $Ind\Psi$ mostly reflects conditions in the upper troposphere. But in September, the contours are slanted and almost horizontal, which indicates that eddy influence increases from the upper to the mid troposphere. Hence, $Ind\Psi$ reflects mid-troposphere conditions of CNRM-AM 5 for this month.

The index derived from the decomposition of the mass streamfunction $Ind\Psi$ closely relates the momentum budget to mass transport of the Hadley cell. Therefore, it contains additional information, as opposed to the rather abstract measure of the local Rossby number *Ro*. However, when using this index the model spread is much larger and the data of the individual models is more noisy than results for *Ro*.

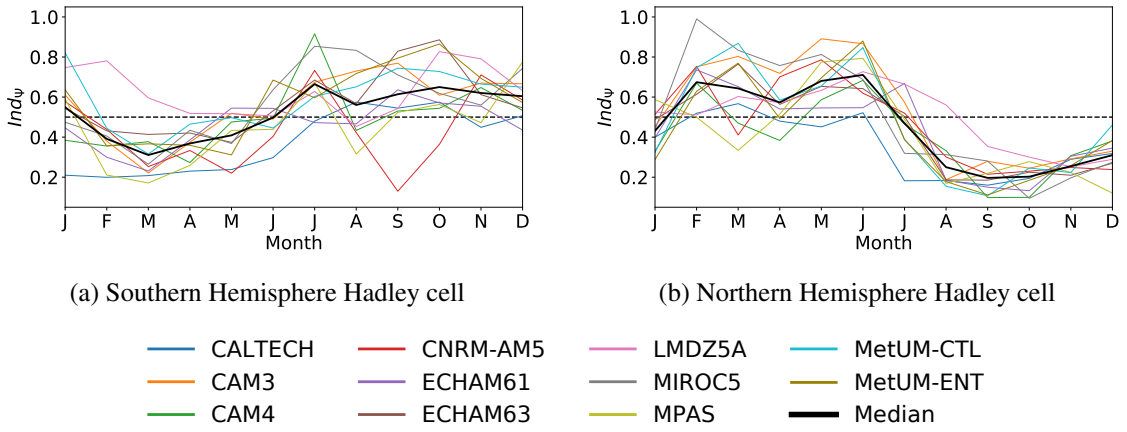

(a) Southern Hemisphere Hadley cell

(b) Northern Hemisphere Hadley cell

Figure 6.30: The evolution of the index derived from the decomposition of the mass streamfunction Ind_Ψ in the models and their median in the upper branch of the Southern Hemisphere (Fig. 6.23a) and Northern Hemisphere (Fig. 6.23b) Hadley cell. If the index exceeds $Ind_\Psi = 0.5$, the mass streamfunction is dominated by **M**.

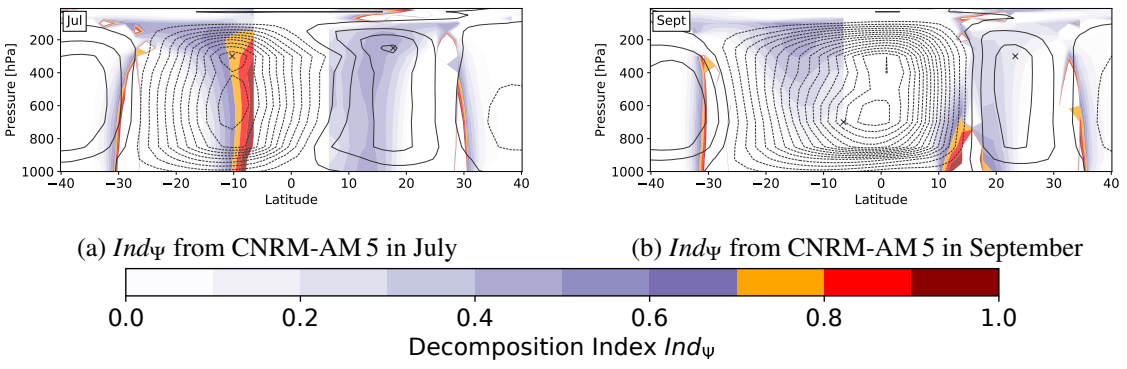

(a) Ind_Ψ from CNRM-AM 5 in July

(b) Ind_Ψ from CNRM-AM 5 in September

Figure 6.31: Comparison of Ind_Ψ in simulations with CNRM-AM 5 in (a) July vs. (b) September

7 Connections to the Energetic Framework

The aim of this chapter is to investigate inhowfar the eddy activity in the tropical momentum budget can explain deviations in this data set from the energetic framework throughout the seasonal cycle. Data for the zonal mean latitudinal ITCZ position δ and the cross-equatorial energy transport of the atmosphere $< \overline{vh} >_0$ are provided by Biasutti and Voigt (2019). Not all models included in Biasutti and Voigt (2019) are also part of this thesis. AM 2.1, GISS ModelE2 and CAM 5 Nor either do not provide the data fields required to investigate the momentum budget or provide erroneous data for the required variables. The ITCZ position is calculated as a centeroid of zonal-mean precipitation.

7.1 *Ro* in Connection with the Energetic Framework

Figure 7.1 is similar to Figure 2.2. It shows the data from TRACMIP AquaControl simulations included in this thesis. Each data point stands for one multiyear monthly mean in one simulation from one model. The color of each individual data point depends on the local Rossby number *Ro* in the Southern Hemisphere Hadley cell (SH) and the Northern Hemisphere Hadley cell (NH).

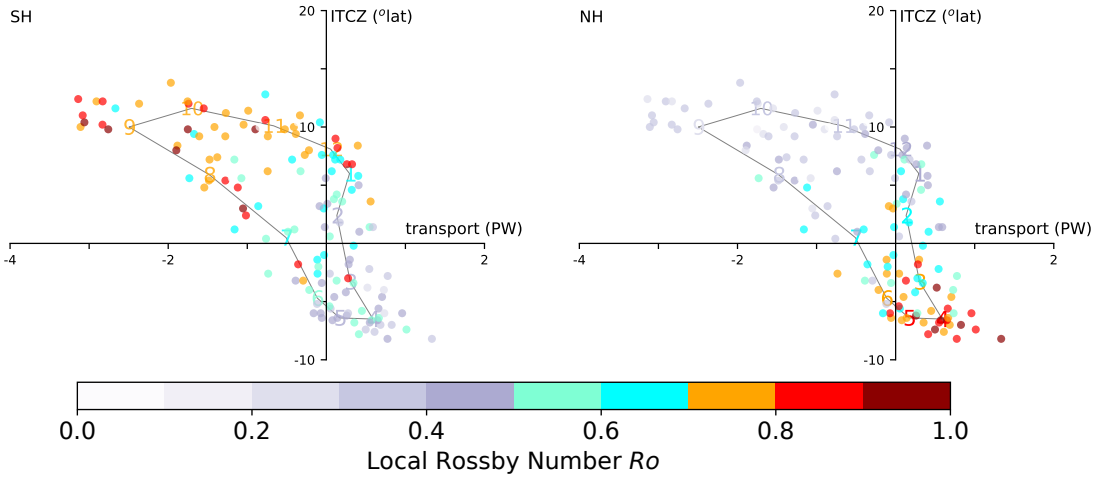

Figure 7.1: ITCZ position calculated as the centeroid of maximum precipitation and the cross-equatorial energy transport for simulations included in this thesis. The coloring is according to local Rossby number *Ro* for the Southern Hemisphere (left) and the Northern Hemisphere Hadley cell (right). Data for the ITCZ centeroid and the cross-equatorial energy transport were provided by Biasutti and Voigt (2019). Numbers indicate the months of the model median for January (1) to December (12).

Let's follow the seasonal cycle of the model median (colored numbers in Figure 7.1) to discuss some general points regarding the output from individual models. The seasonal cycle starts in

July, when the ITCZ migrates from the Southern to the Northern Hemisphere. *Ro* has already significantly increased from June to July in the strengthening Southern Hemisphere Hadley cell. It is the first month, in which it transports energy across the equator to the Southern Hemisphere, while the ITCZ is still located close to the equator.

From July to September, the ITCZ migrates farther into the Northern Hemisphere, as both cross-equatorial energy transport and mass transport by the Southern Hemisphere Hadley cell strengthen. *Ro* becomes larger than $Ro \geq 0.7$ in August, indicating that the eddies lost their influence on the dynamics of the Hadley cell. In September, energy transport into the Southern Hemisphere reaches its maximum.

From September to December, the ITCZ position shifts only slightly, but cross-equatorial energy transport decreases, until it ultimately vanishes in December. On the other hand, *Ro* stays constant during this period. Hence, the changes in cross-equational energy transport might not be connected to eddy influence, as measured by *Ro*. This decline is possibly connected to the emergence of shallow circulation. Such a circulation transports energy in the opposite direction of the Hadley cell. Therefore, vertically integrated energy transport vanishes at the equator. In December, the upper branch of the Hadley cell and the ITCZ are still situated far in the Northern Hemisphere, while the low-level mass transport of the Hadley cell terminates closer to the equator. The Hadley cell strength already decreased markedly compared to September.

From December to March, the Southern Hemisphere Hadley cell becomes very weak. This coincides with a rapid decline of *Ro* and a southward shift of the ITCZ. The ITCZ shifts from the Northern to the Southern Hemisphere from February to March. From March until June, *Ro* remains low in the Southern Hemisphere Hadley cell, indicating a strong influence of eddies.

The Northern Hemisphere Hadley cell goes through a similar seasonal cycle. As the ITCZ migrates southward from December to March, *Ro* increases to $Ro \geq 0.7$ and mass transport strengthens. In April, the Northern Hemisphere Hadley cell transports most energy into the Northern Hemisphere. This coincides with the least eddy influence on and the strongest mass transport by the Hadley cell. From April to May, the vertically integrated cross-equatorial mass transport vanishes, but *Ro* stays constant. This pattern is similar to the behaviour of the Southern Hemisphere Hadley cell from September to December. Therefore, the reasons behind the decline in cross-equatorial energy transport might be the same. Between May and August, the ITCZ migrates southward. The influence of eddies on the Northern Hemisphere Hadley cell increases, as *Ro* declines. Eddy influence remains high until December.

The ITCZ is situated in the Northern Hemisphere for eight months and stays in the Southern Hemisphere for only four months. *Ro* stays above $Ro \geq 0.7$ for five months in the Southern Hemisphere Hadley cell, as compared to four months in the Northern Hemisphere. This suggests a longer period, in which eddies are not relevant in the Southern Hemisphere Hadley cell, at least from a momentum perspective. In the transitioning months of January, February and July, eddies play an important role in both Hadley cells. Moreover, the retreating and weakening Hadley cell always has a small *Ro*, when the ITCZ is close to the equator, while the advancing and strengthening Hadley cell consistently shows high *Ro* within the same months.

Representation of the seasonal cycle differs among models. Figure 7.2, Figure 7.3 and Figure 7.3 show three markedly different examples. In CAM 3 (Fig. 7.2), the data points from March to September associated with high local Rossby numbers $Ro \geq 0.8$ either in the Northern or the

Southern Hemisphere Hadley cell line up. This suggests that the model adheres to the energetic framework, when eddy influence on the stronger Hadley cell is small.

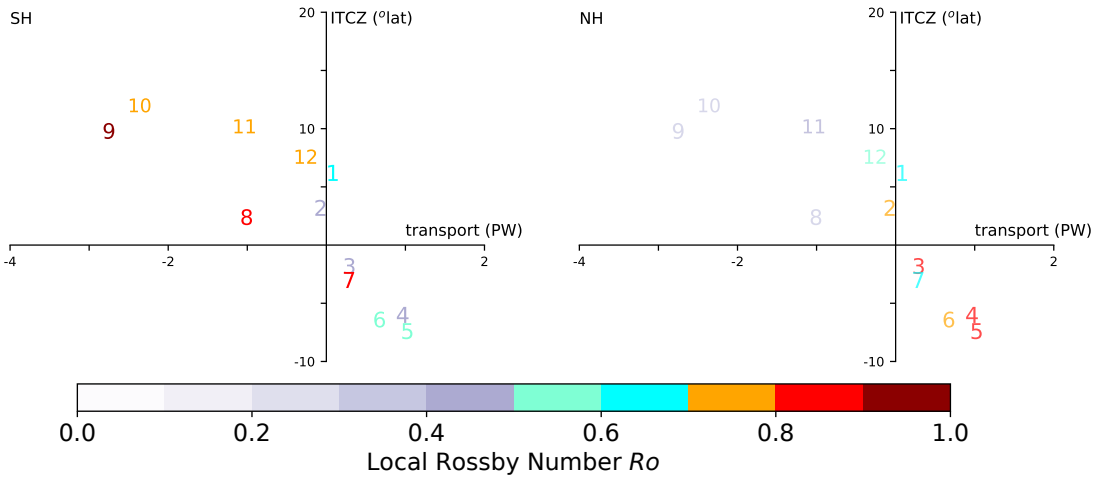

Figure 7.2: ITCZ position calculated as the centeroid of maximum precipitation and the cross-equatorial energy transport for CAM 3. The coloring is according to local Rossby number *Ro* for the Southern Hemisphere (left) and the Northern Hemisphere Hadley cell (right). Data for the ITCZ centeroid and the cross-equatorial energy transport were provided by Biasutti and Voigt (2019). The numbers stand for the months of the data point from January (1) to December (12).

Deviations from this line mostly occur, while the Southern Hemisphere Hadley cell determines the position of the ITCZ from September to February. From October to December, *Ro* is smaller than in September, but stays fairly stable, while the ITCZ position is virtually constant and cross-equatorial energy transport vanishes. From December to March, *Ro* declines in the Southern Hemisphere Hadley cell, while it increases in the Northern Hemisphere Hadley cell. In January, *Ro* is about the same in both Hadley cells. In February, *Ro* of the Northern Hemisphere Hadley cell already exceeds its Southern Hemisphere counterpart. This happens in spite of the ITCZ position still being in the Northern Hemisphere. Maybe this is a precondition for the ITCZ position to cross the equator. The results from CAM 3 therefore suggest that eddy influence on the Hadley cell does play a role between December and March. Moreover, the model adheres to the energetic framework, when eddy influence is exceptionally low in this model. From September to December, other mechanisms must play a role which decrease cross-equatorial transport in these months.

Cross-equatorial energy transport in MIROC 5 is much lower than in CAM 3, but the amplitude of *Ro* is larger (June $Ro \leq 0.4$ to August $Ro \geq 0.9$ in the Southern Hemisphere Hadley cell). From June to August, the ITCZ position also shifts from about 6° S to 3° N. *Ro* increases even faster in the Northern Hemisphere Hadley cell from January to March. Nevertheless, the months with $Ro \geq 0.8$ do not fall in one line as in CAM 3. Hence, in months with very limited eddy influence, *Ro* does not adhere to the linear relationship of the energetic framework.

The last example shows LMDZ5A (Fig. 7.4) which produces a stronger Hadley circulation than CAM 3 and MIROC 5, but shows a different seasonal cycle of *Ro*. In this simulation, *Ro* becomes large only in the Southern Hemisphere Hadley cell, shortly before the ITCZ starts to migrate equatorward in December and January. At least *Ro* decreases in the Southern Hemisphere Hadley cell and increases in its northern counterpart, as the ITCZ migrates more rapidly towards the equator in February and March. Yet this mechanism does not occur from May to July, as the

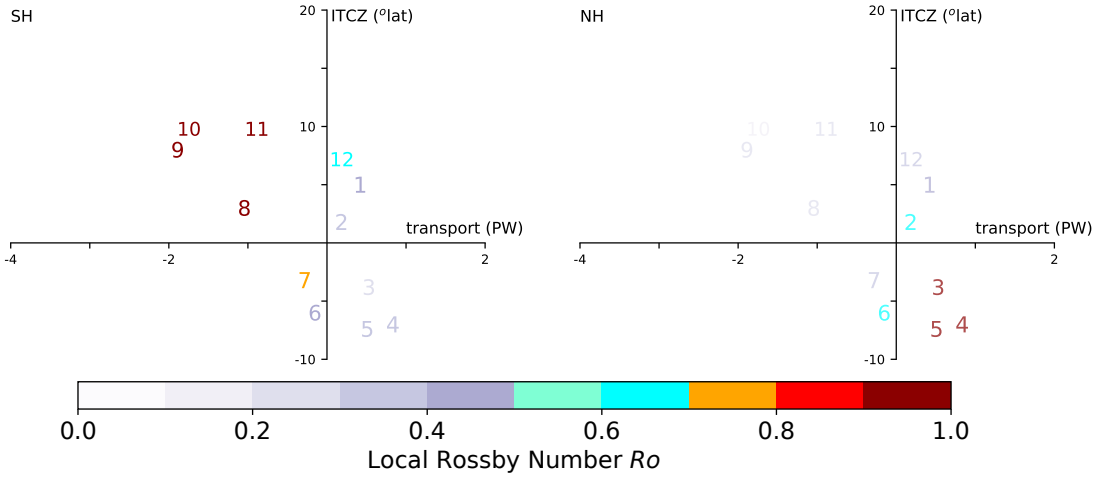

Figure 7.3: ITCZ position calculated as the centeroid of maximum precipitation and the cross-equatorial energy transport for MIROC 5. The coloring is according to local Rossby number *Ro* for the Southern Hemisphere (left) and the Northern Hemisphere Hadley cell (right). Data for the ITCZ centeroid and the cross-equatorial energy transport were provided by Biasutti and Voigt (2019). The numbers stand for the months of the data point from January (1) to December (12).

ITCZ shifts back to the Northern Hemisphere. There, *Ro* only reaches its peak in the Northern Hemisphere Hadley cell in June, when the ITCZ is already close to the equator.

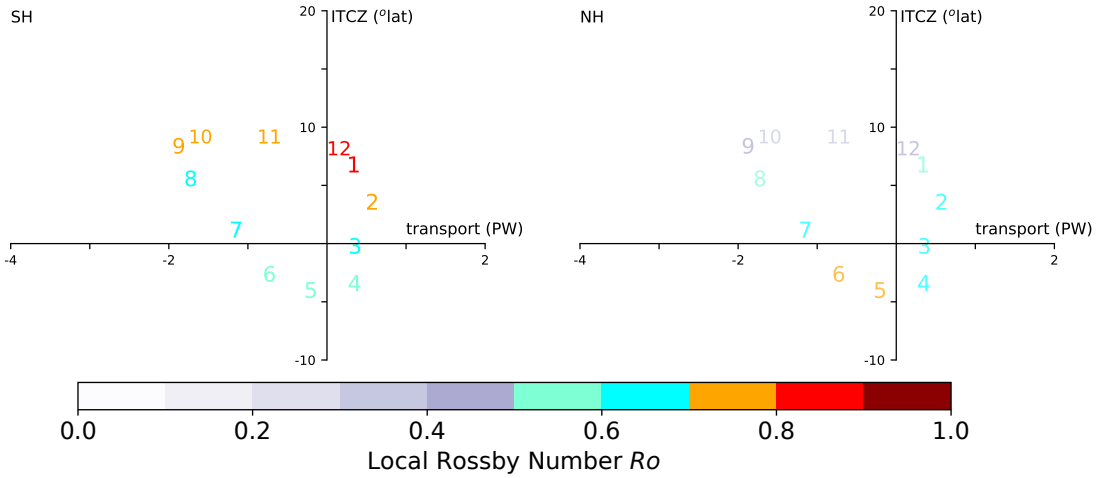

Figure 7.4: ITCZ position calculated as the centeroid of maximum precipitation and the cross-equatorial energy transport for LMDZ5A. The coloring is according to local Rossby number *Ro* for the Southern Hemisphere (left) and the Northern Hemisphere Hadley cell (right). Data for the ITCZ centeroid and the cross-equatorial energy transport were provided by Biasutti and Voigt (2019). The numbers stand for the months of the data point from January (1) to December (12).

Concluding, while the reduction of cross-equatorial heat transport is not connected to a changing eddy influence as measured by *Ro*, the shifts in the ITCZ from December to March and from June to September seem to be connected to changes in eddy influence in the model median, but not in LMDZ5A.

7.2 The Decomposition of the Mass Streamfunction and the Energetic Framework

The index derived from the decomposition of the mass streamfunction Ind_Ψ, as defined in Equation 4.16, is the second index for eddy influence on the Hadley cell. The results of this thesis for Ind_Ψ show a seasonal cycle which is less pronounced than for *Ro*. Additionally, the model spread of Ind_Ψ is larger (cf. Section 6.5.3). The aim of this section is to investigate, whether changes in Ind_Ψ are connected with deviations of the data set from the energetic framework in the model median and in specific models.

Figure 7.5 displays the seasonal cycle of simulation from the data set. Each dot represents on multiyear monthly mean of the ITCZ position and the cross-equatorial energy transport of one simulation from one model. The shading follows the according Ind_Ψ value for each data point.

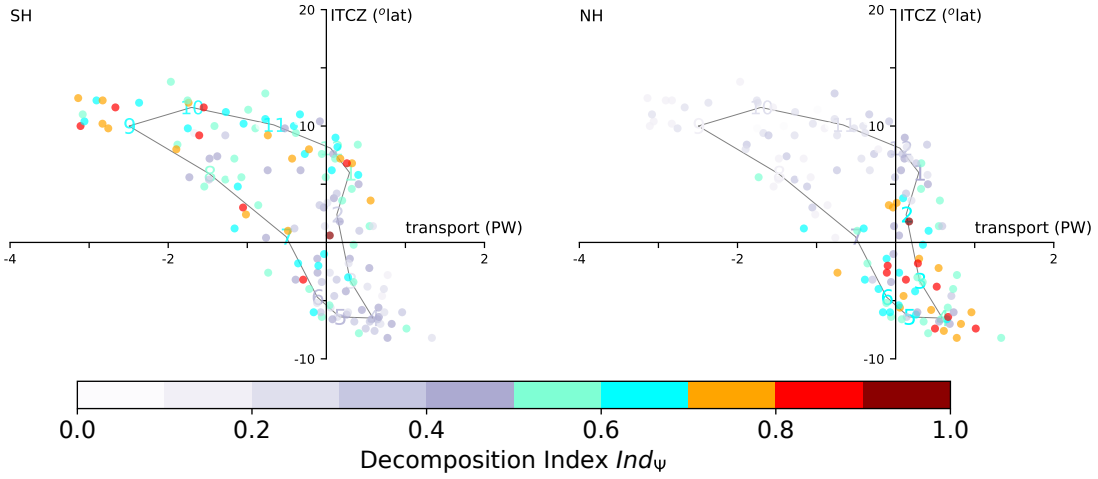

Figure 7.5: ITCZ position calculated as the centeroid of maximum precipitation and the cross-equatorial energy transport for simulations included in this thesis. The coloring is according to Ind_Ψ for the Southern Hemisphere (left) and the Northern Hemisphere Hadley cell (right). Data for the ITCZ centeroid and the cross-equatorial energy transport were provided by Biasutti and Voigt (2019). The numbers stand for the months of the model median from January (1) to December (12).

In the model median (colored numbers in Figure 7.5), the seasonal cycle of Ind_Ψ is similar to *Ro* but not as pronounced.

The Southern Hemisphere Hadley cell is driven by the mean meridional circulation from September to December. These are also the months of maximum excursion of the Hadley cell. From September to December, cross-equatorial energy transport decreases, while the Hadley cell is still predominantly driven by the mean flow. From December to March the Hadley cell retreats back to the Southern Hemisphere. In these months, eddy influence increases drastically. This is in line with the results from *Ro*. Curiously, in the month in which the Southern Hemisphere Hadley cell strengthens most rapidly, in July, eddy influence on the Hadley cell becomes suddenly weak, only to increase again in August.

In the model median, Ind_Ψ in the Northern Hemisphere Hadley cell increases from December to March, when the ITCZ shifts to the Southern Hemisphere and decreases from June to August when the ITCZ shifts back to the Southern Hemisphere, similar to *Ro*.

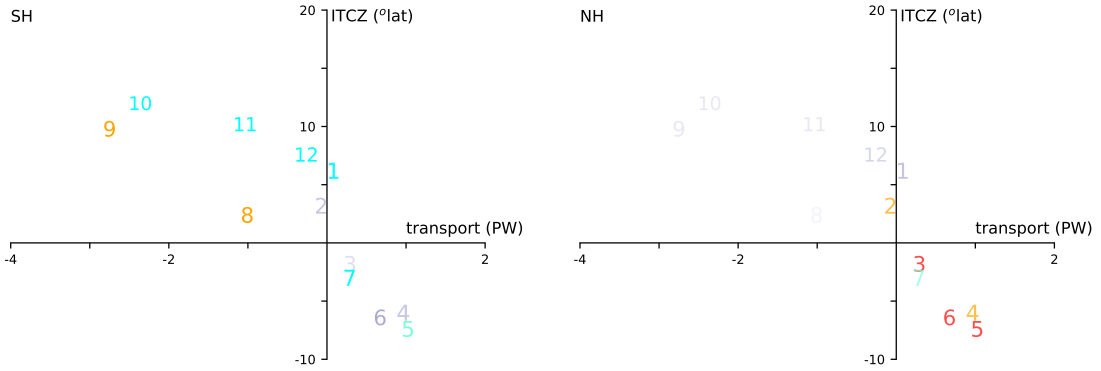

(a) CAM3

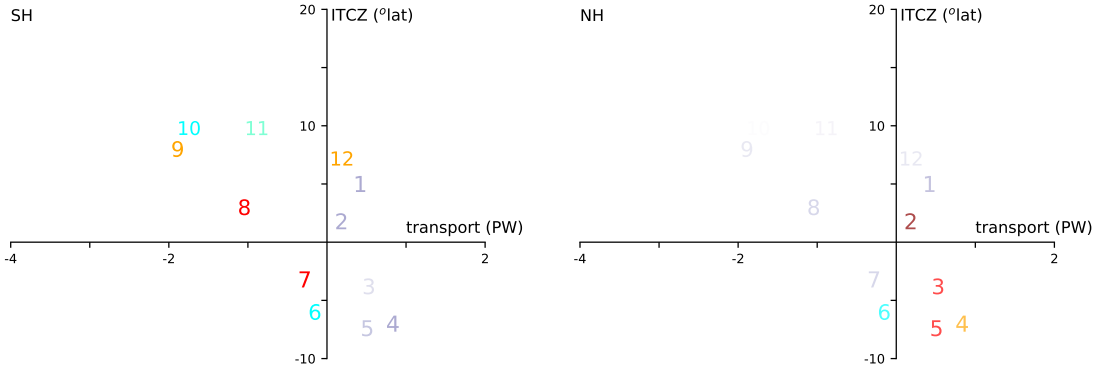

(b) MIROC5

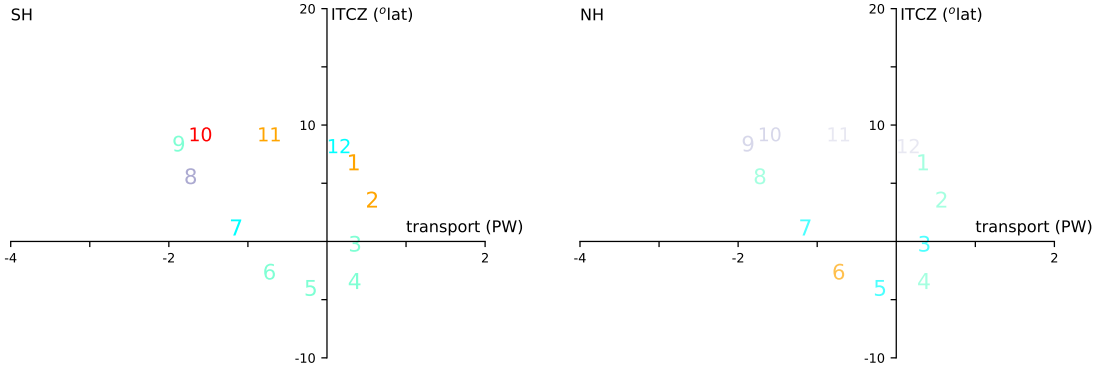

(c) LMDZ5A

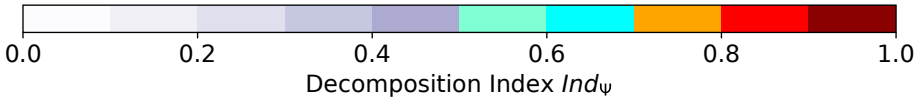

Figure 7.6: ITCZ position calculated as the centeroid of maximum precipitation and the cross-equatorial energy transport for CAM 3, MIROC 5, LMDZ5A. The coloring is according to Ind_Ψ for the Southern Hemisphere (left) and the Northern Hemisphere Hadley cell (right). Data for the ITCZ centeroid and the cross-equatorial energy transport were provided by Biasutti and Voigt (2019). Numbers stand for the months of the respective data point from January (1) to December (12).

$Ind\Psi$ predicts a strong influence of eddies in the Northern Hemisphere Hadley cell in April which is unlikely looking at the momentum divergence in the upper troposphere (cf. Section 6.3). Possibly, the influence of eddies on momentum flux divergence in the mid-troposphere is stronger, which leads to the discrepancy between $Ind\Psi$ and *Ro*.

Using the same three models as before in order to give an insight into the model spread and the differences between *Ro* and $Ind\Psi$, $Ind\Psi$ shows a similar pattern to *Ro* in CAM 3, only with a weaker seasonal cycle. Peculiar is the lower $Ind\Psi$ in April of the Northern Hemisphere Hadley cell. As opposed to this, MIROC 5 shows a very different pattern. In this model, $Ind\Psi$ decreases from September to November indicating an increase of eddy influence in the Southern Hemisphere Hadley cell during these months. Then in December, the Southern Hemisphere Hadley cell is mainly driven by the mean meridional circulation, only to become eddy-driven again in the following months. However, the eddy influence increases faster from January to February according to $Ind\Psi$ in comparison with *Ro*. In LMDZ5A, the pattern is similar to the *Ro*-pattern. With higher values and weaker eddy influence in seasons, in which the Hadley cell is weakening and the ITCZ is shifting back to the equator. A weak eddy influence in months in which the Hadley cell is retreating becomes more frequent than using *Ro*.

In conclusion, the picture from $Ind\Psi$ is not as clear as the results from R_0. This is not surprising, when one takes the results from the previous chapter into account. However, the model median is in line with the overall pattern from the previous section that eddy influence changes, as the ITCZ migrates from one hemisphere into the other from December to March and from June to September.

8 Conclusions

Climate change poses a challenge for the large share of the global population living in the tropics. Especially changes in precipitation patterns have adverse impacts on societies and economies in the region. The main source of precipitation in the tropics is connected to the ITCZ and its seasonal migration pattern. Yet the response of the ITCZ to climate change in simulations is uncertain. Putting a focus on theoretical considerations to better understand the underlying mechanisms of the ITCZ migration will also help to better understand the uncertainties in the simulations.

A lot of insight regarding tropical rainfall and its response to climate change can be gained by the energetic framework. However, in some cases (Biasutti et al., 2018; Wei and Bordoni, 2018; Biasutti and Voigt, 2019), some months of the seasonal cycle deviate from the energetic framework's assumptions (Kang et al., 2009; Frierson et al., 2013; Bischoff and Schneider, 2014; Schneider et al., 2014; Adam et al., 2016). Biasutti et al. (2018) hypothesize that these deviations could be due to the influence of eddies on Hadley cell. This thesis therefore studied the impact of eddies in the tropics using the TRACMIP AquaControl simulations. These are aquaplanet simulations under present-day conditions, with an implemented slab ocean and a q-flux to mimic the meridional ocean heat transport of the Earth's oceans. From a dynamical point of view, eddy influence on the Hadley cell lies somewhere between two extreme cases. One case describes a Hadley cell that is entirely driven by the momentum divergence of the mean meridional circulation which responds directly to thermal changes, similar to the model of (Held and Hou, 1980). In the other case, the Hadley cell is entirely driven by eddies. In this Hadley cell, energy transport is rather dependent on eddy activity than on thermodynamic variables. There is a set of indices and measures to describe in how far the Hadley cell resembles one case or the other, which are inferred from an analysis of the zonal momentum balance. Therefore this thesis took on the task of analyzing the zonal momentum balance of the data set in the annual mean and throughout the seasonal cycle.

The focus was the upper branch of the Hadley cell. In this area, eddies have the strongest influence on the Hadley cell. Two indices, the local Rossby number Ro and the fraction of the mass streamfunction driven by the mean meridional circulation Ind_Ψ, capture the eddy influence of the upper branch down as one number. When the indices have a value of zero, the Hadley cell is driven by eddies only. As these indices approach one, they increasingly resemble the dynamics of the Held and Hou model. Using this method, the thesis has addressed three questions, which can be answered as follows.

How does the meridional momentum budget look like in TRACMIP AquaControl in the annual mean and throughout the seasonal cycle?

In the TRACMIP simulations, in the annual mean momentum is transported meridionally from the Northern to the Southern Hemisphere across the equator in the upper troposphere. Throughout the

seasons, the cross-equatorial momentum transport switches its sign, so that it is in the direction of the summer hemisphere.

Meridional momentum flux divergence occurs in the upper branch and in the near-surface return flow of the Hadley cell, both in the annual mean and throughout the seasonal cycle. Near the surface, the annual mean momentum flux divergence shows three peaks in the tropics, connected to the Hadley cell. It shows momentum flux convergence in the near-surface return flow of the Hadley cell and momentum flux divergence below the ascending region at the equator. The strength of the peaks near the surface varies markedly throughout the seasons. In the boreal summer, the momentum flux convergence in the Northern Hemisphere vanishes and in the boreal winter the same pattern occurs in the Southern Hemisphere. Momentum flux divergence near the equator is especially strong in summer/winter seasons, as opposed to weak momentum flux divergence in the transitioning seasons of spring/autumn. The momentum flux divergence in the upper troposphere is stronger than near the surface and show the opposite pattern. There is momentum flux divergence in the tropical Southern and the Northern Hemisphere while momentum flux convergence can be found above the ascending region around the equator. The peaks may vary strongly in strength and also slightly in their position, but never vanish. In the annual mean, the strongest momentum flux divergence is reached in the upper branch of the Southern Hemisphere Hadley cell. The strongest momentum flux convergence occurs poleward of the strongest divergence in the Ferrell cell. Due to the low agreement among models, the model median may not adequately represent the whole ensemble.

How strong is the influence of eddy momentum transport on the Hadley cell in the annual mean and throughout the seasonal cycle? Is the influence robust across different models?

There is transient eddy momentum transport in the deep tropics. The eddy activity picks up in strong cross-equatorial Hadley cell but this might be connected to deviations in the meridional wind v' rather than to momentum deviations u', especially in the winter cell of the Southern Hemisphere. As opposed to this, some models (MPAS, CAM 4) show eddy activity in the deep tropics which originates there in March and June.

Eddy momentum flux divergence $\mathbf{E}$ is the quantity which directly connects eddies to the strength of the Hadley cell. In the summer cell, $\mathbf{E}$ outside of the deep tropics dominates the Hadley cell. In the winter cell, $\mathbf{E}$ in the deep tropics becomes especially strong for some models in boreal winter and in the model median in boreal summer. But still, momentum flux divergence by the mean meridional circulation $\mathbf{M}$ dominates the winter cell. In the boreal summer, deep tropical $\mathbf{E}$ amounts to about $1/3$ of $\mathbf{M}$. The agreement in the total momentum flux divergence is low which is mostly due to uncertainties in $\mathbf{M}$.

The angular momentum contours are slightly slanted in the model median which indicates weak eddy influence in the deep tropics. Additionally, the upper-tropospheric wind u_{up} is close to the angular momentum conserving wind u_M, at least in the boreal winter in the Northern Hemisphere. This indicates a weak influence of eddies in this region for this season. A opposed to this, u_{up} is farther away from u_M in the Southern Hemisphere in boreal summer which indicates a stronger eddy influence on the Southern than on the Northern Hemisphere winter cell.

The data set shows eddy momentum transport in the deep tropics. This does not have a large effect on the total momentum flux divergence as $\mathbf{M}$ is very strong in the winter cell, when eddy momentum transport occurs. However, the eddy momentum transport of the Ferrel cell does influence the momentum budget and dominates the summer cells. The local Rossby number *Ro* is high from boreal summer until autumn in the Southern Hemisphere. In the Northern Hemisphere Hadley cell, the local Rossby number is high from boreal autumn until the end of its winter. Eddy influence on momentum budget, as measured by *Ro*, can differ between models by factor 2.

Using the decomposition of the mass streamfunction from (Bordoni and Schneider, 2008), there is another useful indicator to describe eddy influence, Ind_Ψ. This indicator is similar to *Ro* when the Hadley cell is relatively weak. Yet it indicates a stronger influence of eddies on the strong Hadley cell in winter, when the Hadley cell's maximum lies within 5° S/N of where *Ro* and Ind_Ψ cannot be calculated. Eddy influence on momentum budget, as measured by *Ro*, can differ between models by factor 4.

When the energetic framework cannot successfully explain the position of the ITCZ, do eddies play a role?

The most prominent deviation from the energetic framework occurs in the ensemble of TRACMIP AquaControl simulations from September to March. From September to December the cross-equatorial energy transport declines, while the position of the ITCZ is virtually constant, and from December to March the ITCZ position changes, while the cross-equatorial energy transport is virtually constant. In the first period, from September to December, *Ro* remains high in the model median with $Ro \geq 0.7$ in the stronger Southern Hemisphere Hadley cell. This is in accordance with $Ind_\Psi \geq 0.5$ in these month for the same Hadley cell. Taking into account that the Southern Hemisphere is much stronger during these months and therefore dictates the ITCZ position, these results suggest that the cross-equatorial energy transport declines independently from the eddy influence. From December to March, *Ro* in the Southern Hemisphere Hadley cell declines (from $Ro \geq 0.4$ to $Ro \leq 0.4$) while it increases in the Northern Hemisphere (from $Ro \leq 0.5$ to $Ro \geq 0.7$). The model median of Ind_Ψ shows a similar pattern. Hence, the migration of the ITCZ from the Northern to the Southern Hemisphere is accompanied by a change in eddy influence in both Hadley cells. Therefore, eddies might be of importance to explain the deviations of this data set from the energetic framework. This might not be true for every model, since eddy influence is depicted differently in some models, but for the model median.

The deviation from the energetic framework from September to December might be connected to other mechanisms, i.e. the shallow convection. Another possibility could be that momentum eddies are not an appropriate proxy for eddy impact on energy transport in the tropics. Therefore, eddies should also be analyzed directly in the energy budget. Although, calculating the eddies of the energy budget is a difficult endeavour.

Bibliography

Adam, O., T. Bischoff, and T. Schneider, 2016: Seasonal and interannual variations of the energy flux equator and ITCZ. Part I: Zonally averaged ITCZ position. *Journal of Climate*, **29 (9)**, 3219–3230.

Adler, R. F., G. J. Huffman, A. Chang, R. Ferraro, P.-P. Xie, J. Janowiak, B. Rudolf, U. Schneider, S. Curtis, D. Bolvin, et al., 2003: The Version-2 Global Precipitation Climatology Project (GPCP) Monthly Precipitation Analysis (1979–Present). *Journal of Hydrometeorology*, **4 (6)**, 1147–1167.

Back, L. and C. Bretherton, 2006: Geographic Variability in the Export of Moist Static Energy and Vertical Motion Profiles in the Tropical Pacific. *Geophysical Research Letters*, **33 (17)**.

Biasutti, M. and A. Voigt, 2019: Seasonal and CO2-induced shifts of the ITCZ: testing energetic controls in idealized simulations with comprehensive models. *accepted: Journal of Climate*.

Biasutti, M., A. Voigt, W. R. Boos, P. Braconnot, J. C. Hargreaves, S. P. Harrison, S. M. Kang, B. E. Mapes, J. Scheff, C. Schumacher, A. H. Sobel, and S.-P. Xie, 2018: Global energetics and local physics as drivers of past, present and future monsoons. *Nature Geoscience*, **11 (6)**, 392–400.

Bischoff, T. and T. Schneider, 2014: Energetic Constraints on the Position of the Intertropical Convergence Zone. *Journal of Climate*, **27 (13)**, 4937–4951.

Bony, S., B. Stevens, D. M. Frierson, C. Jakob, M. Kageyama, R. Pincus, T. G. Shepherd, S. C. Sherwood, A. P. Siebesma, A. H. Sobel, et al., 2015: Clouds, circulation and climate sensitivity. *Nature Geoscience*, **8 (4)**, 261.

Bordoni, S. and T. Schneider, 2008: Monsoons as eddy-mediated regime transitions of the tropical overturning circulation. *Nature Geoscience*, **1 (8)**, 515.

Byrne, M. P., A. G. Pendergrass, A. D. Rapp, and K. R. Wodzicki, 2018: Response of the intertropical convergence zone to climate change: Location, width, and strength. *Current Climate Change Reports*, **4 (4)**, 355–370.

Caballero, R., 2008: Hadley cell bias in climate models linked to extratropical eddy stress. *Geophysical Research Letters*, **35 (18)**.

Collins, W. D., P. J. Rasch, B. A. Boville, J. J. Hack, J. R. McCaa, D. L. Williamson, B. P. Briegleb, C. M. Bitz, S.-J. Lin, and M. Zhang, 2006: The formulation and atmospheric simulation of the Community Atmosphere Model version 3 (CAM3). *Journal of Climate*, **19 (11)**, 2144–2161.

Dima, I. M. and J. M. Wallace, 2003: On the seasonality of the Hadley cell. *Journal of the Atmospheric Sciences*, **60 (12)**, 1522–1527.

Donohoe, A., D. M. W. Frierson, and D. S. Battisti, 2014: The effect of ocean mixed layer depth on climate in slab ocean aquaplanet experiments. *Climate Dynamics*, **43 (3-4)**, 1041–1055.

Donohoe, A. and A. Voigt, 2017: Why future shifts in tropical precipitation will likely be small: the location of the tropical rain belt and the hemispheric contrast of energy input to the atmosphere. *Climate Extremes: Patterns and Mechanisms*, **226**, 115.

Edelman, A., A. Gelding, E. Konovalov, R. McComiskie, A. Penny, N. Roberts, S. Templeman, D. Trewin, M. Ziembicki, B. Trewin, et al., 2014: State of the tropics 2014 report.

Eyring, V., S. Bony, G. A. Meehl, C. A. Senior, B. Stevens, R. J. Stouffer, and K. E. Taylor, 2016: Overview of the Coupled Model Intercomparison Project Phase 6 (CMIP6) experimental design and organization. *Geoscientific Model Development*, **9 (5)**, 1937–1958.

Frierson, D. M. W., Y.-T. Hwang, N. S. Fučkar, R. Seager, S. M. Kang, A. Donohoe, E. A. Maroon, X. Liu, and D. S. Battisti, 2013: Contribution of ocean overturning circulation to tropical rainfall peak in the Northern Hemisphere. *Nature Geoscience*, **6 (11)**, 940–944.

Held, I. M. and A. Y. Hou, 1980: Nonlinear Axially Symmetric Circulations in a Nearly Inviscid Atmosphere. *Journal of the Atmospheric Sciences*, **37 (3)**, 515–533.

Hide, R., 1969: Dynamics of the atmospheres of the major planets with an appendix on the viscous boundary layer at the rigid bounding surface of an electrically-conducting rotating fluid in the presence of a magnetic field. *Journal of the Atmospheric Sciences*, **26 (5)**, 841–853.

Hill, S. A., S. Bordoni, and J. L. Mitchell, 2019: Axisymmetric constraints on cross-equatorial Hadley cell extent. *Journal of the Atmospheric Sciences*, **76 (6)**, 1547–1564.

Holton, J. R. and G. J. Hakim, 2012: *An Introduction to Dynamic Meteorology*, Vol. 88. Academic Press.

Hourdin, F., M.-A. Foujols, F. Codron, V. Guemas, J.-L. Dufresne, S. Bony, S. Denvil, L. Guez, F. Lott, J. Ghattas, et al., 2013: Impact of the lmdz atmospheric grid configuration on the climate and sensitivity of the ipsl-cm5a coupled model. *Climate Dynamics*, **40 (9-10)**, 2167–2192.

Kallberg, P., A. Simmons, S. Uppala, and M. Fuentes, 2004: ERA-40 project report series: 17. The ERA-40 archive. ECMWF. *Reading, Berkshire, UK*.

Kang, S. M., D. M. Frierson, and I. M. Held, 2009: The tropical response to extratropical thermal forcing in an idealized GCM: The importance of radiative feedbacks and convective parameterization. *Journal of the Atmospheric Sciences*, **66 (9)**, 2812–2827.

Lee, S., 1999: Why Are the Climatological Zonal Winds Easterly in the Equatorial Upper Troposphere? *Journal of the Atmospheric Sciences*, **56 (10)**, 1353–1363.

Levine, X. J. and T. Schneider, 2015: Baroclinic eddies and the extent of the Hadley circulation: An idealized GCM study. *Journal of the Atmospheric Sciences*, **72 (7)**, 2744–2761.

Lindzen, R. S. and A. V. Hou, 1988: Hadley circulations for zonally averaged heating centered off the equator. *Journal of the Atmospheric Sciences*, **45 (17)**, 2416–2427.

Neale, R. B., J. Richter, S. Park, P. H. Lauritzen, S. J. Vavrus, P. J. Rasch, and M. Zhang, 2013: The mean climate of the Community Atmosphere Model (CAM4) in forced SST and fully coupled experiments. *Journal of Climate*, **26 (14)**, 5150–5168.

Neelin, J. D. and I. M. Held, 1987: Modeling Tropical Convergence Based on the Moist Static Energy Budget. *Monthly Weather Review*, **115 (1)**, 3–12.

Olhoff, A. and J. M. Christensen, 2018: Emissions Gap Report 2018.

O'Gorman, P. A. and T. Schneider, 2008: The hydrological cycle over a wide range of climates simulated with an idealized GCM. *Journal of Climate*, **21 (15)**, 3815–3832.

Peixoto, J. and A. Oort, 1992: *Physics of Climate*. New York, NY (United States); American Institute of Physics.

Rose, B. E., K. C. Armour, D. S. Battisti, N. Feldl, and D. D. Koll, 2014: The dependence of transient climate sensitivity and radiative feedbacks on the spatial pattern of ocean heat uptake. *Geophysical Research Letters*, **41 (3)**, 1071–1078.

Schneider, T., 2006: The General Circulation of the Atmosphere. *Annual Review of Earth and Planetary Sciences*, **34 (1)**, 655–688.

Schneider, T., T. Bischoff, and G. H. Haug, 2014: Migrations and dynamics of the intertropical convergence zone. *Nature*, **513 (7516)**, 45–53.

Simpson, I. R., T. A. Shaw, and R. Seager, 2014: A Diagnosis of the Seasonally and Longitudinally Varying Midlatitude Circulation Response to Global Warming*. *Journal of the Atmospheric Sciences*, **71 (7)**, 2489–2515.

Singh, M. S., Z. Kuang, and Y. Tian, 2017: Eddy influences on the strength of the Hadley circulation: Dynamic and thermodynamic perspectives. *Journal of the Atmospheric Sciences*, **74 (2)**, 467–486.

Skamarock, W. C., J. B. Klemp, M. G. Duda, L. D. Fowler, S.-H. Park, and T. D. Ringler, 2012: A multiscale nonhydrostatic atmospheric model using centroidal Voronoi tesselations and C-grid staggering. *Monthly Weather Review*, **140 (9)**, 3090–3105.

Stevens, B., M. Giorgetta, M. Esch, T. Mauritsen, T. Crueger, S. Rast, M. Salzmann, H. Schmidt, J. Bader, K. Block, et al., 2013: Atmospheric component of the MPI-M earth system model: ECHAM6. *Journal of Advances in Modeling Earth Systems*, **5 (2)**, 146–172.

Vallis, G. K., 2006: *Atmospheric and Oceanic Fluid Dynamics*. Cambridge University Press.

Voigt, A., M. Biasutti, J. Scheff, J. Bader, S. Bordoni, F. Codron, R. D. Dixon, J. Jonas, S. M. Kang, N. P. Klingaman, R. Leung, J. Lu, B. Mapes, E. A. Maroon, S. McDermid, J.-y. Park, R. Roehrig, B. E. J. Rose, G. L. Russell, J. Seo, T. Toniazzo, H.-H. Wei, M. Yoshimori, and

L. R. Vargas Zeppetello, 2016: The tropical rain belts with an annual cycle and a continent model intercomparison project: TRACMIP. *Journal of Advances in Modeling Earth Systems*, **8 (4)**, 1868–1891.

Voldoire, A., E. Sanchez-Gomez, D. S. y Mélia, B. Decharme, C. Cassou, S. Sénési, S. Valcke, I. Beau, A. Alias, M. Chevallier, et al., 2013: The CNRM-CM5. 1 global climate model: description and basic evaluation. *Climate Dynamics*, **40 (9-10)**, 2091–2121.

Walker, C. C. and T. Schneider, 2005: Response of idealized Hadley circulations to seasonally varying heating. *Geophysical Research Letters*, **32 (6)**.

———, 2006: Eddy influences on Hadley circulations: Simulations with an idealized GCM. *Journal of the Atmospheric Sciences*, **63 (12)**, 3333–3350.

Walters, D., M. Brooks, I. Boutle, T. Melvin, R. Stratton, S. Vosper, H. Wells, K. Williams, N. Wood, T. Allen, et al., 2017: The Met Office unified model global atmosphere 6.0/6.1 and JULES global land 6.0/6.1 configurations. *Geoscientific Model Development*, **10 (4)**, 1487–1520.

Watanabe, M., T. Suzuki, R. O'ishi, Y. Komuro, S. Watanabe, S. Emori, T. Takemura, M. Chikira, T. Ogura, M. Sekiguchi, et al., 2010: Improved climate simulation by MIROC5: mean states, variability, and climate sensitivity. *Journal of Climate*, **23 (23)**, 6312–6335.

Wei, H.-H. and S. Bordoni, 2018: Energetic Constraints on the ITCZ Position in Idealized Simulations With a Seasonal Cycle. *Journal of Advances in Modeling Earth Systems*, **10 (7)**, 1708–1725.

Williamson, L., M. Blackburn, J. Hoskins, K. Nakajima, W. Ohfuchi, O. Takahashi, Y.-Y. Hayashi, H. Nakamura, M. Ishiwatari, L. McGregor, H. Borth, V. Wirth, H. Frank, P. Bechtold, P. Wedi, H. Tomita, M. Satoh, M. Zhao, M. Held, J. Suarez, M.-I. Lee, M. Watanabe, M. Kimoto, Y. Liu, Z. Wang, A. Molod, K. Rajendran, A. Kitoh, and R. Stratton, 2012: *The APE atlas*.

Zurita-Gotor, P., 2019: The role of the divergent circulation for large-scale eddy momentum transport in the tropics. Part I: observations. *Journal of the Atmospheric Sciences*, **76 (4)**, 1125–1144.

Acknowledgement

Foremost, I would like to thank my supervisor, Dr. Aiko Voigt, for his guidance through the process of this thesis. I would also like to thank Prof. Peter Knippertz for his constructive feedback. It was on point and helped me to progress with this thesis. Furthermore, I would like to thank my research group and especially Elzina Bala for their support and feedback on my work.

I want to thank Niklas, Seraphine and Johannes, my office mates, for scientific discussions and mental support.

Finally, I wish to thank family and friends for their support and encouragement throughout my studies. There have been countless conversations that helped me to carry on. Especially, I want to thank Elisabeth, Silvio, Karl, Anton, Gregor, Sebastian, Leonie, Karolina, Max, Jorge and my mom.

Declaration of Authorship

I hereby declare that the thesis submitted is my own unaided work. All direct or indirect sources used are acknowledged as references. I am aware that the thesis in digital form can be examined for the use of unauthorized aid and to determine wether the thesis as a whole or parts incorporated in it may be deemed as plagiarism.
For the comparison of my work with existing sources I agree that it shall be entered in a database where it shall also remain after examination, to enable comparison with future theses submitted. Further rights of reproduction and usage, however, are not granted here. This paper was not previously presented to another examination board and has not been published.

Karlsruhe, 30. 01. 2020

Freia Catherina Then